ON THE CONTROL ELEMENTS

OF

A PARTICULATE PROCESS

Powder Feeders and Measurement of Gas-Solids Flow Rate

Hiroaki Masuda

December, 1972

ON THE CONTROL ELEMENTS OF A PARTICULATE PROCESS

Powder Feeders and Measurement of Gas-Solids Flow Rate

by

Hiroaki Masuda

Department of Chemical Engineering
Kyoto University
Kyoto, Japan

December, 1972

FOREWORD

The research described in this report, "On the control elements of a particulate process" by Hiroaki Masuda was carried out under the direction of Dr. K. Iinoya, Professor, in the Department of Chemical Engineering, Kyoto University, Kyoto, Japan.

I am much indebted to Dr. K. Iinoya for his advice and guidance in the course of this doctoral work as well as in my entire study. I wish to express my thanks to Dr. M. Ikeda, Professor of Department of Applied Mathematics and Physics, Kyoto University, for his valuable suggestions regarding the mathematical treatment of this work. Thanks are extended to each member of Professor Iinoya's Laboratory, Drs. K. Hotta, K. Makino, and S. Yuu. I am also indebted to the members of the Department of Chemical Engineering for their kind interest in this work.

I also wish to thank the collaborators of the following studies, which constitute this dissertation.

1) Masuda, H. and K. Iinoya,"Mean Particle Diameter in an Analysis of a Particulate Process", Memoirs of the Faculty of Eng., Kyoto Univ., 34, No.4, 344 (1972)

2) Masuda, H. and K. Iinoya, "Scatter of Experimental Data due to Particle-Size-Distribution", J. Chem. Eng., Japan, 4, 60 (1971)

3) Masuda, H., T. Masuda, and K. Iinoya, "Experimental Study on the Characteristics of the Various Feeders", J. Res. Assoc. Powder Tech., Japan, 7, 479 (1970)

4) Masuda, H., T. Masuda, and K. Iinoya, "On the Characteristics of a Table Feeder", Kagaku Kōgaku, 35, 559 (1971)

5) Masuda, H., K. Miura, and K. Iinoya, "Some Aspects of the Table Feeder", J. of Society of Materials Sci., Japan, 21, 577 (1972)

6) Masuda, H. and K. Iinoya, "Step Response of Discharge Rate for Scraper Position in a Table Feeder", J. Res. Assoc. Powder Tech., Japan, 9, 227, (1972)

7) Masuda, H., T. Kameda, and K. Iinoya, "On the Static Characteristics of a Rotary Feeder", Kagaku Kōgaku, 35, 917 (1971)

8) Masuda, H., Y. Itō, and K. Iinoya, "Measurement of Gas Flow Rate in Gas-solids Two-phase Flow by use of a Horizontal Diffuser", submitted to the Society of Chem. Engrs., Japan

Thanks are also due to Mr. R. E. Underdown for his help in the preparation of this dissertation.

TABLE OF CONTENTS

Page

PART I

BASIC PROBLEMS

CHAPTER 1 INTRODUCTION 1

1.1 Final Control Means : Powder Feeders 2

1.2 Measurement of Powder Flow Rates 4

1.3 Scope of the Dissertation 6

References 7

CHAPTER 2 MEAN PARTICLE DIAMETER IN THE ANALYSIS OF A PARTICULATE PROCESS 10

2.1 Introduction 10

2.2 Definition of the Mean Particle Diameter 11

2.2-1 The experimental value of the process variable 11

2.2-2 Linear estimate 12

2.2-3 Definition of the mean particle diameter 14

2.2-4 A method of applying the definition term by term 15

2.2-5 A graphical method 15

TABLE OF CONTENTS (continued)

		Page
2.3	Discussion	17
2.3-1	On the definition of mean particle diameter	17
2.3-2	Comments on the use of mean particle diameter	25
2.3-3	Log-normal particle size distribution	26
2.4	Examples	30
2.4-1	$y = \Sigma \kappa_j D_p^{\alpha j}$	30
2.4-2	$\eta_I = 1 + D_p/d - 1/(1 + D_p/d)$	30
2.4-3	Example of six particles	31
2.4-4	Application to other physical processes	33
2.5	Conclusion	33
	Nomenclature	37
	References	38
CHAPTER 3	SCATTER OF EXPERIMENTAL DATA DUE TO PARTICLE SIZE DISTRIBUTION	39
3.1	Introduction	39
3.2	Distribution of the Sample Mean Particle Diameter	41
3.3	Number of Particles Required in an Experiment	46
3.4	Example	50
3.5	Discussion	55
3.6	Conclusion	58

TABLE OF CONTENTS (continued)

Page

Appendix [A] Sampling distribution of mean particle diameter 59

[B] Derivation of Eq.(3.23) 61

Nomenclature 62

References 65

PART II

FINAL MEANS : POWDER FEEDERS

CHAPTER 4 EXPERIMENTAL STUDY ON THE CHARACTERISTICS OF VARIOUS FEEDERS 66

4.1 Introduction 66

4.2 Apparatus and Experimental Methods 66

4.3 Screw feeder 68

4.4 Vibra Screw Feeder 70

4.5 Flo-tron 73

4.6 Belt Feeder 73

4.6-1 Analysis of the step response of the belt feeder 76

4.6-2 Prediction of the step response detected by weighing 79

4.6-3 Discussion of the belt feeder 83

4.7 Conclusion 86

Nomenclature 86

References 87

TABLE OF CONTENTS (continued)

	Page
CHAPTER 5 TABLE FEEDER	89
5.1 Introduction	89
5.2 Characteristics of the Discharge Rate when regulated by the Scraper	90
5.2-1 Apparatus and experimental methods	90
5.2-2 Preliminary observation	92
5.2-3 Shape of the powder bed and the mass flow rate	94
5.2-4 Experimental results and discussion on the shape of the powder bed and the discharged mass flow rate	98
5.2-5 Dynamic characteristics and analysis	101
5.3 Characteristics of the Discharge Rate when regulated by changing the Rotational Speed of the Table	106
5.3-1 Apparatus and experimental methods	106
5.3-2 Static characteristics	108
5.3-3 Dynamic characteristics	111
5.4 Fluctuation of the Mass Flow Rate	113
5.4-1 Cause of the fluctuation	113
5.4-2 Amplitude of the fluctuation	117
5.5 Intercepted Height of the Powder Bed as a Function of the Scraper Position: Y-curve	121
5.5-1 Measurements of Y-curve	122

TABLE OF CONTENTS (continued)

Page

5.5-2 Explanation of the step responses of the discharge rate regulated by the scraper 123

5.5-3 Explanation of the effect of the powder properties on the Y-curve 126

5.6 Conclusion 138

Nomenclature 140

References 143

CHAPTER 6 ROTARY FEEDER 144

6.1 Introduction 144

6.2 Prediction of the Volumetric Efficiency 145

6.2-1 Theoretical study 145

6.2-2 Apparatus and experimental methods 152

6.2-3 Results and discussion 154

6.3 Step Response 164

6.4 Conclusion 165

Nomenclature 166

References 167

PART III

PRIMARY MEANS

MEASUREMENTS OF THE MASS FLOW RATES IN GAS-SOLIDS TWO-PHASE FLOW

CHAPTER 7 MEASUREMENT OF GAS FLOW RATE BY USE OF A HORIZONTAL DIFFUSER 168

TABLE OF CONTENTS (continued)

		Page
7.1	Introduction	168
7.2	Theoretical Approach	169
7.3	Apparatus and Experimental Procedure	177
7.4	Results and Discussions	181
7.5	Conclusion	190
	Nomenclature	191
	References	192
CHAPTER 8	CONCLUSION	195

PART I

BASIC PROBLEMS

CHAPTER 1

INTRODUCTION

Automatic control of particulate processes is an important subject not only as a means of promoting production safely and efficiently, but also as a means of protecting the environment from dust contamination. However, in the existing circumstances, satisfactory control of particulate processes is not easy, nor is it common practice. Generally a control system involves detection of the process variables which are considered indicative of the state of the process, and manipulation of appropriate variables, by some final control device, to maintain the process in the desired condition. In these functions, manipulation of the process variables can be made in response to a signal from a controller whose output varies according to predetermined control actions and settings. Such controllers are widely used in the operation of fluid and other processes, and in principle, should be applicable to the control of systems involving particles. The control theories used in the fluid-systems are also applicable. Therefore, the most important areas in which problems may arise in the automatic control of particulate processes are the primary measuring means

and the final control means; namely, in the development and operation of measuring devices for the powder flow rate, and powder feeders. This chapter will review progress in the fields of powder feeders and measuring devices.

1.1 Final Control Means: Powder Feeders

The final control means in particulate processes is required to control the powder flow rate according to the manipulating signals. Any kind of powder feeder may be used for this purpose. However, it is desirable for satisfactory control that the feeder has a quick response, linear static properties, and reproducible static properties. To obtain these properties, it is necessary that the supply of powder from the hopper to the feeder proceeds smoothly in "mass flow". But this is not achieved easily and has been studied as a problem in the design of a hopper.[7, 11, 18, 19] Recently, studies on the flow pattern in a system where a hopper and a feeder are combined as a unit, were taken up by some investigators.[14. 17, 19] A particular powder feeder may not be suitable for every kind of powder. Therefore, there are a greater variety of feeders [1, 2, 10,19] used in particulate systems, than is general with fluid systems. Available powder feeders will, basically, control the discharged volume, not the mass, flow rate of the powder. As far as the mass flow rate of powder fed in a major process is con-

cerned, therefore, the flow rate must be checked by a mass flow meter. A belt-scale and hopper-scale[9, 21] have this mechanism. Studies concerning feeders with weighing mechanisms, have been reported.[15, 16] It is recommended, at present, to install a subsidiary control loop using a mass flow meter such as the Impact-Line mass flow meter.[20]

Auxiliary control of the final feed mechanism is one of the most important points in control of a particulate process. A feeder without a minor control loop, however, will be practicable[8] when the rate of the change of the environmental conditions is slow. Response of a main process under conditions of changing process variables will involve a time delay. When the time delay is large, and the time lags of the final control device and the primary measuring element are the same or higher than that of the main process, it will be difficult to control the process with this control system. In fact the process may become unstable. The characteristics of the feeder must, therefore, be known beforehand, also whether the feeder is accompanied by a minor control loop, or not.

The characteristics of powder feeder, as a final control means, have not been investigated adequately. The first problem in the application of a feeder as the final control means is, therefore, to analyze its static and dynamic characteristics.

1.2 Measurement of Powder Flow Rates

As reviewed by Beck et al,[3] and Iinoya et al,[13] there are many methods for the measurement of powder flow rate, e.g. weighing methods, nucleonic method, Coriolis force method, static electrical capacitance method, impact force method, and so on. Among the weighing methods, the belt scale and hopper scale are well known. For the study of the dynamic characteristics of the various feeders considered in this dissertation, the Impact-Line mass flow meter was used. This particular flow meter belongs to the group utilizing the impact force method. The force produced by the impact between a powder and an inclined plate is in proportion to the mass flow rate of the powder. The mass of powder adhering to the plate affects the vertical component of the force, but does not affect the horizontal component. Therefore, zero drift of the meter due to the adhering powder is eliminated when the horizontal component is used. The time constant of the system including a recorder is about 0.4 sec., and the accuracy is satisfactory.

It is essential for the measurement of powder flow rate that the flow-meter does not obstruct the flow of powder, and that it has no moving parts. The obstruction of the flow may cause blockage, and the moving parts may suffer damage by the dust. These troubles will also affect the operation of the main process. If these points are taken into consideration in selecting the measuring instruments,

measurements of the flow rate in one-phase powder flow may be carried out with fairly good accuracy.

On the other hand, measurements of the flow rate in two-phase flow, especially in gas-solid two-phase flow, under the existing circumstances, leave much to be desired. However, demands for development in such measurements have become stronger. As reviewed by Boothroyd et al,[5, 6] there are many methods which might be used for the measurements such as pressure drop method, electrostatic method, optical method, heat flux method, hot-wire anemometer method, etc. Not one of them, however, can satisfy all demands. A new method has been reported by Beck et al.[4] They determined the velocity of the powder flow from the transit time of the naturally occurring flow noise pattern between capacitance transducers installed at two points along a pneumatic conveyor. This method does not obstruct the flow. The chief difficulty in the application of this method is the complexity of the treatment of the data.

Other potentially-useful methods for measurement without obstruction of the flow are the detection of the pressure drop over a straight-pipeline and the measurement of the naturally occurring electrostatic current. In systems handling large particles, the former is available with fairly good accuracy, but it has not proved satisfactory in systems involving fine particles. The electrostatic method must be further examined, experimentally and theoretically. Measurements of the gas flow rate in

gas-solids two-phase flow is also one of the important outstanding problems.

1.3 Scope of the Dissertation

Some of the objectives of this research are as follows:

1. To clarify the problems peculiar to particulate processes, namely the determination of the mean particle diameter and the scatter of the data due to the particle-size-distribution.

2. To analyse the static characteristics of various feeders.

3. To analyse the dynamic characteristics of various feeders.

4. To examine the methods available for measuring the mass flow rate in air-solid two-phase flow.

Part I, consisting of Chapter 1, 2, and 3, discusses the basic problems peculiar to the particulate processes. The purpose of Chapter 1 is to provide a framework for the two major subjects with which the dissertation is concerned, namely, the final control means of the control systems, and measurement of the powder flow rate. A further purpose is to outline the subsequent contents of the

dissertation. Chapter 2 discusses the mean particle diameter in relation to the analysis of a particulate process, and Chapter 3, the scatter of the experimental data attributable to the particle-size-distribution.

Part II describes the experimental and theoretical studies of the final control means, namely, powder feeders. Chapter 4 presents the experimental studies on a screw feeder, Vibra screw feeder, Flotron, and a belt feeder. Chapter 5 examines the static and dynamic characteristics of a table feeder. Chapter 6 deals with a rotary feeder.

Part III describes the experimental and theoretical studies on the measurement of the mass flow rate in gas-solids two phase flow. Chapter 7 discusses the Venturi-type gas-flow meter, as a basic device for measuring the powder flow rate in two-phase flow.

References

1) Aoki, R. et al., "Saikin no Funryūtai Kyōkyū Sochi (Modern feeders for powder materials)", Kagaku Kōgaku, 26, 530 (1962)
2) Aoki, R. et al., "Funryūtai no Chosō to Kyōkyū Sōchi (Hoppers and feeders for powder materials)", Nikkan Kōgyō Co. (1963)
3) Beck, M. S., and N. Wainwright, "Current industrial methods of solids flow detection and

measurement", Powder Technol., 2, 189 (1968/69)
4) Beck, M. S. et al., "Particle velocity and mass flow measurement in pneumatic conveyors", Powder Technol., 2, 269 (1968/69)
5) Boothroyd, R. G., and A. S. Goldberg, "Measurements in flowing gas-solids suspensions-Part I", Brit. Chem. Eng. 14, 1705 (1969)
6) Boothroyd, R. G., and A. S. Goldberg, "Measurements in flowing gas-solids suspensions-Part II", Brit. Chem. Eng. 15, 357 (1970)
7) Brown, R. L., and J. C. Richards, "Principles of powder mechanics", Pergamon Press. (1970)
8) Gericke, H. R., "Metering of bulk material" Aufbereitungs-Teckn. Nr. 1, 19 (1971)
9) Hashimoto, Y., "Funtaino Jidō-Keiryō-Sōchi ni tsuite (On the automatic weighing of powder materials)", Kagaku Kōgaku, 32, 1062 (1968)
10) Hyde. R. w., "Feeders and feeding mechanisms", Chemical Engineers' Handbook (J.H. Perry), 3rd. Ed. p. 1370, McGraw-Hill (1950)
11) Igarashi, H., and R. Aoki, "Hopper karano Ryūshitsu (Flow from hopper)", Kagaku Kōgaku, 28, 698 (1964)
12) Iinoya, K., and K. Goto, "Funryūtai no Kenshutsu to Seigyo (Instantaneous measurement and control of the solid flow rate)", J. of the Japan Associ. of Automatic Control Eng., 7, 646 (1963)
13) Iinoya, K., and H. Masuda, "Funtai Ryūryō no Keisoku to Seigyo (Measurements and control of the powder flow rate)", Kagaku-Kōgaku no Shinpo 5 (Advanced Chem. Eng., No. 5) Chap. 8,

Edited by the Society of Chem. Engrs., Japan (1971)

14) Johanson, J. R., "Feeding", Chem. Eng., 76, 75 (October 13, 1969)

15) Kloven, P., "A Novel, gravimetric feeder for powder and granular products", Paper presented at the ISA-70 (October, 1970)

16) Lordi, A. C., "Adjustable-speed feeder drives", Instrumentation Technol., 15, 46 (January, 1968)

17) Miles, J. E. P. and C. Schofield, "Techniques for controlling the flow rate of dry solids", Paper presented to symposium on solids handling, Inst. of Chem. Engrs. (September, 1969)

18) Stepanoff, A. J., "Gravity flow of bulk solids and transportation of solids in suspension", John Wiley & Sons Inc. (1969)

19) Schwedes, J., "Fließverhalten von Schüttgütern in Bunkern", Verlag Chemie, Gm bH (1970)

20) Watanabe, K. and T. Inagaki, "Impact Line Ryūryōkei ni yoru Funryūtai Ryūryō Jidō-Seigyo no Jitsurei (Installation of automatic control of powder and granular materials by Impact-Line flow meter)", J. Res. Assoc. Powder Tech., 7, 538 (1970)

21) Zanetti, R. R., "Continuous proportioning for the food industry", Instrumentation Technol., 18, 42, (March, 1971)

CHAPTER 2

MEAN PARTICLE DIAMETER IN THE ANALYSIS OF A PARTICULATE PROCESS

2.1 Introduction

What has been said previously about the mean particle diameter is not definite enough and this vagueness has caused much trouble. When studying the experimental data obtained for the same particulate process, for example, it is found that some authors employ the arithmetic mean diameter, others, the geometric mean diameter or the mass-surface mean diameter, and so on. Practically, the value of mean diameter varies so much depending on the definition employed, that in some extreme cases, even an assumed mean diameter may be used to bring the experimental data (measured values) into good agreement with the estimated values (theoretical values). If such is the case, one cannot tell whether the theoretical value is correct or not.

Another problem may arise as to what mean diameter to employ in quoting some of the results reported by other investigators. One may only apply such definitions as have been generally used, namely the arithmetic mean diameter, the geometric

mean diameter, and so on.

Another problem to be solved is how the theoretical and experimental results for mono-disperse particulate processes are to be applied to a poly-disperse particulate process.

A solution to such problems as pointed out above is to develop a definition for the mean diameter, which allows the value of the mean particle diameter to be estimated with high accuracy.

In an approach to this C. E. Ангреев and his collaborators[1] defined the mean particle diameter in general form. S. Miwa[2, 3] has commented on their results.

In this chapter, the author, from a consideration of these studies, defines the mean particle diameter in terms of the linear estimate of the process variable, and shows that it may be used to determine the mean diameter in any process. Alternative methods for determining the mean particle diameter are given in detail.

2.2 Definition of the Mean Particle Diameter

2.2-1 The experimental value of the process variable

To describe the state of the particles sampled, two parameters, "mean" and "variance" of the diameters are necessary, even if other conditions such as temperature, moisture or the shape of the particle are considered to be constant. The fre-

quency distribution of the particle size is, therefore, a function of diameter D_p, mean m and variance s^2;

$$f = f\ (D_p,\ m,\ s^2) \qquad (2.1)$$

Generally, the particles sampled vary in each experiment, the experimental value Y being a function of at least two variables, m and s^2. With interaction term γ , Y will be expressed in the form;

$$Y\ (m,\ s^2) = \int_0^\infty y(D_p)\ f(D_p, m, s^2)\, dD_p + \gamma(m, s^2) \qquad (2.2)$$

Here $y(D_p)$ represents either a mono-disperse particulate process variable or a one-particle process variable. The first term of the right hand side, being linear estimate, can be put in the form;

$$\bar{Y}\ (m, s^2) = \int_0^\infty Y(D_p)\ f(D_p, m, s^2)\, dD_p \qquad (2.3)$$

Of course, the term $\int \cdots dD_p$ can be replaced with Σ when a discrete system is concerned.

2.2-2 Linear estimate $\bar{y}(m, s^2)$

Generally, the linear estimate $\bar{y}$ varies with the method of measurement such as weighing the particles or counting the particles and so on. Just

for a simple example, take the case of six spherical particles with the same specific gravity. Four of the six have a diameter 1, and the remaining two have a diameter 2. Each particle follows the equation;

$$y = y(D_p) \qquad \text{e.g. if the process follows Stokes' law } y = K D_p^2 \qquad (2.4)$$

and has no interaction with any of the others (cf. Table 2.1).

Table 2.1 : Description of the six particles

Particle dia.	1	1	1	1	2	2
Process variable	y_1	y_1	y_1	y_1	y_2	y_2
weight ratio	1	1	1	1	8	8

($y_1 = 15$, $y_2 = 30$)

Then the experimental value on the count basis is;

$$Y^{(o)} = \frac{4}{4+2} y_1 + \frac{2}{4+2} y_2 = \frac{2}{3} y_1 + \frac{1}{3} y_2 \qquad (2.5)$$

(mean on count basis)

Here y_i stands for $y(D_{pi})$. On the other hand, the experimental value on the mass basis is;

$$Y^{(3)} = \frac{4}{4+(2\times8)} y_1 + \frac{2\times8}{4+(2\times8)} y_2 = \frac{1}{5} y_1 + \frac{4}{5} y_2 \qquad (2.6)$$

(mean on mass basis)

If $Y_1 = 15$ and $Y_2 = 30$, it is clear that $Y^{(0)} = 20$ and $Y^{(3)} = 27$ from the last two Eqs. (2.5) and (2.6). So, in spite of the fact that the process is the same, the experimental values obtained by the different methods are not the same*). In this example, the experimental value can be estimated only by the linear term. So from this example, if one wants to estimate the experimental values on any basis, it is found desirable to express the linear estimate in the form;

$$\bar{y}^{(\beta)} = \Sigma f^{(\beta)} y = \Sigma f^{(0)} D_p^{\beta} y / \Sigma f^{(0)} D_p^{\beta} \qquad (2.7)$$

If "β" in the above equation is 0, the estimate is on the count basis, if "β" is 1, on the length basis, if "β" is 2, on the area basis, if "β" is 3, on the volume (or mass) basis. As discussed above, these values are different from each other. The method used, therefore, has to be stated definitly, and the experimental values have to be compared with the estimated values on the same basis.

2.2-3 Definition of the mean particle diameter

By use of the linear estimate, the mean particle diameter will be defined by the equation;

$$\bar{D}_p \equiv y^{-1} (\bar{y}) \qquad (2.8)$$

---

*) Note that the mean particle diameter of the six particles cannot be determined at this point. See also § 2.4-3.

2.2-4 A method of applying the definition term by term

When the process variable y is given in the form of the summation of several terms, it is convenient to apply definition (2.8) to each term. That is, if the process variable y is expressed by the equation;

$$y = \sum_{j=1}^{n} y_{(j)} \tag{2.9}$$

Then the mean particle diameters are given by the equation;

$$\bar{D}_{p(j)} \equiv y_{(j)}^{-1} \quad (\bar{y}_{(j)}), \qquad j = 1, 2, 3, \ldots, n \tag{2.10}$$

2.2-5 A graphical method

Now consider the case that the process variable y cannot be expressed in a simple equation of D_p, or cannot be expressed in any equation. In such a case, if the process variable can be expressed graphically or in a table, the mean particle diameter may be obtained directly by use of definition (2.8). Take Fig. 2.1 to explain this method generally. In the figure, $g(D_p)$ is a function of D_p, e.g. Reynolds number, Nusselt number, Peclet number, Sherwood number, Inertia parameter, and so on, and here it is called the characteristic parameter of the particle diameter.

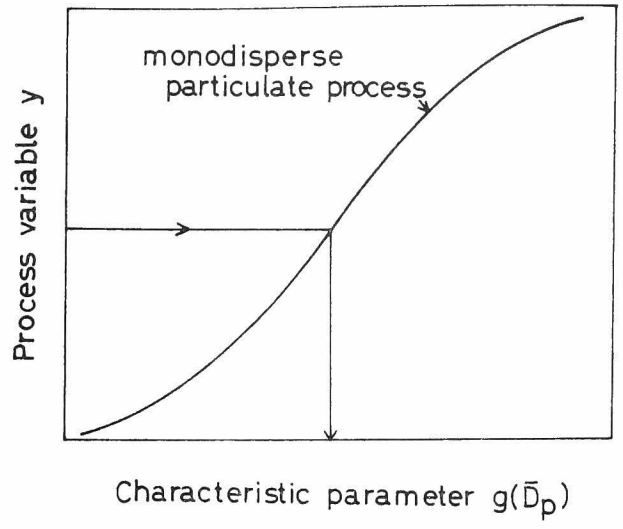

Fig.2.1 Graphical method

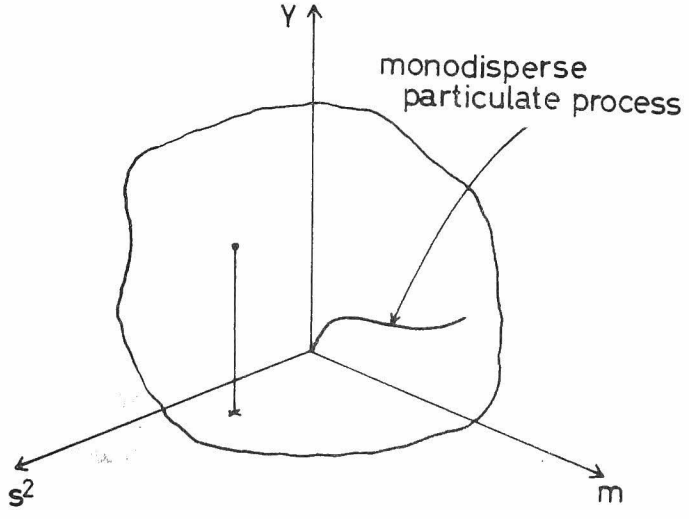

Fig.2.2 General idea of experimental data in the (s^2, m, Y)-space

From Eq. (2.7), the linear estimate $\bar{y}$ is given by the equation;

$$\bar{y} = \sum_i f_i \, y(\; g(D_{pi} \;)) \qquad (2.11)$$

Having calculated $\bar{y}$, the characteristic parameter g of the mean particle diameter is obtained as shown by the arrows in Fig. 2.1. Then, from this value, the mean particle diameter can be determined by the following equation;

$$\bar{D}_p = g^{-1} \; (\bar{g}) \qquad (2.12)$$

2.3 Discussion

2.3-1 On the definition of mean particle diameter

The following discussion shows that definition (2.8) is adequate in scope and is of considerable importance. The discussion is based on the assumption that there is no interaction between particles. From Eq. (2.2), it follows that;

$$Y(m,s^2) = \int_0^\infty y(D_p) f(D_p, \; m,s^2) dD_p = \bar{y}(m,s^2) \qquad (2.13)$$

From this equation it is found that the experimental value $Y(m, \; s^2)$ is a function of m and s^2. Hence, the experimental value $Y(m, \; s^2)$ may be expressed as a point in the $(m, \; s^2, \; Y)$-space (cf. Fig. 2.2).

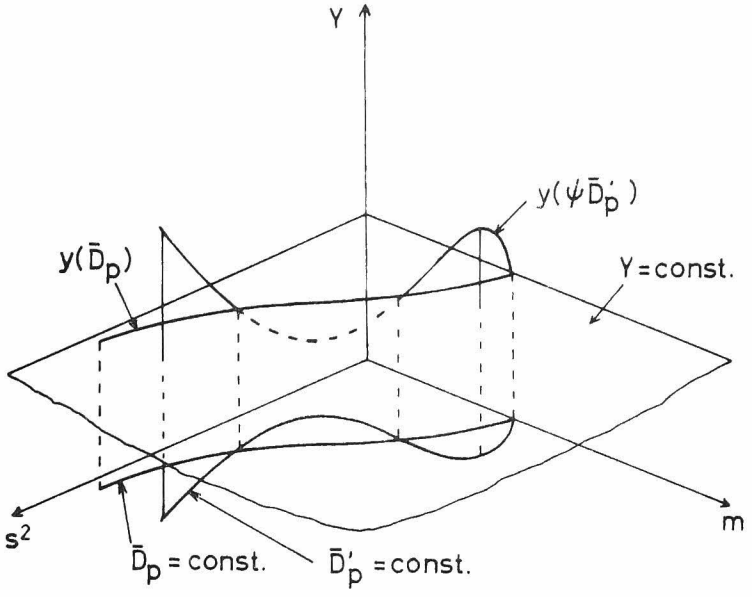

Fig.2.3 Relation between the mean particle diameter and the experimental data

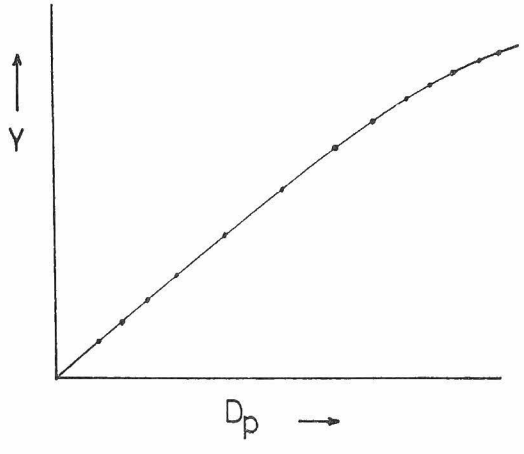

Fig. 2.4 Experimental data represented by use of the mean particle diameter based on definition (2.8)

This is interpreted as implying that if one point (m,s^2) is given, as by sampling the particles, one experimental value $Y(m,s^2)$ will be given. If the mean particle diameter is given in accordance with definition (2.8), it is given by the equation;

$$\bar{D}_p = y^{-1}(\bar{y}(m,s^2)) = y^{-1}(Y(m,s^2)) \qquad (2.14)$$

So, $\bar{D}_p$ = const. gives a curve in a (m, s^2)-space, and from the definition, the experimental values $Y(m,s^2)$ on this curve are constant, that is;

$$Y(m,s^2) = y(\bar{D}_p) = \text{const.} \qquad (2.15)$$

From the above discussion, it may be concluded that the experimental values $Y(m,s^2)$ have a constant value $y(\bar{D}_p)$ on this mean particle diameter $\bar{D}_p$ (cf. Fig. 2.3). This is applicable when the experimental values are studied using the mean particle diameter (cf. Fig. 2.4). On the other hand, any mean particle diameter that is defined other than by Eq. (2.8) has no such characteristic property as mentioned above. Such mean diameters will be discussed briefly here. Generally any one of these mean particle diameters may be formulated with a certain function $\psi(m,s^2)$ as follows;

$$\bar{D}_p' = \bar{D}_p / \psi(m,s^2) = y^{-1}(Y(m,s^2)) / \psi(m,s^2) \qquad (2.16)$$

Therefore,

$$Y(m,s^2) = y(\psi(m,s^2)\cdot \bar{D}_p') \qquad (2.17)$$

The above equation means that $\bar{D}_p' = \text{const.}$ cannot give a constant experimental value. In other words, the experimental values on the curve $\bar{D}_p' = \text{const.}$ vary with each (m,s^2). Fig. 2.3 shows the general idea. Note that if a wrong mean particle diameter is used, the values obtained, even from the most careful experiments, will turn out to scatter as shown in Fig. 2.5. Without any data as to (m,s^2), scarcely any satisfactory results may be obtained from the experiments. The following example will help to make the above discussion clear. A random sampling is carried out from log-normal distributed particles (cf. § 2.3-3). Then an experiment is made on the process to conform to the equation;

$$y = KD_p^2 \qquad (2.18)$$

The mean particle diameter to conform to definition (2.8) is;

$$\bar{D}_p = y^{-1}(\bar{y}) = \sqrt{\int_{-\infty}^{\infty} KD_p^2 f^{(0)}(\ln D_p,\ m,s^2)\, d\ln D_p / K}$$

$$= \exp(m+s^2) \qquad (2.19)$$

(for Q1 shown in Fig. 2.8, $\bar{D}_p = 57.4$ microns)

The experimental value $Y(m,s^2)$ is expressed as;

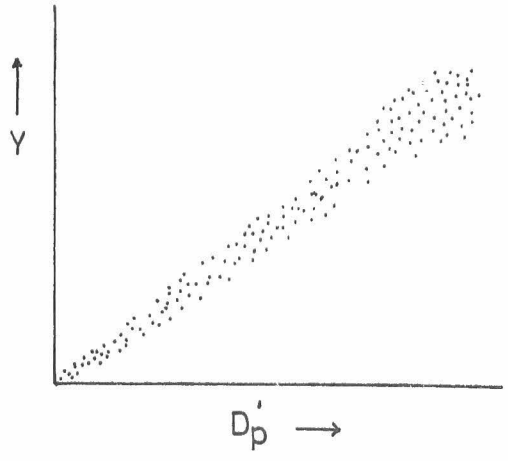

Fig.2.5

Experimental data represented by use of other mean particle diameters than the correct one based on the proposed definition

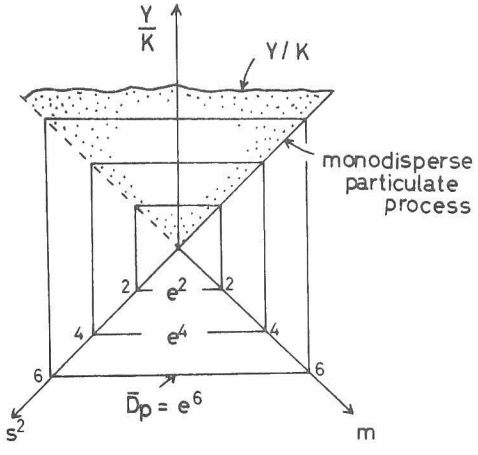

Fig.2.6

The mean particle diameter - surface mean diameter - based on the definition and the experimental data in the (s^2, m, Y/K)-space

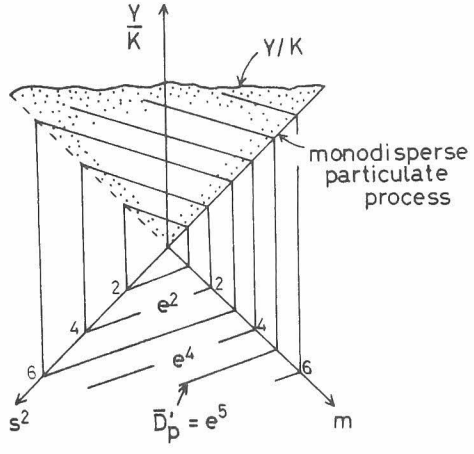

Fig.2.7

The length mean particle diameter and the experimental data in the (s^2, m,Y/K)-space

$$Y(m,s^2) = K \int_{-\infty}^{\infty} D_p^2 f^{(0)}(\ln D_p, m, s^2)\, d\ln D_p = K\bar{D}_p^2 \qquad (2.20)$$

(for Q1, $Y/K = 3295$ microns^2)

If $\bar{D}_p$ = const., the experimental values $Y(m,s^2)$ have a constant value $K\bar{D}_p^2$, independently of the value (m,s^2), and are correctly represented by Eq. (2.18). Such a process as discussed above is shown in Fig. 2.6. On the other hand, if some other mean particle diameter, for example, the length mean diameter;

$$\bar{D}_p' = \int_{-\infty}^{\infty} D_p f^{(0)}(\ln D_p, m, s^2) d\ln D_p = \exp(m+s^2/2) \qquad (2.21)$$

(for Q1, $\bar{D}_p'$ = 54 microns)

is used, the relation between $\bar{D}_p'$ and $\bar{D}_p$ is as follows;

$$\bar{D}_p' = \exp(m+s^2)\exp(-s^2/2) = \bar{D}_p/\exp(s^2/2) \qquad (2.22)$$

$\psi(m,s^2)$ used in the general discussion is $\exp(s^2/2)$. From Eq. (2.17) or Eqs. (2.20) and (2.22), the following equation is obtained.

$$Y(m,s^2) = y(\psi(m,s^2)\bar{D}_p') = K\{\psi(m,s^2)\bar{D}_p'\}^2$$

$$= K\cdot\exp(s^2)\bar{D}_p'^2$$

or,

$$Y(m,s^2)/K = \bar{D}_p'^2 \exp(s^2) \qquad (2.23)$$

This is shown in Fig. 2.7. As shown in Fig. 2.8, the results represented by $\bar{D}_p'$ vary with the variance s^2. Therefore, even if the length-mean particle diameter $\bar{D}_p'$ is constant, the experimental values will scatter through the variance of powders. In general, this scatter has a bias. In this example, the experimental values are always larger than $K \cdot D_p^2$ when $\bar{D}_p'$ is used. In Fig. 2.8, corresponding experimental values for the kinds of powder often used in experiments are indicated by the designated symbols. These powders have fairly small variances. However, the results show about 10 % error. When $\bar{D}_{p50}$ is used instead of $\bar{D}_p'$, the results become worse, and the errors are 20 % or more.

It is most important in determining the mean particle diameters term by term (cf. §2.2-4) that the experimental value is compared with another only at the point where all the mean particle diameters $\overline{Dp}(j)$ coincide with one another. When the process variable is expressed in more than two terms, therefore, it is better to deal with the data using both the mean and the variance. Note that even in such a case, when the graphical method is introduced (cf §2.2-5), it is adequate to study the data with the mean particle diameter or with its characteristic parameter $g(\bar{D}_p)$.

From the above discussion it is clear that to

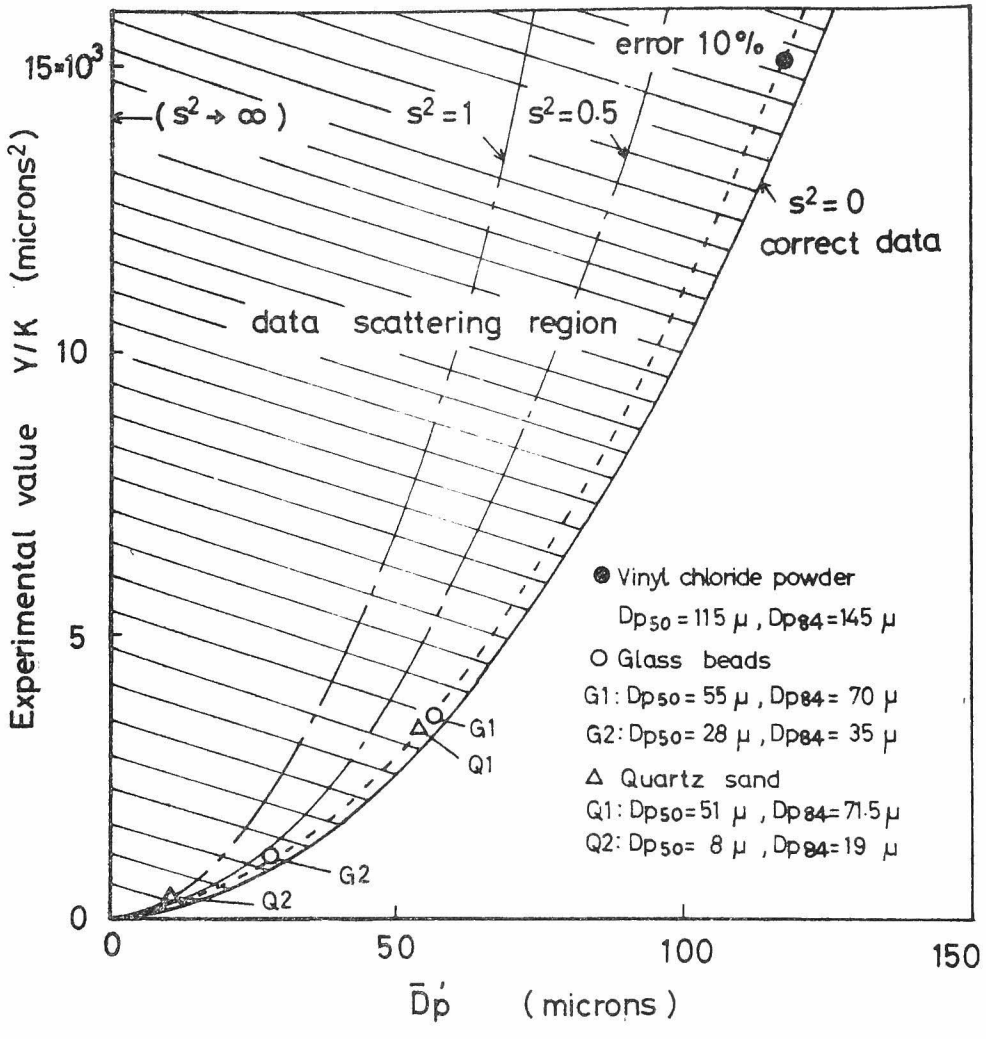

Fig.2.8 Experimental data represented by use of other mean particle diameters than the correct one - e.g.; the length mean diameter

use a properly defined mean particle diameter is very important, not only to study the various experimental values systematically but to attain satisfactory results with little scattering in the data.

2.3-2 Comments on the use of mean particle diameter

The mean diameter being defined by the linear estimate, the process variable estimated using the mean diameter is a linear part of the variable. The non-linear part of it, therefore, has to be discussed separately from the linear part.

Especially in the case where the process variable depends both on the feed and on the product particles, careful consideration must be taken on the linear estimate. When the mean diameters defined term by term are used, the linear estimate is given by the equation;

$$\bar{y} = \sum_{i,j} f_{(F)i} \; f_{(p)j} \; y(D_{p(F)i} \, , \, D_{p(p)j}) \tag{2.24}$$

where the suffixes F and P refer to the feed and the product, respectively. Therefore, the effects of the overlapping of the two frequency distributions are left out of consideration here. In the case where each particle of the product cannot be larger than it was before passing through the process,

$$\sum_{D_{p(F)} < D_{p(P)}} f_{(F)} f_{(P)} Y(D_{p(F)}, D_{p(P)})$$

must be subtracted from the estimate. Then Y is given by the equation;

$$Y = \bar{y} - \sum_{D_{p(F)} < D_{p(P)}} f_{(F)} \cdot f_{(P)} \cdot Y(D_{p(F)}, D_{p(P)}) + \gamma \qquad (2.25)$$

Conversely, when the term "larger than" is replaced with "smaller than" the summation should be carried out on $D_{p(F)} > D_{p(P)}$.

2.3-3 Log-normal particle size distribution

It is convenient to make use of the log-normal particle size distribution;

$$f(\ln D_p, \mu, \sigma^2) = \frac{1}{\sqrt{2\pi\sigma^2}} \exp\left\{-\frac{1}{2} \frac{(\ln D_p - \mu)^2}{\sigma^2}\right\} \qquad (2.26)$$

where,

$$\mu = \int_{-\infty}^{\infty} \ln D_p f(\ln D_p, \mu, \sigma^2) d\ln D_p = \ln D_{p(50\%)} \qquad (2.27)$$

$$\sigma^2 = \int_{-\infty}^{\infty}(\ln D_p - \mu)^2 \, f(\ln D_p, \mu, \sigma^2) d\ln D_p \qquad (2.28)$$

$$\sigma = \ln D_{p(84.1\%)} - \ln D_{p(50\%)} \qquad (2.29)$$

Then, the relation between $\bar{y}^{(0)}$ and $\bar{y}^{(a)}$ is as follows;

$$\begin{aligned} \bar{y}^{(a)}(\mu,\sigma^2) &= \int_{-\infty}^{\infty} y(D_p) D_p^a f^{(0)}(\ln D_p, \mu, \sigma^2) d\ln D_p / \\ &\quad \int_{-\infty}^{\infty} D_p^a f^{(0)}(\ln D_p, \mu, \sigma^2) d\ln D_p \\ &= \int_{-\infty}^{\infty} y(D_p) f^{(0)}(\ln D_p, \mu+a\sigma^2, \sigma^2) d\ln D_p \\ &= \bar{y}^{(0)}(\mu+a\sigma^2, \sigma^2) \end{aligned} \qquad (2.30)$$

That is, if the estimate is made on the count basis, the estimate on some other basis can be calculated with this equation. In more general form, Eq. (2.30) reads

$$\bar{y}^{(a)}(\mu,\sigma^2) = \bar{y}^{(b)}(\mu + (a-b)\sigma^2, \sigma^2) \qquad (2.31)$$

If the estimate is made on any one of the bases therefore, the estimate on another basis can be calculated with this equation. Figures, too, may be of use in the transformation (cf. Fig. 2.9). Let us take the process of terminal velocity for example. If the fact that the particles are of

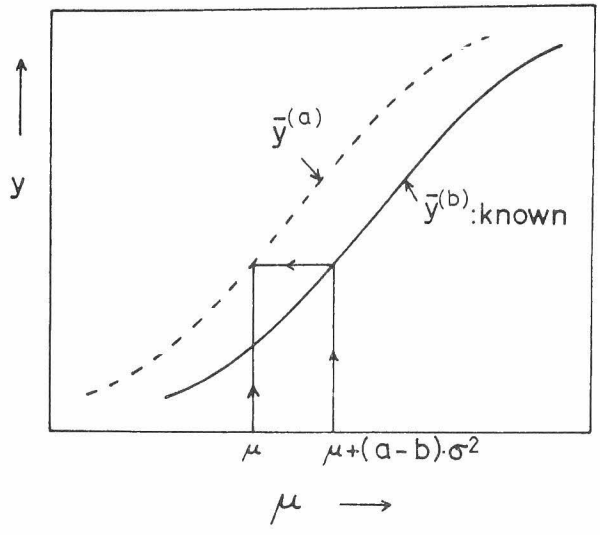

Fig.2.9 The linear estimate of the process variable in case of the log-normal size distribution

$D_p(50\%) = 5\ (\mu)$, $D_p(84.1\%) = 8\ (\mu)$, and $\rho_p = 3$ (g/cm^3) is known, one may obtain $\mu = \ln D_{p(50\%)} = 1.61$, and $\sigma = \ln D_{p(84.1\%)} - \ln D_{p(50\%)} = 0.47$. Now, the Stokes' law, $v_t = \{g(\rho_p - \rho_a)/18\mu_a\}D_p^2$ is applicable. This equation corresponds to the process variable y. Then on the count basis, one may have;

$$\bar{v}_t^{(0)} = \frac{g(\rho_p - \rho_a)}{18\mu_a} \int_{-\infty}^{\infty} D_p^2 f^{(0)} d\ln D_p$$

$$= \frac{g(\rho_p - \rho_a)}{18\mu_a} \exp\ (2\mu + 2\sigma^2) \qquad (2.32)$$

On the other hand, applying Eq. (2.31) to (2.32), $\bar{v}_t^{(3)}$ (on the mass basis) will be

$$\bar{v}_t^{(3)} = \frac{g(\rho_p - \rho_a)}{18\mu_a} \exp\ \{2(\mu + 3\sigma^2) + 2\sigma^2\} \qquad (2.33)$$

From $\mu_a = 0.00018$ (g/cm sec) and $\rho_a = 0.0012$ (g/cm^3), $\bar{v}_t^{(0)}$ and $\bar{v}_t^{(3)}$ will be 0.35 (cm/sec) and 1.33 (cm/sec) respectively. The difference between these two values is due to the fact that they are not on the same basis. For comparison, the calculated mean particle diameters are 6.24 (μ) on the count basis, and 12.1 (μ) on the mass basis. If $\bar{v}_t^{(0)}$ and $\bar{v}_t^{(3)}$ are calculated using these values, it is found that they coincide with the above mentioned values 0.35 and 1.33 respectively.

2.4 Exapmles

2.4-1 $y = \sum_{j=1}^{n} K_j D_p^{\alpha_j}$ (cf. § 2.2-4)

One may have $y_{(j)} = K_j D_p^{\alpha_j}$ by inspection, therefore

$$y_{(j)}^{-1} = (y_{(j)}/K_j)^{1/\alpha_j}, \text{ and } \bar{y}_{(j)} = K_j \Sigma_i f_i D_{pi}^{\alpha}$$

Then Eq. (2.10) reads

$$\bar{D}_{p(j)} = (K_j \Sigma_i f_i \cdot D_{pi}^{\alpha_j}/K_j)^{1/\alpha_j} = (\Sigma f D_p^{\alpha_j})^{1/\alpha_j},$$

$$j = 1, 2, 3, \ldots\ldots\ldots n \qquad (2.34)$$

2.4-2 $\eta_I = 1 + D_p/d - 1/(1 + D_p/d)$ (cf. §2.2-4)

As the first term is a constant, it is omitted for now, then $y_{(1)} = D_p/d$ and $y_{(2)} = -1/(1 + D_p/d)$, therefore

$$y_{(1)}^{-1} = d \cdot y_{(1)}, \bar{y}_{(1)} = \sum_i f_i D_{pi}/d, \; y_{(2)}^{-1} = -d(1+1/y_{(2)})$$

and

$$\bar{y}_{(2)} = -\Sigma\{f_i/(1 + D_{pi}/d)\}$$

From Eq. (2.10), we have

$$\bar{D}_{p(1)} = d \Sigma f_i D_{pi}/d = \Sigma f D_p,$$

$$\bar{D}_{p(2)} = -d\left\{1 + \frac{-1}{\Sigma \frac{f_i}{1+\frac{D_{pi}}{d}}}\right\} = \frac{1}{\Sigma \frac{f}{d+D_p}} - d \qquad (2.35)$$

Here, $\bar{D}_{p(1)} = \Sigma f D_p$ is the length mean diameter, but $\bar{D}_{p(2)}$ has never been taken into consideration before.

2.4-3 Example of six particles (cf §2.2-5)

In this section the graphical method (cf. § 2.2-5) will be explained in a less abstract way. Here the six particles (cf. §2.2-1) will be dealt with again. Now put $v\rho_a/\mu_a = 10$, and $D_{p1} = 1$ and $D_{p2} = 2$, and one may have $R_{e1} = 10$ and $R_{e2} = 20$. On the assumption that the process variable y is obtained as in Fig. 2.10, $\bar{R}_e^{(0)} = 11$ and $\bar{R}_e^{(3)} = 15$ are found from the figure. They were represented as $\bar{g}$ in §2.2-5. It is found that $R_e = D_p\, v\rho_a/\mu_a$, and then $g^{-1}(\bar{g}) = \mu_a \bar{R}_e/v\rho_a$. It follows that $\bar{D}_p^{(0)} = 11\mu_a/v\rho_a = 1.1$, and $\bar{D}_p^{(3)} = 15\ \mu_a/v\rho_a = 1.5$. These results are interpreted to mean that the estimates of this process are 20 on the count basis and 27 on the mass basis, and the mean diameters of the particles (six particles) are 1.1 on the count basis and 1.5 on the mass basis. Experimental values for this process may be plotted at the point of mean diameter 1.1 on the count basis and 1.5 on the mass basis, and they may be compared with the

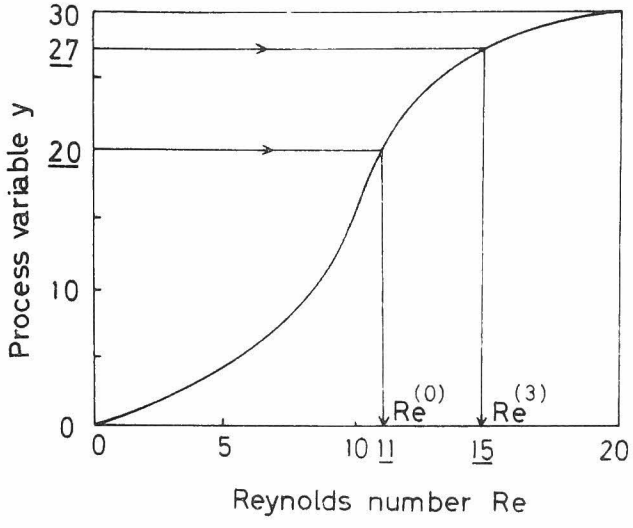

Fig.2.10 Process variable in a six particle system

estimates on their respective bases. A comparison such as described above is the most systematic and proper way to deal with experimental and estimated values.

2.4-4 Application to other physical processes

The procedure discussed in this chapter may be extended to other physical processes. The conclusions reached when this is done are listed in Table 2.2, should have wide application. They were obtained through the method described in §2.2-3 and §2.2-4. To use these mean diameters effectively, it must be kept in mind that they may be used to express the quantities in the left hand side of the equations in column 2, but not to express other quantities such as the square of them, a function of them, and so on.

2.5 Conclusion

The mean particle diameter is defined as $y^{-1}(\bar{y})$, where y^{-1} is an inverse function of the mono-disperse particulate process variable and $\bar{y}$ a linear estimate of the poly-disperse particulate process variable. When the mean particle diameters determined using the definition have the same values, the linear parts of the process variable also have the same values even if the parameters

Table 2.2 Mean particle diameters in the key processes

Process	Representative equation	Mean particle Dia.	Comment
Absorption	$\Delta p=\frac{150(1-\varepsilon)}{R_e}\frac{h(1-\varepsilon)G^2}{g_c\varepsilon^3 D_p\rho_a}$ $+ 1.75\frac{h(1-\varepsilon)G^2}{g_c\varepsilon^3 D_p\rho_a}$	$\bar{D}_{p(1)}=\sqrt{1/(\Sigma f/D_p^2)}$ $\bar{D}_{p(2)}= 1/(\Sigma f/D_p)$ $\bar{R}_e = \bar{D}_{p(1)}v\rho/\mu$	Pressure drop in packed beds , S.Ergun. Chem. Eng. Progr., 48, 89 (1952)
Adsorption	$J = \frac{k}{v}F\ (\frac{\mu}{\rho D_p})^{2/3}$	$\left\{\frac{1}{\Sigma\frac{f}{D_p^{2/3}}}\right\}^{3/2}$	Fluid film coefficient C.Chu,et al., Chem.Eng. Progr., 49, 141 (1953)
	$HETP = 2\lambda D_p + \frac{2\gamma D}{v}$ $+ \frac{8Hd}{\pi^2(1+Hd)^2}\frac{d_f^2 v}{D_e}$	$\Sigma f D_p$	Effective height of theoretical plate van Deemter, et al., Chem. Eng. Sci., 5, 271 (1956)
Agglomeration	$\sigma_z = \frac{9(1-\varepsilon)}{8\pi D_p^2}kF$	$\frac{1}{(\Sigma f/D_p^2)^{1/2}}$	Adhesive strength of packed particles H.Rumpf, & E.Turba., Ber.Dtsch. Keram.Ges., 41, 78 (1964)
	$\sigma_z = 8(1-\varepsilon)T/\varepsilon D_p$	$1/(\Sigma\ f/D_p)$	

Process	Representative equation	Mean particle dia.	Comment
Drying	$p = 2cT/D_p$	$1/(\Sigma f/D_p)$	Capillary suction pressure
	$\theta_{min} = 0.23L/N^{0.9}SD \pm 9.85 \times LG/FD_p^{0.5}$ + counter-current - co-current	$\frac{1}{(\Sigma \frac{f}{\sqrt{D_p}})^2}$	Minimum residence time of a rotary dryer S.J.Friedman & W.R. Marshall Jr., Chem. Eng.Progr., 45, 482, 572 (1949)
Dust and mist collection	$U_t = n_e V/\{3\pi\mu D_p R \cdot \ln(R_2/R_1)\}$	$1/(\Sigma f/D_p)$	Electrical method; moving velocity of a particle
Evaporation	$k_s a = 0.148(k_s a)_0 w/D_p$	$1/(\Sigma f/D_p)$	Capacity coefficient in crystallization
Fluidized beds	$N_u = 0.004(D_p v\rho/\mu)^{1.5}$	$(\Sigma f D_p^{3/2})^{2/3}$	R.Toei , Kagakukikai Gijutsu(Japan),No.15, 22 (1963)
	$\rho_{MB} = 0.356\rho_p(\log D_p - 1)$	$\log^{-1}(\Sigma f \log D_p)$	Maximum bed density
	$\bar{U}_{mf} = (\frac{g\phi^2 D_p^2}{200}) \times (\frac{\rho_s - \rho_f}{\mu_f})/F(\varepsilon)\ \varepsilon=\varepsilon_{mf}$	$\sqrt{\Sigma f D_p^2}$	Minimum velocity for fluidization

Process	Representative equation	Mean particle dia.	Comment
Heat transfer	$k_e^\circ/k_g = \varepsilon\left[1+\frac{h_{rv}D_p}{k_g}\right] + \frac{3}{2}\frac{k_s}{k_g}\left[1-\frac{1}{1+\frac{2k_g}{3\phi k_s}+\frac{2h_{rs}D_p}{3k_s}}\right]$	$\bar{D}_{p(1)} = \Sigma f D_p$ $\bar{D}_{p(2)} = \frac{1}{\Sigma\frac{f}{A+D_p}} - A$ $A = (\frac{3}{2}k_s + \frac{k_g}{\phi})/h_{rs}$	Effective thermal conductivities in packed beds S.Yagi & D.Kunii, A.I. Ch.E. Journal, 3, 373 (1957) Kagaku Kogaku, 18, 576 (1954)
	$q_p = \frac{6(1-\varepsilon)}{D_p\phi_s} h_p(t-t_p)_{av.}$	$1/(\Sigma f/D_p)$	Heat transfer between packings and fluids

- e.g. mean and variance - are not the same. If the experimental data are studied by use of this mean particle diameter, therefore, no scattering in the data due to the wrong use of the mean particle diameter is observed. On the other hand, use of other mean particle diameter will lead to unsatisfactory results with scattering in the data. Thus, the various experimental data may be systematically studied only by use of the proposed definition. Futhermore, when the size distribution is log-normal in form, it is found that the linear estimate on the "a" basis with the mean μ is the same as on the "b" basis with the mean $\mu + (a - b)\sigma^2$, where σ^2 is the variance. As is clear from this fact, the determination of the mean particle diameter is much simplified.

Nomenclature

D_p	particle diameter
f	particle size distribution
$g(D_p)$	characteristic parameter of the particle diameter
m	sample mean particle diameter
s	sample standard deviation
Y	experimental value
y	process variable
$\bar{y}$	linear estimation
β	basis number (β = 0 for the count basis, and β = 3 for the mass basis)

$\gamma(m,s^2)$	interaction term, Eq. (2.2)
μ	population mean particle diameter
μ_a	viscosity of air
ρ_a	density of air
σ	population standard deviation
ψ	certain function of m and s^2, Eq. (2.16)

References

1) Андреев, С. Е., В. В. Товаров и В. А. Перов; "Закономерности измельчения и исчисление характеристик гранулометрического состава", Науи-Техни изд (1959)

2) Miwa S.; "Imports of the mean particle diameter and its representation", Kagaku Kōgaku, Japan 28, 789 (1964).

3) Miwa S.; "Physical imports of the mean diameter for particulate materials", J. Res. Assoc. Powder Tech., Japan, 3, 562 (1966).

CHAPTER 3

SCATTER OF EXPERIMENTAL DATA DUE TO PARTICLE SIZE DISTRIBUTION

3.1 Introduction

One of the most important subjects in the study of particulate process is why the experimental data obtained for the process scatter more widely than in other processes. With regard to this matter, it has been said that the scatter may arise from agglomeration, adhesion, and some other causes. But there has never been any explanation that satisfactorily accounts for the cause.

It is sure that such complicated phenomena as agglomeration, adhesion, and others may be some of the causes of the scatter. More fundamentally, however, the scatter might be attributed to the size distribution of the particles.

Another cause of the scatter is that the mean particle diameter is often determined rather carelessly. The results scatter, if studied by use of an incorrect mean particle diameter. This is not scatter in the ordinary sense. No curve fitted to these data by various curve-fitting methods represents the properties of the process.

In this study the undesirable scatter due to wrong use of the mean particle diameter is eliminated

by use of the correct mean particle diameter. Another sort of scatter due to the size distribution is theoretically discussed. The scatter caused by the size distribution will be found negligibly small if the size distribution of sample particles is obtained for each experiment. Usually, however, only the size distribution of population particles is obtained. Consequently, the theoretical value of a process variable can be estimated by use of the population parameters (the mean and the variance, for example). It is expected, therefore, that the data will scatter around the estimate (the theoretical value). Practically, as will be discussed in this chapter, there is some bias. It will be negligible, however, if the sample size is fairly large in number.

One of the most interesting problems here is how many particles should be sampled to attain satisfactory results. Generally, the approach to the problem is very difficult. The following discussion is, therefore, based upon the assumptions that the particle size distribution is log normal, and that the interaction between particles is negligible. Then the experimental value $Y(m,s^2)$ of process variable is given by;

$$Y(m, s^2) = \bar{y}(m, s^2) \qquad (3.1)$$

where $\bar{y}$ is a linear estimate.

3.2 Distribution of the Sample Mean Particle Diameter

A simple but most important process may be written in the form;

$$y = KD_p^{\alpha} \tag{3.2}$$

where K, α : const. $\neq 0$
This chapter deals only with the process represented by the above equation. If the distribution of sample mean particle diameter is obtained, the distribution of experimental data is known from the relation;

$$Y = K\bar{D}_p^{\alpha} \tag{3.3}$$

For this process, the population mean particle diameter on β-basis (for the count basis, $\beta = 0$ and for the mass basis, $\beta = 3$) is given by the equation[1];

$$\begin{aligned}\bar{D}_p^{\bullet} &= y^{-1}(\bar{y}) \\ &= \left\{ \frac{1}{K} \frac{K\int D_p^{\beta} D_p^{\alpha} f(\ln D_p, \mu^{(0)}, \sigma^2) d\ln D_p}{\int D_p^{\beta} f(\ln D_p, \mu^{(0)}, \sigma^2) d\ln D_p} \right\}^{1/\alpha} \\ &= \exp.(\mu^{(0)} + c\sigma^2) = \exp.(\mu^{(\beta)} + \frac{\alpha}{2}\sigma^2)\end{aligned} \tag{3.4}$$

where $c = \beta + \alpha/2$, and $\mu^{(0)} + \beta\sigma^2 = \mu^{(\beta)}$ (3.5)
And $\mu^{(0)}$ is the logarithmic mean diameter for the number distribution of the population and σ^2 is its

variance;

$$\mu^{(0)} = \int_{-\infty}^{\infty} \ln D_p \cdot f(\ln D_p, \mu^{(0)}, \sigma^2) d\ln D_p = \ln D_{p50}$$

$$\sigma = \ln D_{p84} - \ln D_{p50}$$

On the other hand, the mean particle diameter of the random sample of size n is shown by;

$$\bar{D}_p = \exp(m + cs^2) \tag{3.6}$$

where $m = \frac{\Sigma \ln D_p}{n}$, and $s^2 = \frac{\Sigma (\ln D_p - m)^2}{n}$ (3.7)

It may be assumed that the sample size n is sufficiently large. Then, by statistical theory[6], $\chi^2 \equiv (n/\sigma^2)s^2$ follows a normal distribution with the mean $\nu \equiv n - 1$ and the variance 2ν. Therefore, the simultaneous distribution $\phi(m, s^2)$ of m and s^2 is given by;

$$\phi(m, s^2) = \frac{n}{\sigma^3\sqrt{2\pi}} \sqrt{\frac{n}{2\nu}} \exp\left\{ -\frac{n}{2\sigma^2} (m-\mu^{(0)})^2 - \frac{1}{4\nu} \left(\frac{n}{\sigma^2}s^2 - \nu\right)^2 \right\} \tag{3.8}$$

The subject of this section is to seek the distribution of the mean particle diameter. It is found from Eq. (3.6) that the equation $\bar{D}_p$ = const. gives a curve in (m, s^2)-space. Now for the sake of simplicity, the natural logarithm of the mean particle diameter, $\ln\bar{D}_p$, is used instead of $\bar{D}_p$. Then

the distribution of $\ln\bar{D}_p$ can be obtained if the simultaneous distribution of m and s^2 is rewritten for that of $\ln\bar{D}_p$ and s^2. This will be shown in the following paragraph.

First of all, from Eq. (3.6), the following equation is obtained.

$$d\ln\bar{D}_p = dm + cd(s^2) \tag{3.9}$$

Therefore,

$$d(s^2)dm = d(s^2)\wedge dm = d(s^2)\wedge d\ln\bar{D}_p - cd(s^2)\wedge d(s^2)$$

$$= d(s^2)\wedge d\ln\bar{D}_p \tag{3.10}$$

where symbol $d(s^2)\wedge dm$ denotes the outer product of $d(s^2)$ and dm. From Eq. (3.10), the simultaneous distribution may be rewritten as follows.

$$1 = \int_{-\infty}^{\infty}\int_{0}^{\infty} \phi(m, s^2)d(s^2)dm$$

$$= \int_{-\infty}^{\infty}\left\{\int_{0}^{\infty}\phi(\ln\bar{D}_p - cs^2, s^2)d(s^2)\right\} d\ln\bar{D}_p \tag{3.11}$$

(here symbol $\wedge$ is omitted as usual). If a certain function $f(\ln\bar{D}_p)$ is defined by;

$$f(\ln\bar{D}_p) \equiv \int_{0}^{\infty} \phi(\ln\bar{D}_p - cs^2, s^2)d(s^2) \tag{3.12}$$

it is evident that the function $f(\ln\bar{D}_p)$ satisfies the condition;

$$\int_{-\infty}^{\infty} f(\ln\bar{D}_p)\, d\ln\bar{D}_p = 1 \qquad (3.13)$$

Therefore, it represents the distribution of $\ln\bar{D}_p$.

The above simple and definite method is the first developed to obtain the distribution of $\ln\bar{D}_p$, as far as the author knows. And it is the basis of the whole theory in this chapter.

Before proceeding with the problem of determining the distribution, it may be convenient to introduce a dimensionless quantity κ by the equation;

$$\kappa = \bar{D}_p/\bar{D}_p^{\cdot} \qquad (3.14)$$

Then, Eq. (3.13) is rewritten as;

$$\int_{-\infty}^{\infty} f(\ln\kappa + \ln\bar{D}_p^{\cdot})\, d\ln\kappa = 1 \qquad (3.15)$$

That is, the distribution f is also the distribution of $\ln\kappa$, which is denoted by $f_{\ln\kappa}$, namely;

$$f_{\ln\kappa} \equiv f(\ln\kappa + \ln\bar{D}_p^{\cdot})$$

If $\kappa = 1$, the mean particle diameter of the sample coincides with that of the population. This fact

shows that the experimental value coincides with the theoretical value. This will be discussed in detail in the next section. It is better to use the distribution $f_{\ln\kappa}$ instead of $f(\ln\bar{D}_p)$ when comparing the experimental results with the theoretical.

Now the distribution $f_{\ln\kappa}$ can be obtained by carrying out the integration of Eq. (3.12) as follows;

$$f_{\ln\kappa} \simeq \frac{\sqrt{n}}{\sigma\sqrt{2\pi}\ \sqrt{2c^2\sigma^2+1}}\, e^{-\frac{\varphi^2}{2}} \cdot \Phi(z)$$

where, $\varphi \simeq \dfrac{\sqrt{n}(\ln\kappa + c\sigma^2/n)}{\sigma\sqrt{2c^2\sigma^2 + 1}}$

$$z \simeq \frac{\sqrt{n}}{\sqrt{2(2c^2\sigma^2 + 1)}} \cdot (2c\ln\kappa + 2c^2\sigma^2 + 1) \qquad (3.16)$$

and $\Phi(z) \equiv \dfrac{1}{\sqrt{2\pi}} \int_{-\infty}^{z} e^{-\frac{z^2}{2}} dz$, $\nu \simeq n$

(see also Appendix A)

This sampling distribution shows the bias, $\bar{D}_p\{\exp(-c\sigma^2/n) - 1\}$, which has been studied by other workers[2,3,4], only numerically.

Equation (3.16) will prove useful when the problem "how many particles should be sampled in an experiment" is discussed.

3.3 Number of Particles Required in an Experiment

The distribution of experimental value Y is obtained by use of the distribution $f_{\ln\kappa}$. If Y^* denotes $Y(\mu^{(0)}, \sigma^2)$, ratio λ of $Y(m, s^2)$ to Y^* is related to κ by the following equation.

$$\lambda \equiv Y/Y^* = (\bar{D}_p/\bar{D}_p^*)^{\alpha} = \kappa^{\alpha} \tag{3.17}$$

For a certain function $f_{\ln\lambda}$, therefore, the following equation is set up.

$$f_{\ln\lambda}\, d\ln\lambda = \alpha\, f_{\ln\lambda}\, d\ln\kappa$$

So, if the function $f_{\ln\lambda}$ is defined by;

$$f_{\ln\lambda} \equiv f_{\ln\kappa}/\alpha = f(\ln\lambda/\alpha + \ln\bar{D}_p^*)/\alpha \tag{3.18}$$

it satisfies the relation;

$$\int_{-\infty}^{\infty} f_{\ln\lambda}\, d\ln\lambda = 1 \tag{3.19}$$

Therefore, $f_{\ln\lambda}$ represents the distribution of $\ln\lambda$.

By use of the above distribution, the probability $P(|e| \leq \delta)$ that experimental data may be in the range of relative error $-\delta$ to $+\delta$, is

obtained.
The relative error is defined as

$$e \equiv \frac{Y - Y^{\cdot}}{Y^{\cdot}} = \lambda - 1 \tag{3.20}$$

Therefore, the probability $P(|e| \leq \delta)$ can be evaluated as follows;

$$P(|e| \leq \delta) = \int_{\ln(1-\delta)}^{\ln(1+\delta)} f_{\ln\lambda}\, d\ln\lambda = \left| \int_{\frac{\ln(1-\delta)}{\alpha}}^{\frac{\ln(1+\delta)}{\alpha}} f_{\ln\kappa}\, d\ln\kappa \right| \tag{3.21}$$

When studying the problem "how many particles should be sampled to get a satisfactory result", the following assumption is acceptable.

$$0 \leq \frac{\delta}{|\alpha|} << \sigma \tag{3.22}$$

It may be assumed that n is larger than 50. Then from Eq. (3.16) it can be shown for the whole range of $\ln\kappa$ that (cf. Appendix B);

$$z \geq \{\sqrt{2c^2\sigma^2 + 1} - \frac{2\delta\sqrt{c^2}}{|\alpha|\sqrt{2c^2\sigma^2 + 1}}\} \cdot \sqrt{\frac{n}{2}} \tag{3.23}$$

However from Eq. (3.22), the following relation can be obtained;

$$\frac{\delta}{|\alpha|} << \sigma < \frac{2c^2\sigma^2 + 1}{2\sqrt{c^2}}$$

And therefore;

$$\frac{2\delta\sqrt{c^2}}{|\alpha|\sqrt{2c^2\sigma^2 + 1}} << \sqrt{2c^2\sigma^2 + 1}$$

Then Eq. (3.23) reads;

$$z \gtrsim \sqrt{2c^2\sigma^2 + 1} \cdot \sqrt{\frac{n}{2}} \geq \sqrt{\frac{n}{2}} > 5$$

Therefore, $\Phi(z) \simeq 1$.

This simplifies Eq. (3.21) as follows.

$$P \simeq \frac{\sqrt{n}}{\sigma\sqrt{2c^2\sigma^2 + 1}} \frac{1}{\sqrt{2\pi}} \left| \int_{-\delta/\alpha}^{\delta/\alpha} e^{-\frac{\varphi^2}{2}} \, d\ln\kappa \right|$$

$$= \frac{1}{\sqrt{2\pi}} \{ \int_{-\infty}^{\infty} e^{-\frac{\varphi^2}{2}} \, d\varphi - \int_{-\infty}^{-|u|} e^{-\frac{\varphi^2}{2}} \, d\varphi - \int_{|u|}^{\infty} e^{-\frac{\varphi^2}{2}} \, d\varphi \}$$

$$= 1 - 2\Phi(-|u|) \qquad (3.24)$$

where,

$$u \equiv \frac{\sqrt{n}\ \delta}{\alpha\sigma\ \sqrt{2c^2\sigma^2 + 1}} \tag{3.25}$$

Another expression of Eq.(3.24) is;

$$\Phi(-|u|) = \frac{1 - P}{2} \tag{3.26}$$

If P is given, u can be obtained from the above equation, and the number of particles n is determined from Eq. (3.25). "n" thus given is defined as "the number of particles required" and denoted by n_*. Then from Eq.(3.25);

$$\log n_* = -2 \log\delta + \log\omega \tag{3.27}$$

where,

$$\omega \equiv u^2\ \alpha^2\ \sigma^2\ (2c^2\ \sigma^2 + 1) \tag{3.28}$$

(see also Fig. 3.4)
Parameter ω is given numerically, if the probability P is assigned and the variance $\sigma^2$of the population-particles, the exponent α of the process variable,

and the basis number β of the experiment are known. Practical use of this equation will be shown in § 3.4.

3.4 Example

Following example will be of help in understanding of the theory developed in the previous section.

Example;

particle size	$D_p(50\%)=5[\mu]$, $D_p(84.13\%)=8[\mu]$
parameters	$\mu^{(0)}=1.61$ ($\mu_g=\exp\mu^{(0)}=5[\mu]$)
	$\sigma^2=0.2209$ ($\sigma=0.47$, $\sigma_g=\exp\sigma=1.6$)
process variable	$y=KD_p^2$ ($\alpha=2$) (3.29)

Eq. (3.29) represents a process that follows Stokes' law. From Eq.(3.4) the population-mean particle diameter $\bar{D}_p^{\cdot}$ is given by;

$$\bar{D}_p^{\cdot} = \exp(1.61 + 0.2209 \cdot c) \qquad (3.30)$$

Basis-numbers 'β' for the count and the mass are 0 and 3, respectively. The exponent α is 2, and Eq.(3.5) gives;

$$c^{(0)} = 1, \text{ and } c^{(3)} = 4$$

denoting $c^{(0)}$ on the count basis and $c^{(3)}$, on the mass basis. From Eq.(3.30), therefore, the population-mean particle diameters are $\bar{D}_p^{\cdot(0)} = 6.24$ [μ] and $\bar{D}_p^{\cdot(3)} = 12.1$ [μ]. On the other hand, from Eq.(3.6) the sample-mean particle diameters are given by;

$$\bar{D}_p^{(0)} = \exp(m + s^2) \text{ and } \bar{D}_p^{(3)} = \exp(m + 4s^2)$$

Therefore,

$$\kappa^{(0)} = \frac{\exp(m + s^2)}{6.24} \quad , \quad \kappa^{(3)} = \frac{\exp(m + 4s^2)}{12.1}$$

The distribution $f_{\ln\kappa}$ for the count and the mass bases can be obtained as shown in Figs. 3.1 and 3.2, respectively. $P(|e| \leq 0.05)$, which is the probability that the experimental data may be in the relative error ±5%, increases as the sample size n becomes larger. This is shown in Fig. 3.3.

The number of particles required in the experiment can be determined for the given requirement that p% of data should be in the region of relative error ± q%, where p and q are given numerically. In this example, the parameters ω on the count and the mass bases respectively are given as functions of u as follows;

$$\omega^{(0)} = 1.27u^2 \quad \text{and} \quad \omega^{(3)} = 7.13u^2 \qquad (3.31)$$

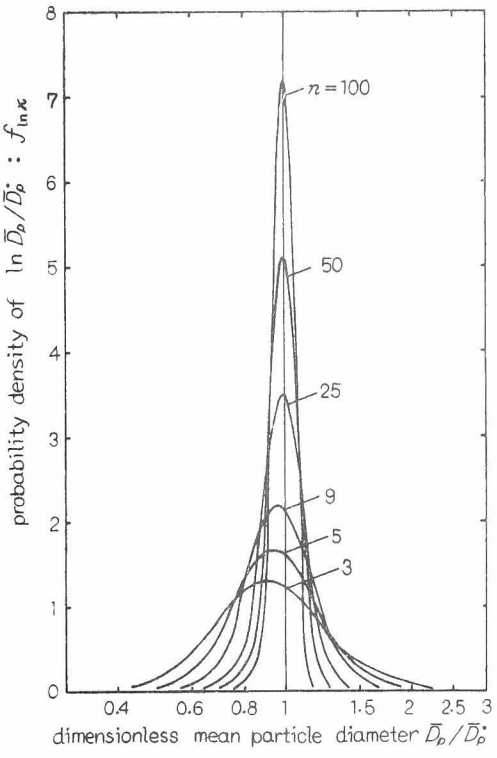

Fig.3.1 Distribution of $\ln \bar{D}_p/\bar{D}_p^{\cdot}$ for the count basis

$\alpha=2$, $\beta=0$, $\sigma_g=1.6$

Eq.(A-10) is used in calculation for small n

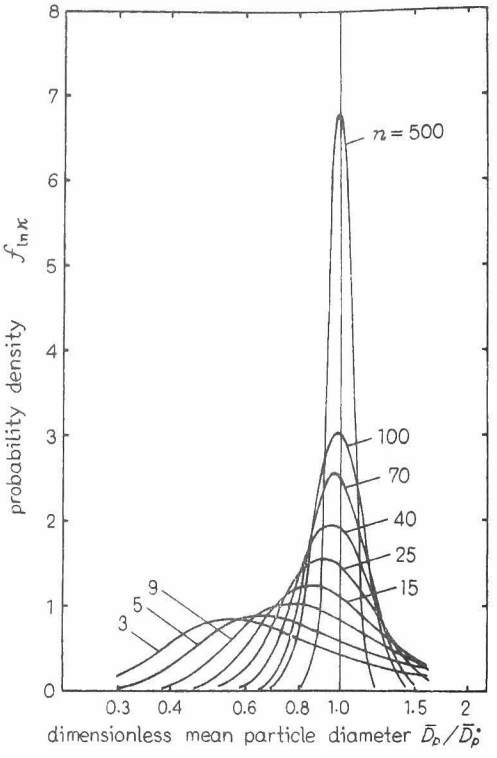

Fig.3.2 Distribution of $\ln \bar{D}_p/\bar{D}_p^{\cdot}$ for the mass basis

$\alpha=2$, $\beta=3$, $\sigma_g=1.6$

Eq.(A-10) is used in calculation for small n

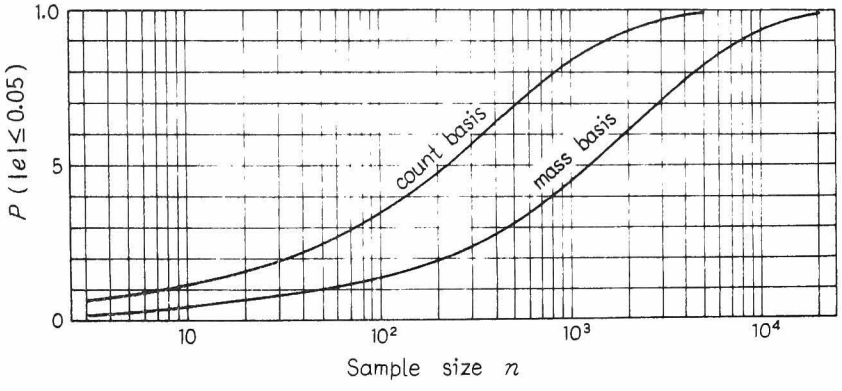

Fig.3.3 Probability P(|e|<0.05) vs. sample size n

Eq.(A-10) is used in calculation for small n

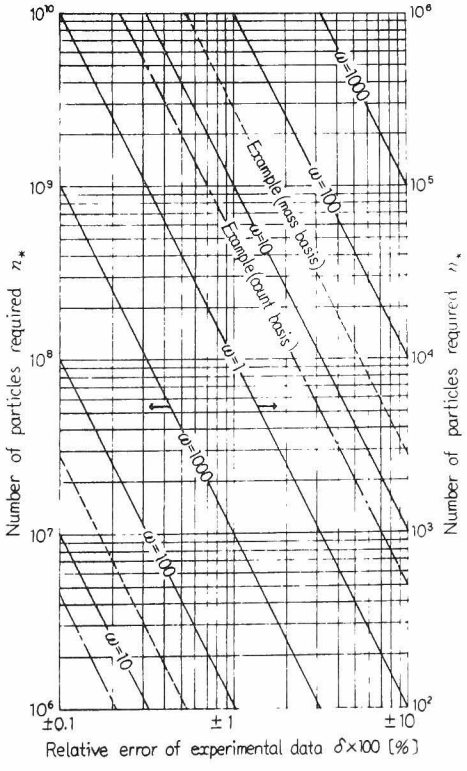

Fig.3.4 Number of particles required in an experiment

$\omega = u^2 \alpha^2 \sigma^2 (2c^2 \sigma^2 + 1)$

When 95% of the data is required to be in the region of the relative error ±q% (where q is arbitrary), for example, u = 1.96 from Eq.(3.26). In this case Eq.(3.31) gives $\omega^{(0)} = 4.87$ and $\omega^{(3)} = 27.4$, as shown in Fig.3.4. From the figure or from Eq.(3.27), "the number of particles required" is determined as follows;

$$n_*^{(0)}(95\%, \pm 10\%) = 487, \qquad n_*^{(3)}(95\%, \pm 10\%) = 2{,}740,$$
$$n_*^{(0)}(95\%, \pm 5\%) = 1{,}900, \qquad n_*^{(3)}(95\%, \pm 5\%) = 11{,}000,$$
$$\cdots\cdots\cdots\cdots, \qquad \cdots\cdots\cdots\cdots$$

where $n_*^{(\beta)}(p\%, \pm q\%)$ denotes the number of particles required in β-basis experiment when the requirement is that p% of data should be in the region of relative error ±q%. For any probability P, n_* will be obtained in the same manner. Just for reference, $n_*(95\%, \pm 5\%)$ is rewritten in terms of weight as specific gravity $\rho_p = 2$ g/cm^3 as shown in Table 3.1.

Table 3.1. Weight of particles required in the experiment (cf.Example in §3.4)

$P(|e| \leq 0.05) = 0.95$, $\sigma_g = 1.6$

$\sqrt[3]{\Sigma f^{(0)} D_p^3}$ *)	Count basis	Mass basis
1 micron	2×10^{-6} mg	1.2×10^{-5} mg
10 micron	2×10^{-3} mg	1.2×10^{-2} mg
100 micron	2 mg	12 mg
1 mm	2 g	12 g
1 cm	2 kg	12 kg

*) $\sqrt[3]{\Sigma f^{(0)} D_p^3}$; 50 wt% diameter

It is found from Fig. 3.4 that if 50,000 particles are used, 95% of the data will be in the region of relative error ±1% on the count basis, and ±2.5% on the mass basis.

3.5 Discussion

The first discussion concerns the number of particles that should be sampled to attain satisfactory results. Eq.(3.27) gives a part of the solution of this problem. The number of particles required is graphically shown in Fig.3.4, in which ω is the only parameter. The figure shows that the number of particles required, n_*, increases with the value of ω and at the same time the scatter of the data also increases. These facts suggest that the parameter ω shows the amount of scatter. It is given by Eq.(3.28). From the equation it is known that the scatter of data increases as the exponent 'α', variance 'σ^2' or basis number 'β' increases. In the previous example $\omega^{(3)}$ was larger than $\omega^{(0)}$. Comparison between Figs. 3.1 and 3.2 shows that the scatter of the data in Fig.3.2 is wider than in Fig.3.1.

The parameter ω is in direct proportion to u^2 as shown in Eq.(3.28) or (3.31). And u increases with P. Consequently, the parameter ω increases if more of the data are included in the given range of error. This fact suggests that the scatter increases relatively to the given range of error, and that u shows the amount of scatter relative to the range.

From the above discussion it is found that the scatter of data is related to the standard geometric deviation σ_g, experimental basis -count or mass -(represented by parameter β), and the exponent α which represents the process itself.

The results described above are quantitatively applicable only when the log-normal distribution is valid, but qualitatively they may apply when other distributions are used.

Our next discussion is about whether the various assumptions given in deriving Eq.(3.27) are appropriate or not. The extent of application of the equation will also be discussed.

One of the assumptions is that sample size n is larger than 50. From the fact that particles with sample size of less than 1,000 are very rarely used in the usual experiments, this assumption is acceptable. When the sample size is small and the standard geometric deviation is larger than 2 for some reason, however, special care should be taken. As shown in Fig.3.2, there is some bias in the sampling distribution of $\ln\kappa$. Fortunately, when σ_g is smaller than 1.6 ($\sigma < 0.6$), or the dispersion exponent for Rosin-Rammlar size distribution is larger than 2~3, in a loose sense of the word, no special care is required about such bias. Outside of the above-mentioned range, the number of particles required is larger than n_* which is determined by the method developed in this chapter.

The next assumption given in deriving Eq.(3.27)

is that $\delta/|\alpha| << \sigma$. This assumption is easy to use, for it is independent of parameter β. However, it is not always necessary, because sample size n is much larger than 50. In short, the condition that parameter z in Eq.(3.16) is larger than 5 is sufficient, because the relation, $\Phi(z) \simeq 1$ is valid. If this remark is taken into consideration, there will be no ambiguity about the assumption.

Further discussion is concerned with the assumption that the population follows the log-normal size distribution. The log-normal size distribution has various advantages which were revealed by Hatch and Choate.[5] In most cases, size distribution is skewed, and it can be approximated by the log-normal distribution, which is of practical use.

Only the process that is represented by Eq.(3.2) has been studied in this chapter, but this equation can be used to represent other processes locally. The application of Eq.(3.27) to other processes will be therefore very interesting. The study of this possibility will be the subject of future work.

From the example in §3.4, it may be said that the error due only to the size distribution is not so large as we usually experience. However, data with a little error are sometimes obtained when particles that have high fluidity are concerned. In such a case the theory developed in this chapter applies well and Eq.(3.27) is useful in examining the data. In the process where fine particles are dealt with, adhesion and agglomeration may be the principal

causes. They may bring about some change in the "effective" mean particle diameter in the process. Also, the particles may interact with each other. Further investigation into these problems is necessary.

3.6 Conclusion

In the particulate process that can be expressed by the equation $y = KD_p^{\alpha}$, the scatter of data caused by the size distribution increases as the standard geometric deviation 'σ_g' (= expσ) of population-particles, parameter "β" representing the experimental basis, and exponent 'α' representing the process itself, increase.

The number of particles required to get a certain per cent of the data in a certain range of error changes depending on the amount of scatter. And the number of particles required increases as the scatter increases. At the same time the number increases relatively to the magnitude of error required in the experiment. This can be represented by use of parameter u. When u increases, the number increases, too. If the log-normal size distribution is valid, all of these facts can be expressed by Eq.(3.27) with only one parameter $\omega = u^2\alpha^2\sigma^2(2c^2\sigma^2 + 1)$. It is possible to use this equation in calculating the number of particles required in the experiment, and also in estimating the error when the number of particles is given.

Appendix

[A] Sampling distribution of mean particle diameter

In the general case, simultaneous distribution is given by[6)]

$$\phi(m,s^2) = \frac{\sqrt{n}}{\sigma\sqrt{2\pi}} e^{-\frac{n}{2\sigma^2}(\mu^{(0)}-m)^2} \cdot \frac{\left(\frac{n}{2}\right)^{\frac{n-1}{2}}}{\sigma^2\Gamma\left(\frac{n-1}{2}\right)} \cdot \left(\frac{s^2}{\sigma^2}\right)^{\frac{n-3}{2}} \cdot e^{-\frac{n}{2\sigma^2}s^2} \tag{A-1}$$

If n is odd, and can be written n = 2k + 1, k = 1,2,....., the above equation reads;

$$\phi(m,s^2) = \frac{\sqrt{n}\ \left(\frac{n}{2}\right)^k}{\sigma^3\sqrt{2\pi}\Gamma(k)} \left(\frac{s^2}{\sigma^2}\right)^{k-1} \cdot e^{-\frac{n}{2\sigma^2}\{(\mu^{(0)}-m)^2+s^2\}} \tag{A-2}$$

From Eqs. (3.4) and (3.6), we have;

$$\ln\bar{D}_p^{\cdot} = \mu^{(0)} + c\,\sigma^2 \tag{A-3}$$

$$\ln\bar{D}_p = m + cs^2 \tag{A-4}$$

$$\therefore \quad \ln\bar{D}_p^{\cdot}/\bar{D}_p = \mu^{(0)} - m + c(\sigma^2 - s^2) \tag{A-5}$$

Therefore,

$$-\frac{n}{2\sigma^2}\{(\mu^{(0)}-m)^2+s^2\}$$

$$=-\frac{n}{2\sigma^2}(\ln\kappa+c\sigma^2)^2-\frac{n}{2\sigma^2}(1-2c\ln\kappa-2c^2\sigma^2)s^2-\frac{nc^2}{2\sigma^2}s^4 \qquad (A\text{-}6)$$

If we put;

$$s^2=\frac{\sigma}{\sqrt{n}|c|}t \qquad (A\text{-}7)$$

substituting Eqs.(A-6) and (A-7) into Eq.(A-2), the following equation is obtained, by use of Eq.(3.12), as the sampling distribution of $\ln\kappa$.

$$f_{\ln\kappa}=\frac{n^{\frac{k+1}{2}}\,e^{-\frac{n}{2\sigma^2}(\ln\kappa+c\sigma^2)^2}}{\sigma^{k+1}\sqrt{2\pi}\cdot 2^k|c|^k\Gamma(k)}\int_0^\infty t^{k-1}\cdot e^{-xt-\frac{1}{2}t^2}dt \qquad (A\text{-}8)$$

where,

$$x=\frac{\sqrt{n}}{2\sigma|c|}(1-2c\ln\kappa-2c^2\sigma^2) \qquad (A\text{-}9)$$

Eq.(A-8) can be rewritten by use of Weber's function $D_{-k}(x)$ as;

$$f_{\ln\kappa} = \frac{n^{\frac{k+1}{2}} \; e^{-\frac{n}{2\sigma^2}(\ln\kappa+c\sigma^2)^2}}{\sigma^{k+1}\sqrt{2\pi}\cdot 2^k \cdot |c|^k} \; e^{\frac{x^2}{4}} D_{-k}(x) \qquad \text{(A-10)}$$

[B] Derivation of Eq.(3.23)

From Eq.(3.16), we have

$$z \equiv \sqrt{\frac{n}{2(2c^2\sigma^2+1)}} \; (2c \ln\kappa + 2c^2\sigma^2 + 1) \qquad \text{(B-1)}$$

The range of $\ln\kappa$ is

$$\ln(1-\delta) \leq \alpha \ln\kappa \leq \ln(1+\delta) \qquad \text{(B-2)}$$

This can be approximated by

$$-\delta/|\alpha| \lesssim \ln\kappa \lesssim \delta/|\alpha| \qquad \text{(B-3)}$$

Moreover, it can be assumed that c is positive, because if c is negative then the following derivation can be made over by reversing the order.

When $\ln\kappa \geq 0$, the value of z satisfies the following relation, from Eq.(B-1);

$$z \geq \sqrt{2c^2\sigma^2 + 1}\sqrt{\frac{n}{2}} > \sqrt{\frac{n}{2}} > 5 \quad (\because n > 50) \tag{B-4}$$

On the other hand, when $-\delta/|\alpha| \leq \ln\kappa < 0$, we have

$$z \geq \{\sqrt{2c^2\sigma^2 + 1} - \frac{2\delta\sqrt{c^2}}{|\alpha|\sqrt{2c^2\sigma^2 + 1}}\}\sqrt{\frac{n}{2}} \tag{B-5}$$

This is Eq.(3.23).

Nomenclature

c	$\beta + \alpha/2$, Eq.(3.5)
D_p	particle diameter
$\bar{D}_p$	sample mean particle diameter
$\bar{D}_p^{\cdot}$	population mean particle diameter
e	relative error defined by Eq.(3.20)
$f(\ln\bar{D}_p)$	sampling distribution of $\ln\bar{D}_p$

$f_{\ln\kappa}$	sampling distribution of $\ln\kappa$
K	constant, Eq.(3.2)
m	logarithmic mean diameter for a random sample of size n (sample mean), Eq.(3.7)
n	sample size
n_*	number of particles required in an experiment
$P(\|e\| \leq \delta)$	probability that the experimental data may be in the range of relative error $-\delta$ to $+\delta$
p	preassigned probability, [%]
q	preassigned relative error, [%]
s	sample standard deviation
u	$\sqrt{n}\delta/\{\alpha\sigma\sqrt{2c^2\sigma^2 + 1}\}$
$Y(m, s^2)$	experimental value
y	process variable
$\bar{y}(m, s^2)$	linear estimate
z	$\sqrt{\frac{n}{2(2c^2\sigma^2 + 1)}} \cdot (2c\ln\kappa + 2c^2\sigma^2 + 1)$

α	constant, in Eq.(3.2)
β	basis number ($\beta = 0$ for the count basis, and $\beta = 3$ for the mass basis)
δ	relative error
κ	dimensionless mean particle diameter of sample: $= \bar{D}_p / \bar{D}_p^{\cdot}$
λ	$= Y/Y^{\cdot} = \kappa^{\alpha}$, Eq.(3.17)
$\mu^{(0)}$	logarithmic mean diameter for the number distribution of population (population mean)
μ_g	geometric mean particle diameter
ν	$\equiv n - 1$
ρ_p	specific gravity of particle
σ	population standard deviation
σ_g	standard geometric deviation
$\Phi(z)$	error function
φ	$= \dfrac{\sqrt{n}(\ln\kappa + c\sigma^2/n)}{\sigma\sqrt{2c^2\sigma^2 + 1}}$
$\phi(m, s^2)$	simultaneous distribution of m and s^2
χ^2	$(n/\nu^2)s^2$
ω	$u^2\alpha^2\sigma^2(2c^2\sigma^2 + 1)$

References

1) Chakravarti, I. M., R. G. Laha, and T. Roy; "Handbook of Methods of Applied Statistics", vol. I, p. 153, John Wiley & Sons, Inc., New York (1967)

2) Mercer, T. T., "Sampling Distributions of Surface and Mass Statistics of a Log-normal Distribution when Estimated by the Method of Weighted Frequencies", Powder Technol., 3, 65 (1969/70)

3) Mori, Y. and A. Suganuma, "The Statistical Bias of the Weight Mean Particle Diameter", Kagaku Kōgaku, 32, 1099 (1968)

4) Mori, Y. and A. Suganuma, "Significance of Statistical Bias of Sample Mean Particle Diameter", Kagaku Kōgaku, 34, 445 (1970)

5) Hatch, T. and S. P. Choate, "Statistical Description of the Size Properties of Non-uniform Particulate Substances", J. Franklin Inst., 207 369 (1929)

6) Taguchi, G., "Jikken-keikakuhō (Design of Experiments)", 2nd Ed., P. 851, Maruzen, Japan (1963)

PART II

FINAL CONTROL MEANS: POWDER FEEDERS

CHAPTER 4

EXPERIMENTAL STUDY ON THE CHARACTERISTICS OF VARIOUS FEEDERS

4.1 Introduction

The applicability of several powder feeders to the control system of a particulate process is examined in this chapter. Step responses of these feeders are obtained experimentally, and discussed briefly. Powder feeders used in the experiments are a screw feeder, Vibra screw feeder, Flo-tron, and a belt feeder. The mechanisms of these feeders will be described in each section.

4.2 Apparatus and Experimental Methods

Fig.4.1 shows the apparatus for studying the dynamic characteristics of the feeders. Mass flow rate responses to step changes in the operating variables were detected by a powder flow meter[1,2,3] (Impact Line Flow Meter, which, as mentioned already,

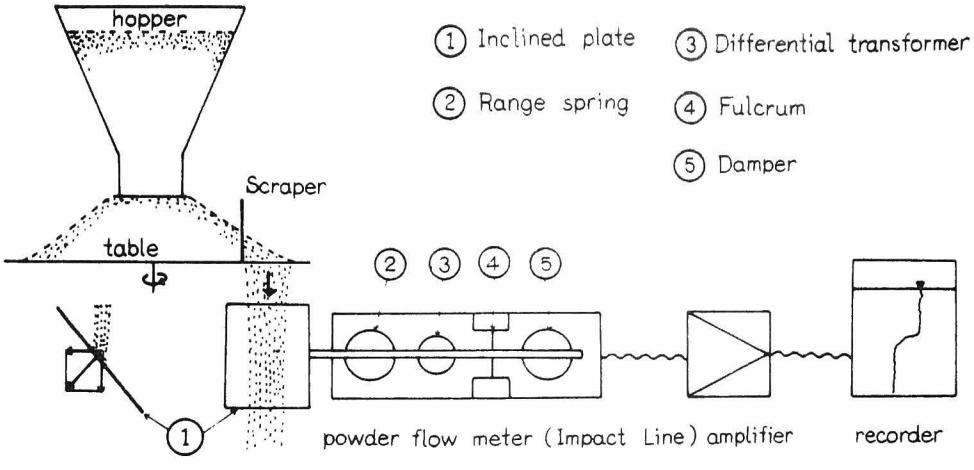

Fig.4.1 Schematic diagram of experimental arrangement

detects the horizontal component of the impact force.). The detected signals were amplified and recorded. The time constant of this system is about 0.4 second.

The properties of the powder materials used in this study are shown in Table 4.1. The angles of repose shown in the table were measured by the injection method using a 150 mmϕ disc.

Table 4.1. Properties of the powder materials

materials	mass median diameter [microns]	angle of repose [degree]	bulk density [g/cm^3]
quartz sand (No. 8)	68	38.1	1.23
calcium carbonate(coarse)	350	40.9	1.58
calcium carbonate (fine)	7.5	38.0	0.541
polyethylene pellet	3500	35.0	0.545

4.3 Screw Feeder

The screw feeder used is shown in Fig. 4.2. Powder is extruded by a rotating screw. The operating variable of interest in this feeder is the number of revolutions per unit time of the screw.

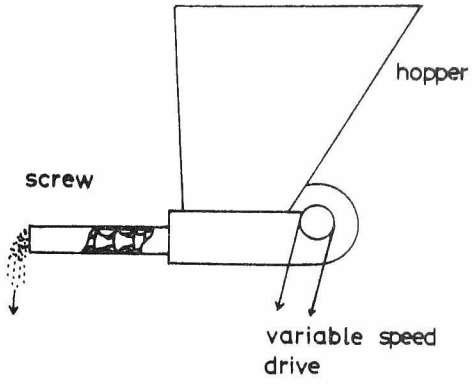

Fig.4.2 Screw feeder

(screw dimension;
pipe length = 280mm,
pipe dia. = 47mm,
pitch = 34mm)

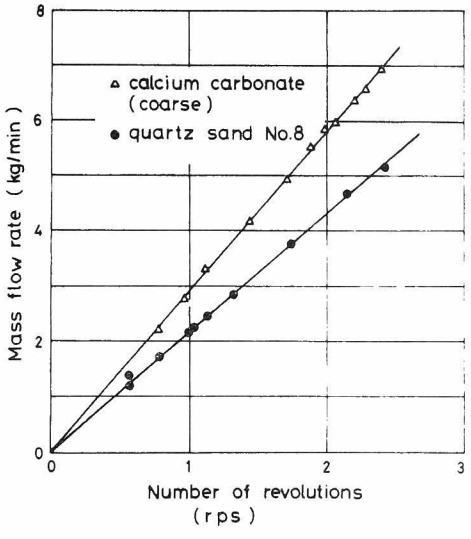

Fig.4.3 Static characteristics of a screw feeder

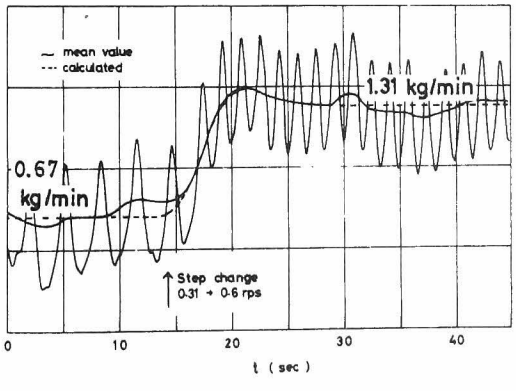

Fig.4.4 Step response of a screw feeder
(quartz sand No.8)

Fig. 4.3 shows the static characteristics of the feeder. This figure indicates the fact that the discharged mass flow rate is in proportion to the rate of revolution of the screw in the range of this experiment. The response of the mass flow rate following a step change in the rate of revolution of the screw is shown in Fig. 4.4. The dotted line in this figure shows the results calculated by the following equation.

$$0.664\frac{d^3W(t)}{dt^3} + 3.95\frac{d^2W(t)}{dt^2} + 2.44\frac{dW(t)}{dt} + W(t)$$

$$= 2.17N \qquad (4.1)$$

where W(t) is the mass flow rate, and N is the number of revolution per second of the screw. This equation represents a 3rd order time delay. As found in Fig. 4.4, the detected mass flow rate fluctuates periodically with fairly large amplitude. The period of this oscillation corresponds to the time for one revolution of the screw.

4.4 Vibra Screw Feeder

The Vibra Screw Feeder used is shown in Fig. 4.5. Vibration is introduced at the hopper and the screw. The screw of this feeder is helical. The operating

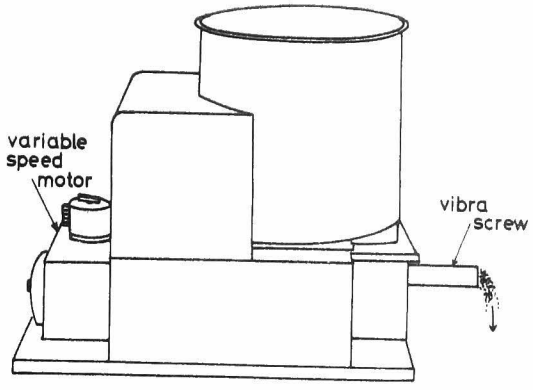

Fig.4.5 Vibra screw feeder

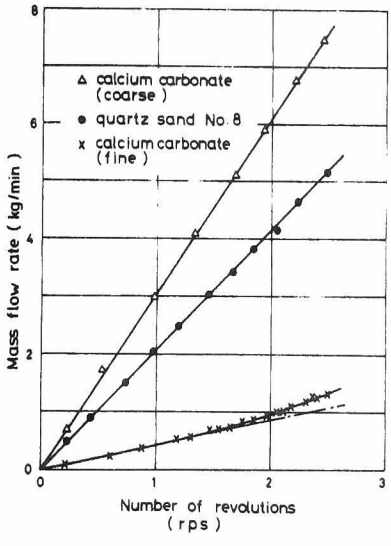

Fig.4.6 Static characteristics of a vibra screw feeder

(screw dia. = 2")

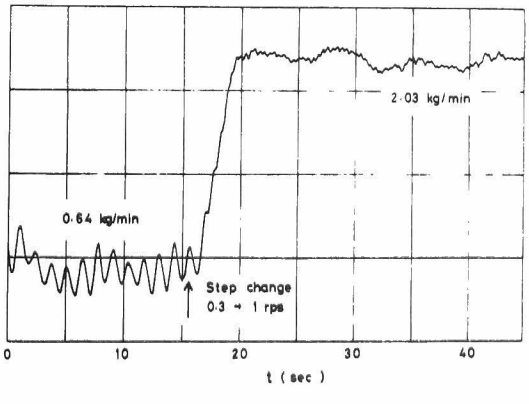

Fig.4.7 Step response of a Vibra screw feeder (quartz sand No.8)

variable studied is the number of revolution per unit time of the screw. Fig. 4.6 shows the static characteristics of this feeder. The discharged mass flow rates for coasely powdered calcium carbonate and for quartz sand No. 8 are in proportion to the number of revolution per second of the screw. But this linear relationship between the mass flow rate and the rate of revolution does not hold for fine calcium carbonate powder. The mass median diameters of the calcium carbonate used are 350 and 7.5 microns respectively. The response of the mass flow rate following a step change in the rate of revolution of the screw is shown in Fig. 4.7. Oscillations in the mass flow rate are the resultant of two components. One of the two arises from the revolution of the screw itself, and the other, from the vertical vibration applied to the rotating screw. When the rate of revolution is small, the amplitude of this oscillation is fairly large, but it becomes smaller as the rate of revolution increases. This may be attributable to the fact that the screw is helical and its center axis is empty. Under condition of large mass flow rate, powder can flow through the central space. Therefore, the effect of the rate of revolution of the screw on the oscillations in mass flow rate may be small, and this is reflected in the fact that the amplitude of the mass flow rate oscillation is also small.

4.5 Flo-tron

The Flo-tron used in this experiment is shown in Fig. 4.8. Powder is fluidized on the vibration plate, and is discharged from the lower part. The operating variable used for this feeder is the applied voltage. Fig.4.9 shows the static characteristics. The relation between the discharged powder flow rate and the applied voltage is non-linear. The response of the mass flow rate for a step change in the applied voltage is shown in Fig. 4.10. This response has a time delay of first order when the applied voltage is small. When applied voltage is high, however, it becomes oscillatory. The discharged mass flow rate is very sensible to the height of the powder in the hopper. Therefore, it is necessary to control the powder pressure in the hopper if constant feed properties are to be obtained. Segregation of particles was also observed.

4.6 Belt Feeder

Fig.4.11 shows the belt feeder. The operating variables of interest in this feeder are belt speed and gate opening. Fig. 4.12 shows the response of mass flow rate to a step change in gate opening. The response is proportional to the magnitude of the change following step increases in the gate opening,

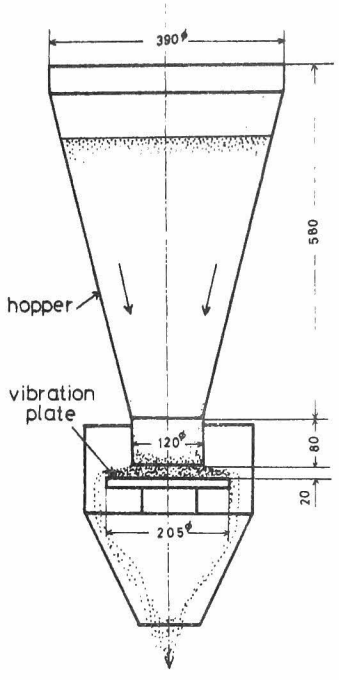

Fig.4.8 Flo-tron

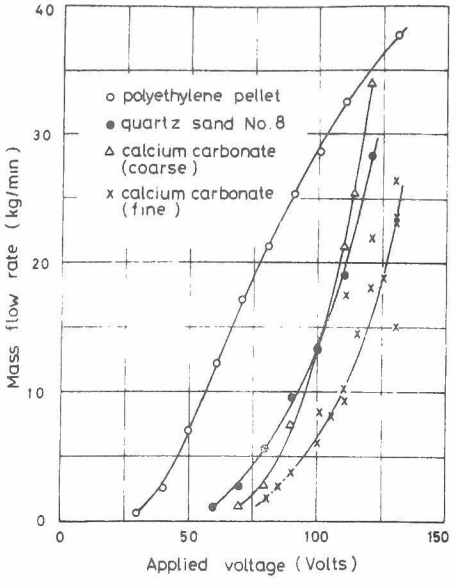

Fig.4.9 Static characteristics of Flo-tron

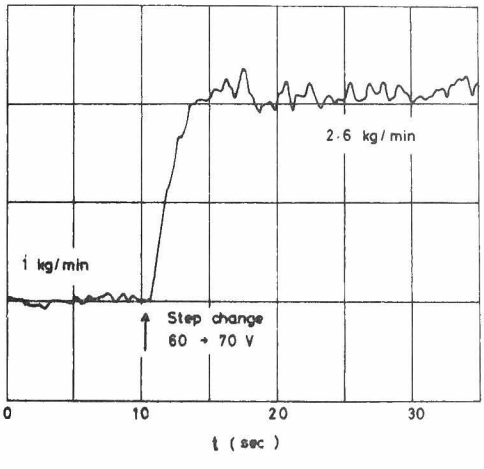

Fig.4.10 Step response of Flo-tron (quartz sand No.8)

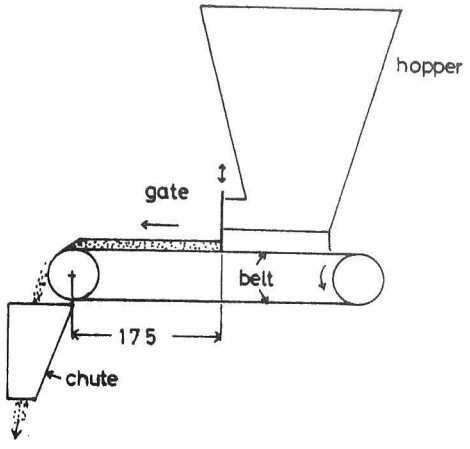

Fig.4.11 Belt feeder (belt speed;16.3 mm/sec)

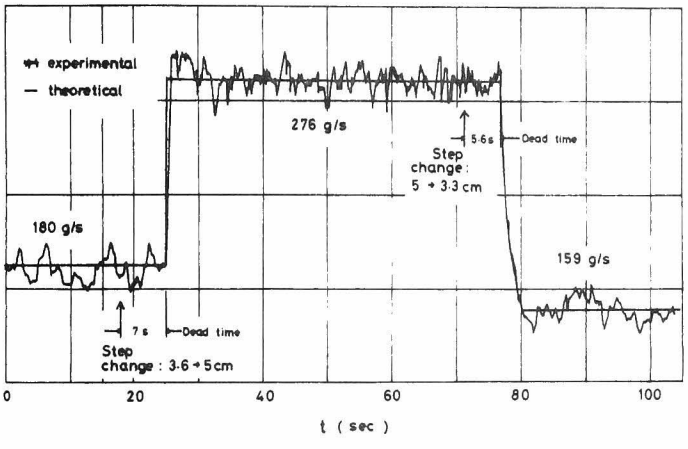

Fig.4.12 Step response of a belt feeder (quartz sand No.8)

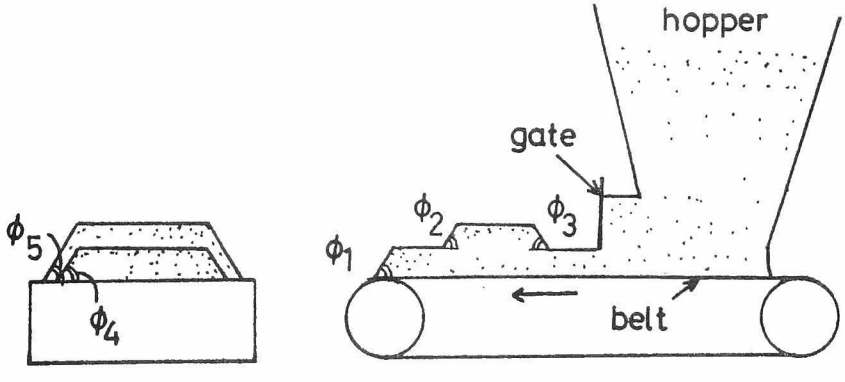

Fig.4.13 Shape of the powder bed on the belt

but this is not so for step decreases of the gate opening. This phenomena will be analysed in the next section. The static characteristic will also be predicted theoretically.

4.6-1 Analysis of the step response of the belt feeder

Fig. 4.13 shows the shape of the powder bed on the belt. ϕ_1 is the angle at which powder is flowing down from the belt. $\phi_2 \sim \phi_5$ are angles of the powder bed after crumbling. In general, the belt speed is very low, (1.63 cm/sec in this experiment), so the effect of speed on these angles is negligible. Then, it is possible to put

$$\phi_1 \simeq \phi_2 \simeq \cdots\cdots\cdots \simeq \phi_5 \equiv \phi \qquad (4.2)$$

Usually this angle ϕ is smaller than the angle of repose. Now, assuming that the shape of the powder bed is as shown in Fig.4.13, analysis for the step response may be carried out as follows:

(i) When the gate is lowered

Fig.4.15 shows the shape of the powder bed when the gate is lowered. The discharged mass flow rate, W(t), is the mass per unit time which goes through an imaginary plane inclined with angle ϕ. This may

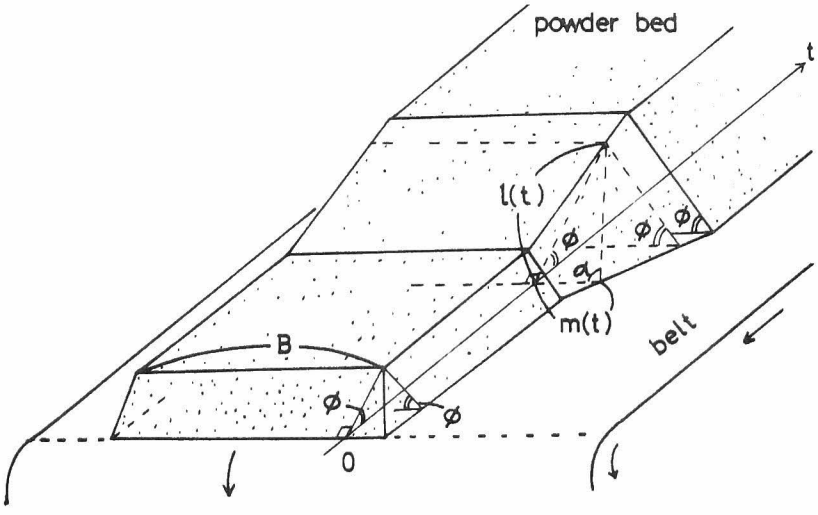

Fig.4.14 Time axis embedded in the belt feeder system

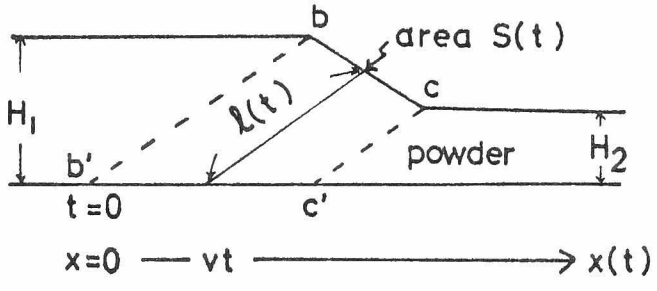

Fig.4.15 Shape of the powder bed (gate opening ; large → small)

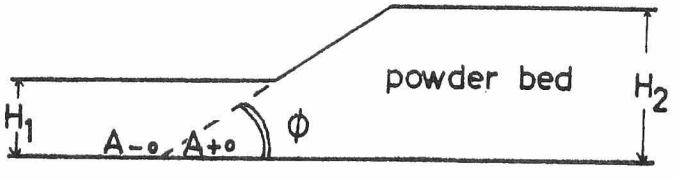

Fig.4.16 Shape of the powder bed (gate opening ; small → large)

be read that the plane goes through the powder bed in the opposite direction with the belt speed v, as shown in Fig.4.15. Until the moving plane reaches the position bb', the mass flow rate W is constant. If the initial point of the time axis is taken at b', the area S(t) of the moving plane at time t is obtained from Figs.4.14 and 15 as follows:

$$S(t) = \{ B + m(t) \} \ell(t) \tag{4.3}$$

where,

$$\ell(t) = \frac{H_1}{\sin \phi} - \frac{v}{2 \cos \phi} t \tag{4.4}$$

and

$$m(t) = \ell(t)/\tan \alpha \tag{4.5}$$

Therefore, Eq.(4.3) reads after some manipulation,

$$S(t) = \frac{v^2}{4 \tan \alpha \cos^2 \phi} t^2 - \left\{ \frac{vB}{2 \cos \phi} + \frac{H_1 v}{\tan\alpha \cos\phi \sin\phi} \right\} t + \left\{ \frac{H_1 B}{\sin \phi} + \frac{H_1^2}{\tan \alpha \sin^2 \phi} \right\} \tag{4.6}$$

And the step response W(t) is obtained as follows:

$$W(t) = S(t)\rho_B v \sin\phi$$

$$= \frac{v^3 \tan\phi}{4\tan\alpha\cos\phi}\rho_B \cdot t^2 - \left\{ \frac{B}{2}\tan\phi + \frac{H_1}{\tan\alpha\cos\phi} \right\} v^2 \rho_B t$$

$$+ \left\{ B + \frac{H_1}{\tan\alpha\sin\phi} \right\} H_1 v \rho_B \qquad (4.7)$$

(ii) When the gate is raised

Fig.4.16 shows the shape of the powder bed when the gate is raised. The mass flow rate W is constant before reaching the position A_{-0}, and is also constant after passing over the position A_{+0}. Therefore, the step response is proportional to the gate opening.

In this treatment, the width of the powder bed has been taken as constant as shown in Fig. 4.14. This approximation is satisfactory under the experimental condition but in higher speed operation it may be necessary to modify the width B and height H.

4.6-2 Prediction of the step response detected by weighing

In this section, the step response detected by the weighing method is predicted. It is assumed that the scale, such as load cell, weighs the mass of the powder which is just on the scale. Following the procedure in section 4.6-1, the mass is obtained as a function of time t. Then the mass flow rate detected by the scale can be predicted as a quotient of the mass and s/v (= Δt), where s is a width of the scale. The results are as follows:

(I) When $s \leq \dfrac{H_2 - H_1}{\tan \phi}$, $(S \leq 1)^*$

(I-1) For, $0 \leq t \leq s/v$, $(0 \leq T \leq S)^*$

Detected mass flow rate W(t) will be given by

$$W(t) = \frac{1}{3s}\tan\phi \cdot v^4 \rho_B t^3 + \left\{ \frac{1}{2s} B \tan\phi + \frac{H_1}{s} \right\} v^3 \rho_B t^2 + B H_1 v \rho_B + \frac{H_1^2 v \rho_B}{\tan\phi} \qquad (4.9)$$

(I-2) For, $s/v \leq t \leq (H_2 - H_1)/v \tan\phi$, $(S \leq T \leq 1)$

---

*) dimensionless representation,

$$S \equiv \frac{\tan \phi}{H_2 - H_1} \cdot s \quad , \qquad T \equiv \frac{\tan \phi}{H_2 - H_1} vt \qquad (4.8)$$

$$W(t) = v^3\rho_B \tan\phi \cdot t^2 + (B\tan\phi + 2H_1 - s\tan\phi)v^2\rho_B t$$

$$+ (BH_1 - \frac{B\tan\phi}{2}s + \frac{H_1^2}{\tan\phi} - H_1 s + \frac{1}{3}\tan\phi \cdot s^2)v\rho_B$$

(4.10)

(I-3) For, $\frac{H_2 - H_1}{v\tan\phi} \leq t \leq \frac{H_2 - H_1}{v\tan\phi} + \frac{s}{v}$,

$(1 \leq T \leq 1 + S)$

$$W(t) = -\frac{1}{3s}\tan\phi \cdot v^4\rho_B t^3 + (\tan\phi - \frac{H_1}{s} - \frac{B\tan\phi}{2s})v^3\rho_B t^2$$

$$+ \left\{\frac{BH_2}{s} + \frac{H_2^2}{s\tan\phi} + 2H_1 - s\tan\phi - \frac{H_1^2}{s\tan\phi} + B\tan\phi\right.$$

$$\left. - \frac{BH_1}{s}\right\} v^2\rho_B t$$

$$+ \frac{BH_1}{s}\left\{\frac{H_2 - H_1}{\tan\phi} + s\right\}v\rho_B + \frac{B\tan\phi}{2s}\left\{\frac{H_2-H_1}{\tan\phi} + s\right\}^2 v\rho_B$$

$$- B\tan\phi\ (\frac{H_2-H_1}{\tan\phi} + s)v\rho_B + \frac{H_1^2}{\tan\phi}\left\{\frac{H_2-H_1}{\tan\phi} + s\right\}\frac{v\rho_B}{s}$$

$$+ \frac{H_1 v\rho_B}{s}\left\{\frac{H_2-H_1}{\tan\phi} + s\right\}^2 - 2H_1 v\rho_B\left\{\frac{H_2-H_1}{\tan\phi} + s\right\}$$

$$+ \frac{\tan\phi}{3s} v\rho_B \left\{ \frac{H_2 - H_1}{\tan\phi} \right\}^3 + \frac{1}{3} \tan\phi \cdot s^2 v\rho_B$$

$$- \frac{BH_2}{s} v\rho_B \left\{ \frac{H_2 - H_1}{\tan\phi} \right\} - H_2^2 \left\{ \frac{H_2 - H_1}{\tan\phi} \right\} \frac{v\rho_B}{s} \qquad (4.11)$$

(II) When $s > \frac{H_2 - H_1}{\tan\phi}$, $(S > 1)$

(II-1) For, $0 \le t \le \frac{H_2 - H_1}{v \tan\phi}$, $(0 \le T \le 1)$

Mass flow rate W(t) is given by Eq.(4.9)

(II-2) For, $\frac{H_2 - H_1}{v \tan\phi} \le t \le \frac{s}{v}$, $(1 \le T \le S)$

$$W(t) = \left\{ \frac{H_2 + H_1}{\tan\phi} + B \right\} \frac{v^2 \rho_B t}{s} + BH_1 v\rho_B$$

$$+ \frac{H_1^2 v\rho_B}{\tan\phi} + \left\{ \frac{H_2 - H_1}{\tan\phi} \right\} \frac{Bv\rho_B}{s} + (H_1 - H_2)$$

$$+ \frac{H_2 - H_1}{\tan\phi} \cdot \frac{v\rho_B}{s \tan\phi} \cdot (H_1^2 - H_2^2)$$

$$+ \frac{B \tan\phi}{2s} \left\{ \frac{H_2 - H_1}{\tan\phi} \right\}^2 v\rho_B + \frac{H_1 v\rho_B}{s} \left\{ \frac{H_2 - H_1}{\tan\phi} \right\}^2$$

$$+ \frac{\tan \phi}{3s} v\rho_B \left\{ \frac{H_2 - H_1}{\tan \phi} \right\}^3 \qquad (4.12)$$

(II-3) For, $\frac{s}{v} \leq t \leq \frac{H_2 - H_1}{v \tan \phi} + \frac{s}{v}$, $(S \leq T \leq 1 + S)$

Mass flow rate W(t) is given by Eq.(4.11).

When $h = H_1$, mass flow rate W_1 is predicted by the equation:

$$W_1 = (B + H_1 / \tan \phi) H_1 v\rho_B \qquad (4.13)$$

For $h = H_2$, the mass flow rate is

$$W_2 = (B + H_2 / \tan \phi) H_2 v\rho_B \qquad (4.14)$$

Then, the dimensionless expression will be given by the following equation:

$$[W] = \frac{W(t) - W_1}{W_2 - W_1} \qquad (4.15)$$

4.6-3 Discussion of the belt feeder

The comparison between the theoretically predicted step responses and the experimental results

is shown in Fig.4.12. When the gate is raised, the experimental result shows a small delay. This delay is attributable to the measuring system. When the gate is lowered, it is found that the coincidence between the experimental and predicted results is very good.

Fig.4.17 shows the prediction of the step responses detected by the weighing method. With regard to the responses of a belt feeder, the previous studies dealt only with the dead time, or distance-velocity lag. But from Fig.4.17, it can be seen that the width of the scale causes a serious delay in the detected responses. This fact must be taken into consideration in the automatic control of a particulate system.

Further discussion is concerned with the dead time observed in the response. A powder bed may crumble after a step change in the gate opening. In which case the dead time does not equal L/v, where L is the distance between the gate and the tip of the belt, and v the belt velocity. The correct dead time can be obtained through a geometrical consideration allowing for the crumbling of the powder bed. In this experiment, the difference between the correct and the apparent dead times has reached 5 seconds. Dead times of this order may become significant in the automatic control of multi-component mixing processes.

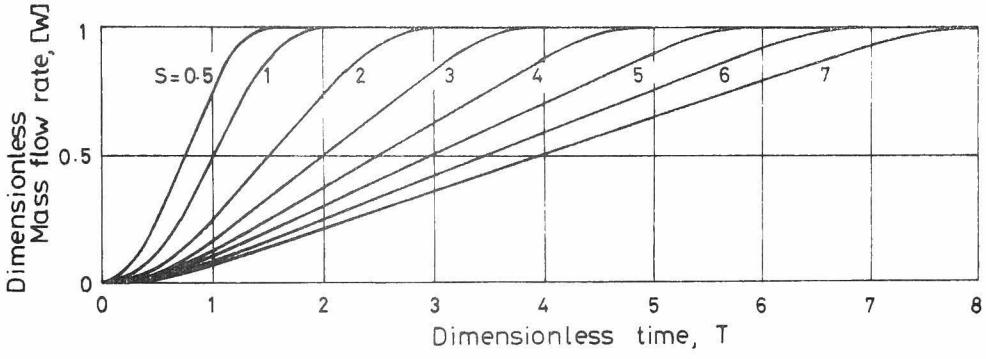

Fig.4.17 Step responses detected by a load cell

$$[W] = \frac{W(t) - W_1}{W_2 - W_1}$$

$$T = \frac{v \tan \phi}{H_2 - H_1} t$$

$$S = \frac{s \tan \phi}{H_2 - H_1}$$

4.7 Conclusion

The static and dynamic characteristics of a screw feeder, Vibra-screw feeder, Flo-tron, and a belt feeder have been studied experimentally. As the result of this study, it is found that these feeders have transfer lags in their dynamic characteristics. The gate-operated belt feeder has a noticeable dead time. These dynamic characteristics are not favorable for control purposes. The step responses of the belt feeder have been analysed theoretically with particular consideration of the shape of the powder bed on the belt. It is also shown that the weighing method for detecting the powder discharge rate of the belt feeder has a serious time delay in the response because of the crumbling of the powder. This fact must be taken into consideration in the automatic control of a particulate process, such as a multi-component mixing process.

Nomenclature

B	width of the powder bed, Fig.4.14
H	height of the powder bed
$\ell(t)$	length shown in Fig.4.14

$m(t)$	$= \ell(t)/\tan\alpha$, length shown in Fig.4.14
N	number of revolution per unit time
$S(t)$	area of the moving plane, Fig.4.15
s	width of a scale
t	time
v	belt speed
$W(t)$	discharged mass flow rate
$[W]$	dimensionless expression of $W(t)$
α	angle, $\tan\alpha = \tan\phi/\sin\phi$
ρ_B	bulk density of powder
ϕ	angle, $(\phi \equiv \phi_1 \sim \phi_5)$, Fig.4.13

References

1) Iinoya, K., T. Yoneda, and N. Kimura, "Fandamental experiments on a solid particle flow meter", Kagaku Kōgaku, 29, 88 (1965)

2) Iinoya, K., T. Yoneda, N. Kimura, K. Watanabe, and T. Shimizu, "Experiments on a particle flow meter", J. Res. Assoc. Powder Tech., Japan 3, 424 (1966)

3) Watanabe, K., and T. Inagaki, "Installation of automatic control of powder and granular materials by Impactline flow meter", J. Res. Assoc. Powder Tech., Japan, 7, 538 (1970)

CHAPTER 5

TABLE FEEDER

5.1 Introduction

A table feeder is generally used as a continuous type powder feeder. Kuwai et al[1], Toyama[2] and Muchi et al[3] studied the static characteristics of a table feeder. Kuwai et al examined the mechanics of the feeding process. However the mechanism is very complicated and has not been elucidated fully yet. The effect of the table friction factor on the discharge rate was studied by Toyama. This effect may be avoidable if there is a gap between the table and the scraper. Muchi et al were concerned with the estimation of the discharge rate as a function of the scraper position. These studies on the table feeder were carried out only for very slow revolutions of the table.

This chapter will be devoted to the static and dynamic problems of the feeder over a rather wide range of operation. The characteristics of the feeder when the scraper is operated, and the characteristics when the number of revolution is varied, will be discussed in §5.2 and §5.3, respectively. §5.4 is concerned with the fluctuation of the discharged mass flow rate which is observed by a flow

meter. A detailed explanation of the step responses observed when the scraper is operated, will be given in §5.5. Further discussion about the relation between the dynamic characteristics and the powder properties will be given also.

5.2 Characteristics of the Discharge Rate when regulated by the Scraper

5.2-1 Apparatus and experimental methods

The table feeder used in this study is shown schematically in Fig.5.1. The diameter of the table is 23 cm. The distance between the lower end of the hopper and the table (denoted by H, or called skirt clearance) is adjustable. The radial distance of the scraper from the center of the table (denoted by R, or called scraper position) can also be varied incrementally. Experiments were carried out for the range of 4 cm < R < 9 cm, and 3 cm < H < 5 cm. The effects of variation in the inserted angle of the scraper were also investigated. The level of powder in the hopper was maintained in the range where the effects of varying level were negligible.

The apparatus used for studying the dynamic characteristics of the feeder was described in §4.2.

The angular velocity of the table was maintained constant at 4.62 radians per second throughout the experiments. The properties of the powder materials used in the experiments are summarized in Table 5.1.

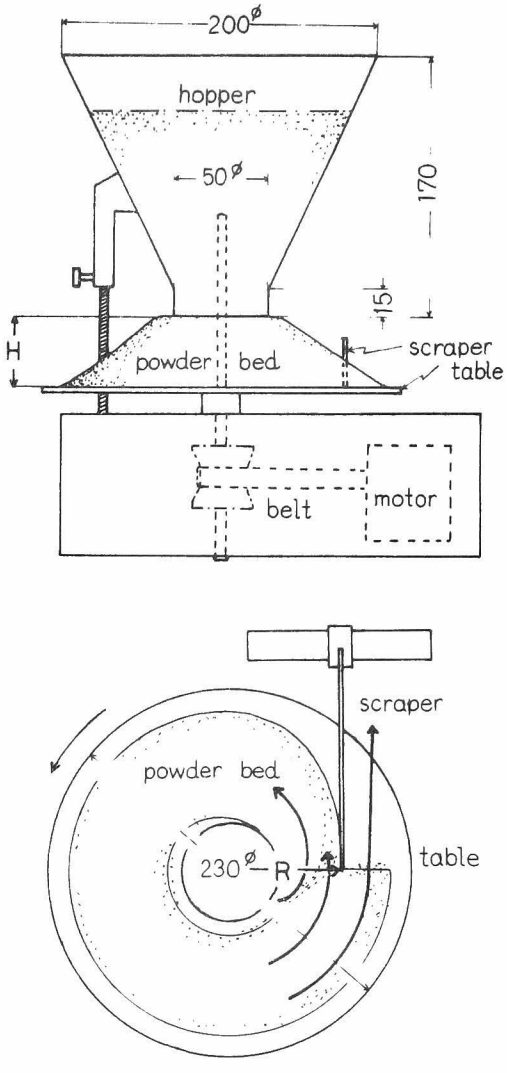

Fig.5.1 Schematic diagram of a table feeder

Table 5.1 Properties of the powder materials

Material	bulk density ρ_B [g/cm^3]	angle of repose φ_r [degree]	particle friction factor $\mu=\tan\varphi_r$ [—]	mass median diameter [microns]
Millet seed	0.794	33.3	0.657	980
Quartz sand No.5	1.36	35.5	0.713	440
Quartz sand No.8	1.23	38.1	0.748	68
Calcium carbonate	1.58	40.9	0.865	350

5.2-2 Preliminary observations

When the feed table is turned, particles flow down with helical trajectories out of the hopper, but after travelling some distance they have the trajectories of concentric circles. Particles outside the scraper are discharged from the feeder. The inserted angle of the scraper is usually fixed, however it was varied in the course of these experiments. When the angle is not zero, a dead zone in the flow of particles is observed at the tip of the scraper. The dead zone is unstable, and its growth or disappearance may be observed. As the

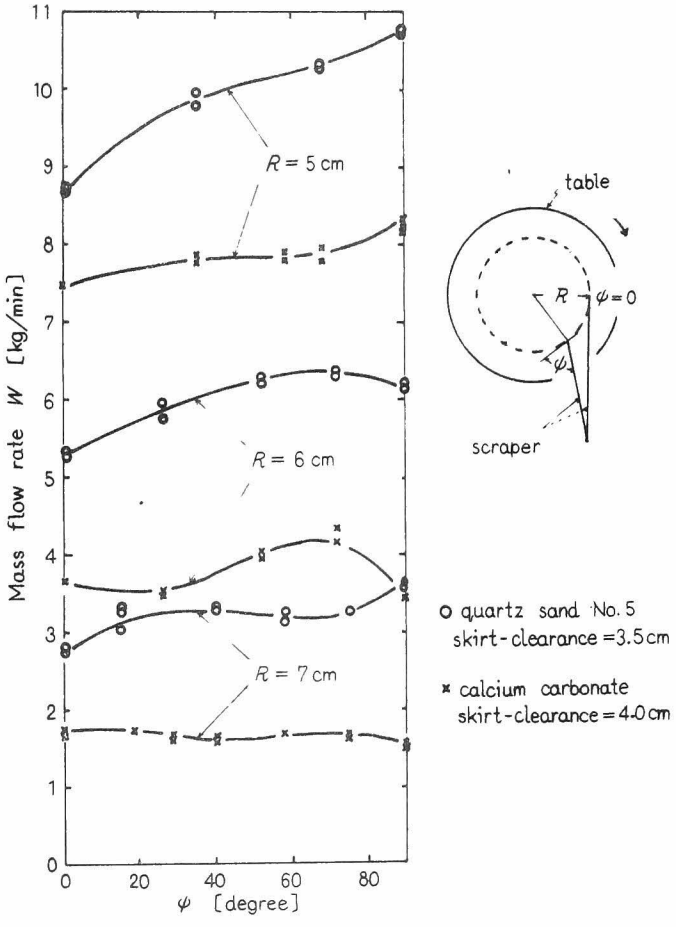

Fig.5.2 Effect of inserted angle of scraper on mass flow rate

dead zone grows it affects the mass flow rate as if the scraper position R was smaller than the actual R, which means that the mass flow rate becomes larger. Fig.5.2 shows the effect of the inserted angle of the scraper on the discharged mass flow rate, in the steady state. It can be seen that the mass flow rate varies appreciably with the inserted angle ψ. For large R, the effect of inserted angle is small, because the amount of particles contributed by this effect is small. However, the effect becomes more serious when R is small. As mentioned above the dead zone is unstable, and causes the deterioration of the constant feed property of a table feeder. In this regard, the scraper should be inserted tangentially to a concentric circle, that is $\psi = 0$. Then, the dead zone disappears and constant feed properties may be obtained.

5.2-3 Shape of the powder bed and the mass flow rate

In this section, the shape of the powder bed on the table will be represented by a theoretical equation. The discharged mass flow rate is also represented by an analytical equation, where the shape of the powder bed is taken into consideration.

From the preliminary observations, it can be said that a particle, just before reaching the

scraper, moves in a concentric circle. Now the equation representing the shape of the powder bed can be obtained by giving consideration to the forces acting on a particle. As shown in Fig.5.3,

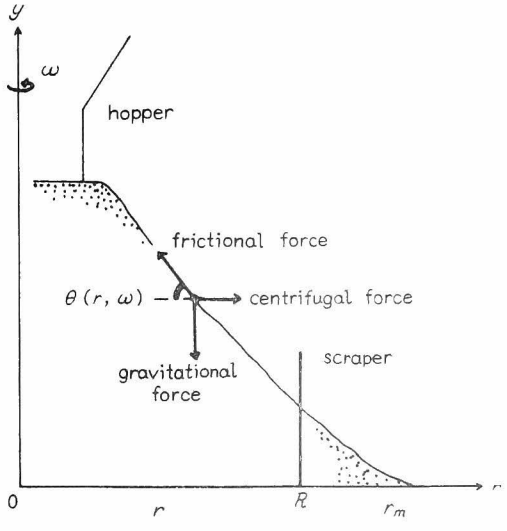

Fig.5.3 Forces acting on a particle

these forces are gravitational, centrifugal, and frictional. If the friction factor is denoted by μ, the following force balance equation can be written:

$$m\mu g \cos\theta - m\mu r\omega^2 \sin\theta = mr\omega^2 \cos\theta + mg \sin\theta \tag{5.1}$$

This equation indicates that the angle θ is a function of position r and angular velocity ω. That is,

$$\tan \theta(r, \omega) = \frac{\mu g - r\omega^2}{g + \mu r\omega^2} \tag{5.2}$$

When $\omega = 0$, this equation reduces to $\tan \theta(r,0) = \mu$, which means that the friction factor μ is a tangent of the angle of repose.

Now, from the definition of $\tan \theta(r, \omega)$, the following differential equation is also established.

$$\frac{dy}{dr} = - \frac{\mu g - r\omega^2}{g + \mu r\omega^2} \tag{5.3}$$

Integration of this equation under the condition:

$y = Y$ at $r = R$,

gives us

$$y = Y - \frac{g}{\omega^2} \left\{ 1 + \frac{1}{\mu^2} \right\} \ln \frac{g + \mu r\omega^2}{g + \mu R\omega^2} + \frac{1}{\mu} (r - R) \tag{5.4}$$

which is the equation for representing the shape of the powder bed. When R denotes the scraper position and Y denotes the height of the powder bed at $r = R$, the discharge rate W will be given by the following equation.

$$W = \frac{\rho_B \omega}{2\pi} \left\{ \int_0^Y \pi r^2 dy - \int_0^Y \pi R^2 dy \right\}$$

By use of Eq. (5.3), this equation can be rewritten as follows:

$$W = \frac{\rho_B \omega}{2} \left\{ \int_R^{r_m} r^2 \left(\frac{\mu g - r\omega^2}{g + \mu r \omega^2} \right) dr - YR^2 \right\} \qquad (5.5)$$

In this equation, r_m represents the maximum radius of the powder bed, which can be obtained as r for y = 0 in Eq. (5.4). Eq.(5.5) may be integrated to yield

$$W = \frac{\rho_B \omega}{2} \left[(\mu + \frac{1}{\mu}) \left\{ - \left(\frac{g}{\mu\omega^2} \right)^2 \left\{ - \left(\frac{g}{\mu\omega^2} \right)^2 (r_m - R) \right. \right. \right.$$

$$\left. + \frac{1}{2} \left(\frac{g}{\mu\omega^2} \right) (r_m^2 - R^2) + \left(\frac{g}{\mu\omega^2} \right)^3 \ln \frac{g + \mu r_m \omega^2}{g + \mu R \omega^2} \right\}$$

$$\left. - \frac{1}{3\mu} (r_m^3 - R^3) - YR^2 \right] \qquad (5.6)$$

This is the equation for predicting the mass flow rate, where the shape of the powder bed is taken into consideration.

Equation (5.6) may be rewritten as a dimensionless expression as follows:

$$\frac{2}{\rho_B \omega} \frac{W}{R^3} = \left[\left(\mu + \frac{1}{\mu}\right) \left\{ -\left(\frac{1}{\mu Z}\right)^2 (R_m - 1) + \frac{1}{2}\left(\frac{1}{\mu Z}\right)^2 \right.\right.$$

$$\left.\left. + \left(\frac{1}{\mu Z}\right)^3 \ln \frac{1+\mu Z R_m}{1 + \mu Z} \right\} - \frac{1}{3\mu}(R_m^3 - 1) - \frac{Y}{2} \right]$$

(5.7)

where Z is a centrifugal effect number ($R\omega^2/g$), and R_m is the dimensionless maximum radius of the powder bed (r_m/R).

5.2-4 Experimental results and discussion on the shape of the powder bed and the discharged mass flow rate

The shape of the powder bed was projected on screen by means of a beam of parallel light under steady state conditions. The projected profile was transcribed onto rectilinear graph paper. These experimental profiles, are compared with the calculated ones in Fig.5.4, which shows satisfactory coincidence

Fig.5.5 compares the measured and predicted mass flow rates. In this prediction, measured Y values were used. If the shape of the powder bed is approximated by a trapezium;

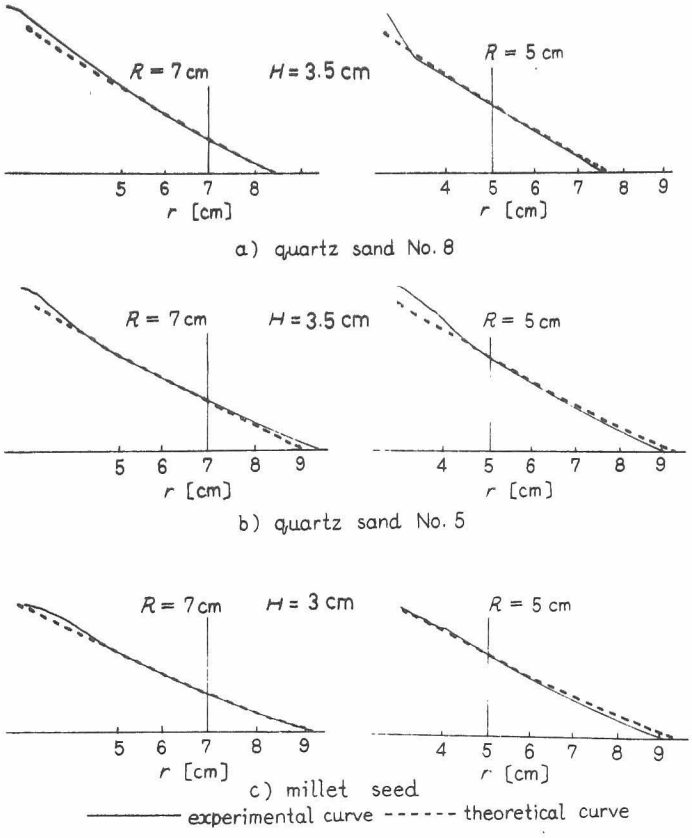

Fig.5.4 Shape of powder bed

ω = 4.62 [rad/sec]

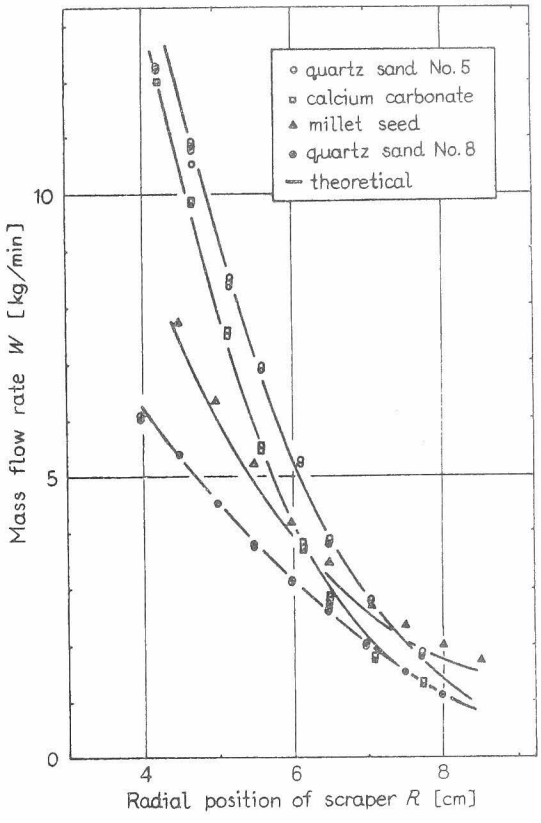

Fig.5.5 Mass flow rate as a function of scraper position

ω=4.62 [rad/sec]

○ H=3.5cm
□ H=4.0 "
△ H=3.0 "
● H=3.5 "

Theoretical lines are obtained by Eq.(5.6)

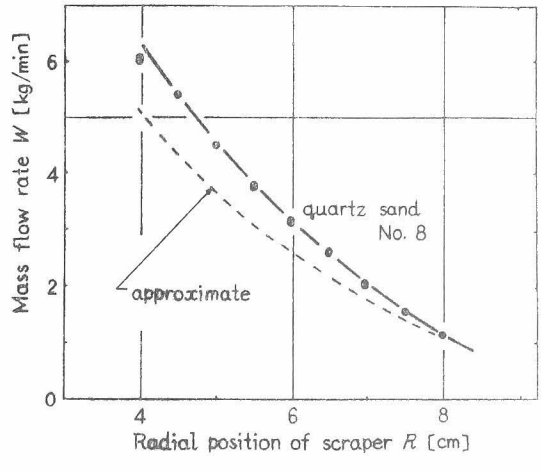

Fig.5.6 Mass flow rate calculated by the approximate equation

(the shape of the powder bed is not considered)

$$y = Y - \tan\theta \cdot (r - R) \qquad (5.8)$$

then an approximate equation for mass flow rate may be written as follows;

$$W = \frac{\rho_B \omega}{2} \frac{Y^2}{\tan\theta} \left(\frac{1}{3} \frac{Y}{\tan\theta} + R\right) \qquad (5.9)$$

where θ is a constant angle, but not the angle of repose. Predicted results obtained using this equation are shown in Fig.5.6. From a comparison between Fig.5.5 and Fig.5.6, it can be recognized that the shape of the powder bed must be taken into consideration when the angular velocity ω is large. Equation (5.5) or (5.6) was examined under the condition of ω = constant for the purposes of this section, but the subject will be discussed further in §5.3 with varying angular velocity.

5.2-5 Dynamic characteristics and analysis

In accordance with the conclusions reached in §5.2-2, the scraper was inserted tangentially to a concentric circle, and was mounted so that it could be moved successively from one position to another

along a selected diameter of the table. A step change in the position of the scraper produces a change in the discharge rate, which is recorded as shown in Fig.5.8. There are two types of response according to the kind of powder material and the operating conditions. These factors will be discussed in detail in §5.5.

Fig.5.7 shows the approximate shape of the powder bed after a step decrease in the position of the scraper.

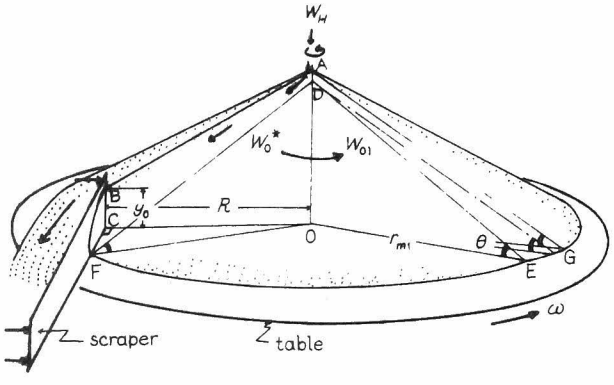

Fig.5.7 Shape of the powder bed after a step change in the position of the scraper

In this context the term decrease means that the scraper blade is moved closer to the center of the feed table. AOG is a final section of the initial bed. The mass flow rate at which the powder enters the face ABCO is

$$W_0^* = \frac{\rho_B \omega}{2} R^2 \left(y_0 + \frac{1}{3} R \tan \theta\right) \qquad (5.10)$$

and the rate at which it leaves the face DEO is

$$W_{01} = \frac{\rho_B}{6} r_{m1}^2 \quad \omega \tan \quad \theta \qquad (5.11)$$

where r_{m1} is the maximum radius OE. In addition, powder flows down from the hopper at a flow rate denoted by W_H, which may be equal to the mass flow rate at the steady state. Now, from the material balance, we have

$$W_0^* + W_H = W_{01} \qquad (5.12)$$

Combining Eqs.(5.10), (5.11) and (5.12), the maximum radius r_{m1} is obtained as follows:

$$r_{m1} = R\sqrt[3]{1 + \frac{3\ y_0}{R \tan \theta} + \frac{6\ W_H}{R^3 \rho_B \omega \tan \theta}} \qquad (5.13)$$

Therefore, when the table turns once, the height of the powder bed at r = R is given by

$$y_1 = (r_{m1} - R) \tan\theta$$

$$= R \left(\sqrt[3]{1 + \frac{3\, y_0}{R \tan\theta} + \frac{6\, W_H}{R^3 \rho_B \omega \tan\theta}} - 1 \right) \tan\theta \qquad (5.14)$$

Then, the height of the powder bed at r = R, at the n-th revolution will be represented by the following equation:

$$y_n = R \left(\sqrt[3]{1 + \frac{3\, y_{n-1}}{R \tan\theta} + \frac{6\, W_H}{R^3 \rho_B \omega \tan\theta}} - 1 \right) \tan\theta \qquad (5.15)$$

The mass flow rate corresponding to y_n may be obtained from the following equation:

$$W_n = \frac{\rho_B \omega}{2} \frac{y_n^2}{\tan\theta} \left(\frac{1}{3} \frac{y_n}{\tan\theta} + R \right) \qquad (5.16)$$

When y_0 and W_H (= W) are given beforehand, the step response can be predicted by Eqs. (5.15) and (5.16). The comparison between the experimental step responses and the predicted ones is shown in Fig.5.8. Both the derivative and proportional type responses

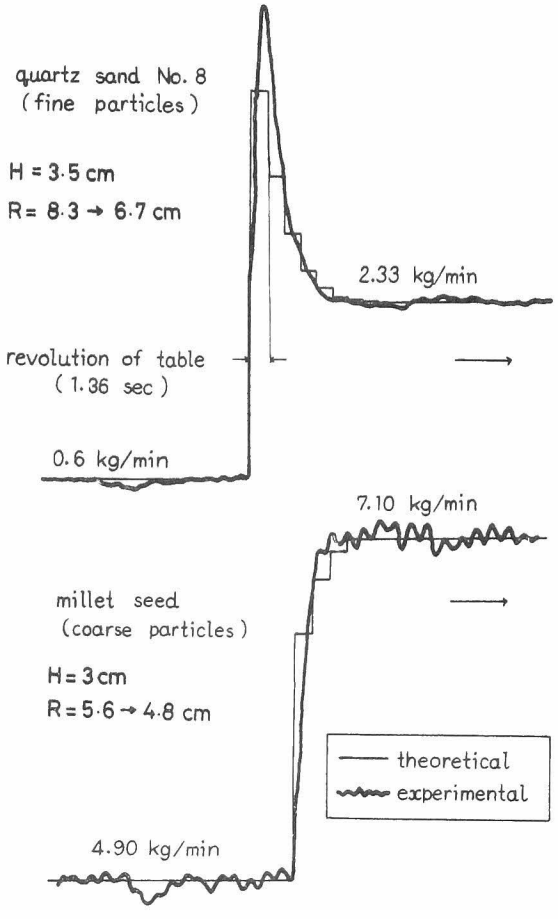

Fig.5.8 Step responses of a table feeder

ω=4.62 [rad/sec]

Theoretical line is obtained by Eq.(5.15) and (5.16).

are represented satisfactorily. The theoretical line will be smoothed, if the crumbling of the powder bed shown as AGED in Fig.5.7 is taken into consideration.

5.3 Characteristics of the Discharge Rate when regulated by changing the Rotational Speed of the Table

5.3-1 Apparatus and experimental methods

The table feeder used in this study is shown in Fig.5.9. As described already, in accordance with the results obtained in §5.2-2, the tip of the scraper is inserted tangentially to a concentric circle, and the blade mounted so that it moved along a selected diameter of the table. In this study, the scraper is fixed at several positions corresponding to pre-selected values of R, and the rotational speed of the table is varied in the range of $\omega = 0 \sim 3$ rad/sec. Responses to step changes in the rate of revolution are obtained with the apparatus shown in §4.2. The powder materials used are quartz sand No.5, quartz sand No.8, glass beads, and millet seeds. Their properties are shown in Table 5.2.

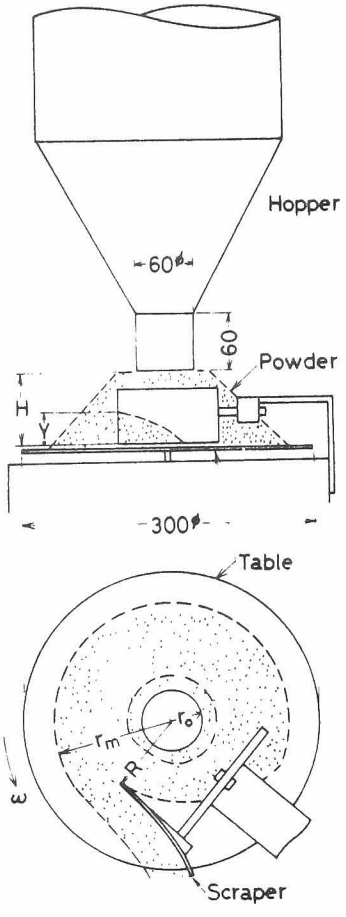

Fig. 5.9 Schematic diagram of a table feeder

Table 5.2 Properties of the powder materials

Material	Bulk density ρ_B (g/cm^3)	Angle of repose φ_r (degr)	Mass median dia. D_{p50} (microns)
Quartz sand No. 5	1.36	35.5	440
Quartz sand No. 8	1.23	38.1	68
Glass beads	1.47	24.0	438
Millet seeds	0.79	33.3	980

5.3-2 Static characteristics

A set of results showing the discharged mass flow rate as a function of table velocity in the steady state is shown in Fig.5.10. It is found that the mass flow rate is in proportion to the angular velocity ω up to 1 rad/sec. Within this operating range, the approximate equation (5.9) is applicable. For the limit of the range, where the mass flow rate is proportional to the angular velocity, the corresponding centrifugal effect number Z is about 0.005. As the dimensionless expression (5.7) for the mass flow rate also contains the dimensionless maximum radius R_m of the powder bed, the limit is also a

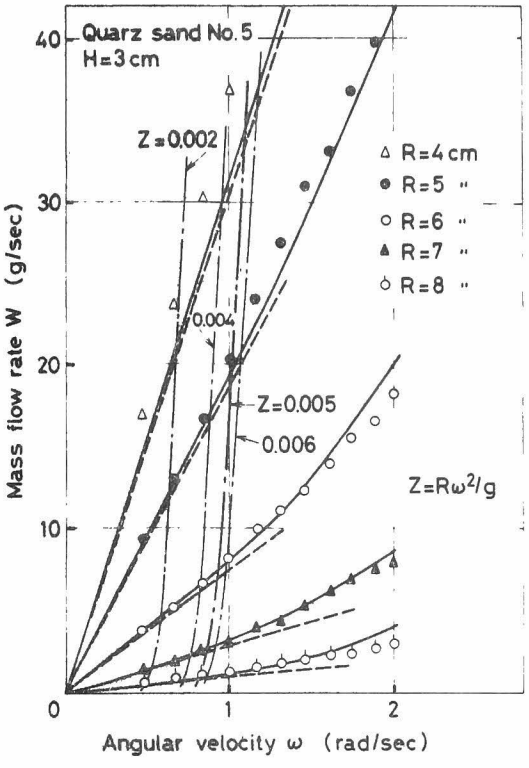

Fig.5.10 Mass flow rate as a function of the angular velocity of a table

- - - - Eq.(5.9)

——— Eq.(5.17)

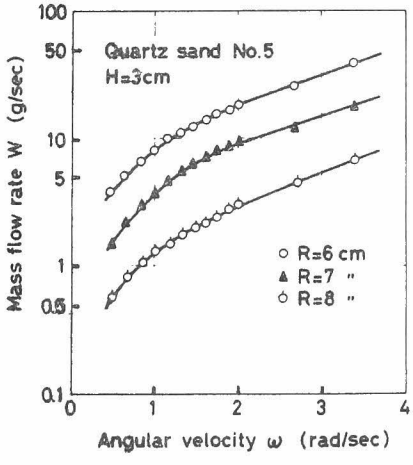

Fig.5.11 Semi-log plot for the mass flow rate

function of R_m. However, the centrifugal effect number can be used as an approximation of the limit. In practice, the operating range of the table feeder seems to be in this region.

On the other hand, the mass flow rate at higher angular velocity ($0.02 < Z$) can be estimated by Eqs. (5.4) and (5.5). For rather low speed revolution, ($0.005 < Z < 0.02$), the shape of the powder bed outside the scraper may be approximated by a straight line. Then Eq. (5.5) gives the following equation:

$$W = \frac{\rho_B \omega Y}{6} (r_m^2 + r_m R - 2 R^2) \qquad (5.17)$$

where r_m can be obtained as r for $y = 0$ in Eq.(5.4). The mass flow rate calculated by this equation is represented by a solid line in Fig. 5.10. The dotted line in the same figure shows a result calculated using Eq.(5.9). It is recognized that Eq.(5.7) can be used with fairly good accuracy when the angular velocity ω is smaller than 1 rad/sec ($Z < 0.005$). However, for higher values of ω this equation may not be applied. Conversely, Eq.(5.17) is applicable to rather high values of ω($0.005 < Z < 0.02$). The lower accuracy of the estimation for samll R means that the approximation for the shape of the powder bed deteriorates due to the curvature in the shape of the powder bed.

It is also found that the mass flow rate increases exponentially in the range of $\omega > 2$ rad/sec

as shown in Fig.5.11.

5.3-3 Dynamic characteristics

Responses of the discharged mass flow rate to a step change in angular velocity of the table are shown in Fig.5.12. It is found that the responses are divided into two groups as in the case of §5.2-5, and they are:

(1) Proportional type response (Fig.5.12-a)
(2) Derivative type response (Fig.5.12-b)

Proportional type responses are observed when the scraper position R is small. Derivative type responses are observed at large R. When the angular velocity of the table is decreased step wise, these two types of responses are also observed. If the shape of the powder bed does not vary due to the step change, the bed height Y at the scraper does not vary either, and step responses of the proportional type are observed. However, a step increase of the angular velocity brings about an expansion of the powder bed. This expansion may arise from the tangential force $r|d\omega/dt|$, which acts on the powder bed in the reverse direction to that of revolution.[4] On the other hand, a step decrease of the angular velocity acts so that the tangential force on the powder bed is in the direction of

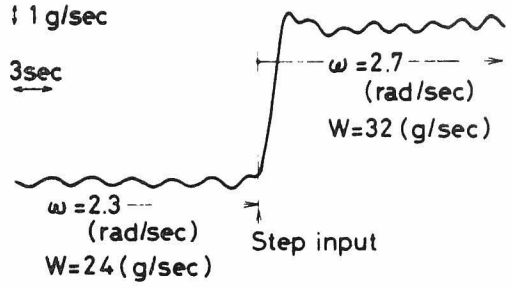

(a) R=8cm, H=2cm
glass beads

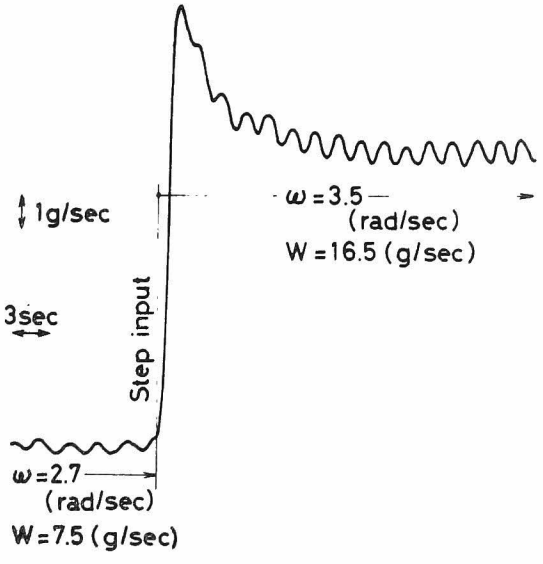

(b) R=10cm, H=2cm
glass beads

Fig.5.12 Step responses of a table feeder
(Rate of revolution was changed)

revolution, and the powder bed shrinks. The effective time of this action may be very short. In this short period of time, the shape of the powder bed varies, and gradually tends to that of the steady state. Expansion of the powder bed brings about an increase of the mass flow rate of the powder, and the shrinkage brings about a decrease. Therefore, the responses will be derivative in nature.

When the scraper position R is small, the effect of the force $r|d\omega/dt|$ is also small. Apart from this fact, the distance between the tip of the scraper and the discharge part of the table is large. Therefore, the response in this case is made smoothly while the powder moves along the scraper, and thus loses its derivative nature.

5.4 Fluctuation of the Mass Flow Rate

Periodic fluctuation of the discharged mass flow rate as shown in Fig.5.12, was observed using the Impact-Line flow meter. It is found that the period coincides with that of revolution of the table. This section discusses the cause of this fluctuation and the relationship between the amplitude and the rate of revolution of the table.

5.4-1 Cause of the fluctuation

To avoid complication, the Impact-Line flow

meter and the motor drive were removed from the system. The table was turned slowly by manual operation, and the discharged powder was sampled for each rotation of 60°. That is, six samples were collected each revolution. The fluctuations determined in this way are shown in Fig.5.13. The lines in this figure indicate the sinusoidal nature of the results. These preliminary data show that the cause of the fluctuation is in the table feeder itself. The observations concerning this fluctuation are as follows:

[Summary of observations]

(1) The recorded mass flow rate can be approximated by a sine curve whose period coincides with that of the revolution of the table.

(2) The edge of the table makes a vertical-sinusoidal motion with amplitude of about 1 mm. The horizontal motion is negligible. As a result of this vertical oscillation, the gap between the table and the scraper varies periodically, the period coinciding with that of the revolution of the table.

The observed behaviour could originate in a number of ways. These are listed below.

[Possible causes]

(i) The connection between the table and the shaft of revolution is not perpendicular.

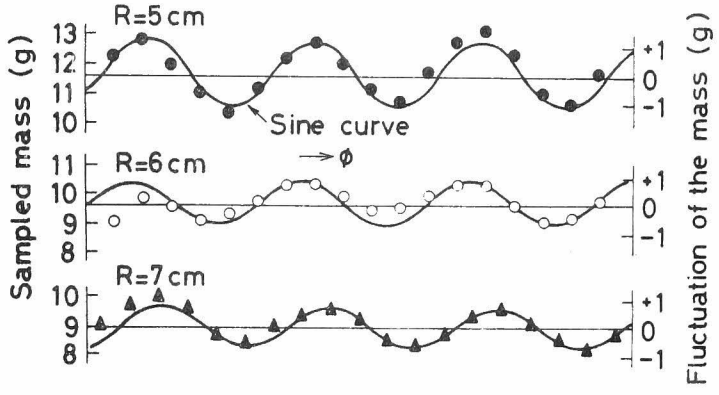

(a) Quartz sand No.5, H=3cm

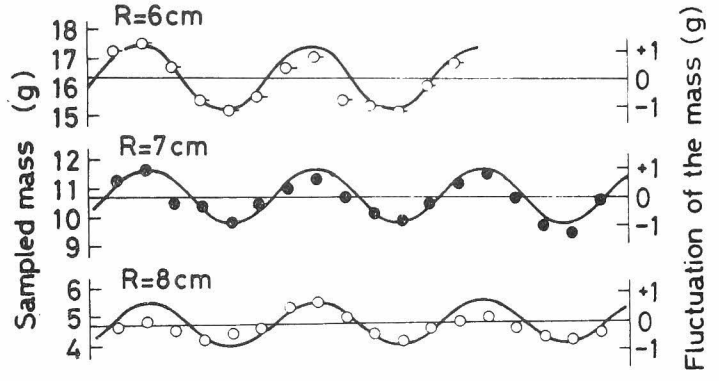

(b) Glass beads, H=2cm

Fig.5.13 Fluctuation of mass flow rate
(weight of the powder sampled while the table was turned slowly through 60°)

(ii) The shaft of revolution is not vertical

(iii) A combination of the above causes.

(iv) The center line of the hopper does not coincide with that of the table.

(v) The center of the table makes a circular motion because the shaft is bent slightly.

(vi) The center of the table makes a elliptical motion.

(vii) The scraper is not horizontal.

(viii) The rotation of the motor drive has some irregularity.

None of the postulated conditions (i), (ii), (iv), (v) or (vii) causes fluctuation of the discharged mass flow rate in the steady state. In the case of (vi) or (viii), the fluctuation will arise in the steady state, but these situations conflict with observations (1) and (2). Situation (iii), however, may cause the fluctuation in steady state, and also satisfies the observed facts. This may be explained as follows.

The powder bed shown in Fig.5.14-a, will turn to Fig.5.14-b after a revolution of 180° of the table. It is assumed that the table is horizontal in Fig.5.14-a, in which case angle $\alpha = \varphi_r$ and the powder bed is stable. The dotted line in Fig.5.14-b shows the powder bed turned through 180°. In this situation, the angle $\beta < \varphi_r$, and the powder bed

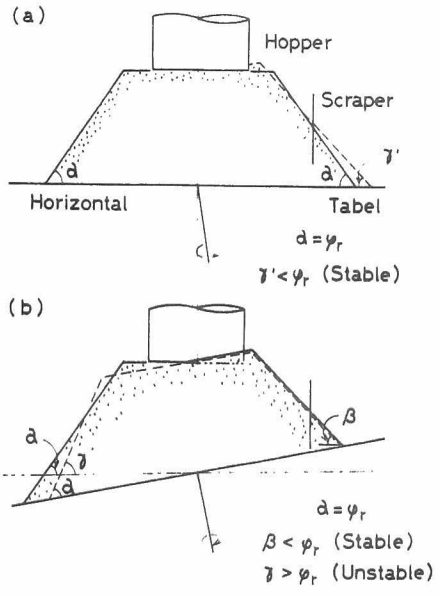

Fig.5.14 Explanation for the cause of the fluctuation in mass flow rate

would appear to be stable. However, the angle $\gamma > \varphi_r$, and the powder bed crumbles to take the shape indicated by the solid line. Consequently, the powder bed becomes stable. A further rotation of 180° is denoted by the dotted line in Fig.5.14-a, where the powder bed is also stable. It is clear that the discharged mass flow rate fluctuates periodically in the steady state. The observed facts(1) and (2) are also satisfied.

5.4-2 Amplitude of the fluctuation

Fig.5.15 shows the variation of the amplitude

of the fluctuations as a function of the angular velocity ω of the table. It is found that the amplitude increases linearly with ω at small ω, and that it decreases in the range of ω = 1.5 ~ 2.5 rad/sec. The amplitude increases again, at higher rotational speeds. The data shown in Fig.5.13 are represented by $A'\sin\phi$, where ϕ is the angle of revolution. Then the fluctuation ΔW of the mass flow rate will be represented by the following equation:

$$\Delta W = A \sin\omega t, \quad A \equiv A'\omega \tag{5.18}$$

because the following relation is applicable.

$$\int_0^{\pi} A'\sin\phi d\phi = \int_0^{\pi/\omega} A\sin\omega t \, dt \tag{5.19}$$

Noting that the data shown in Fig.5.13 are integrated values over 60° of revolution, the measured amplitude A" shown in the figure satisfies the following equation:

$$A'' = \left| \int_{\phi}^{\phi+\frac{\pi}{3}} A' \sin\phi \, d\phi \right|_{max}$$

$$= \left| -\sqrt{3} A' \sin\left(\phi + \frac{\pi}{6}\right) \right|_{max}$$

$$= \sqrt{3} A' \tag{5.20}$$

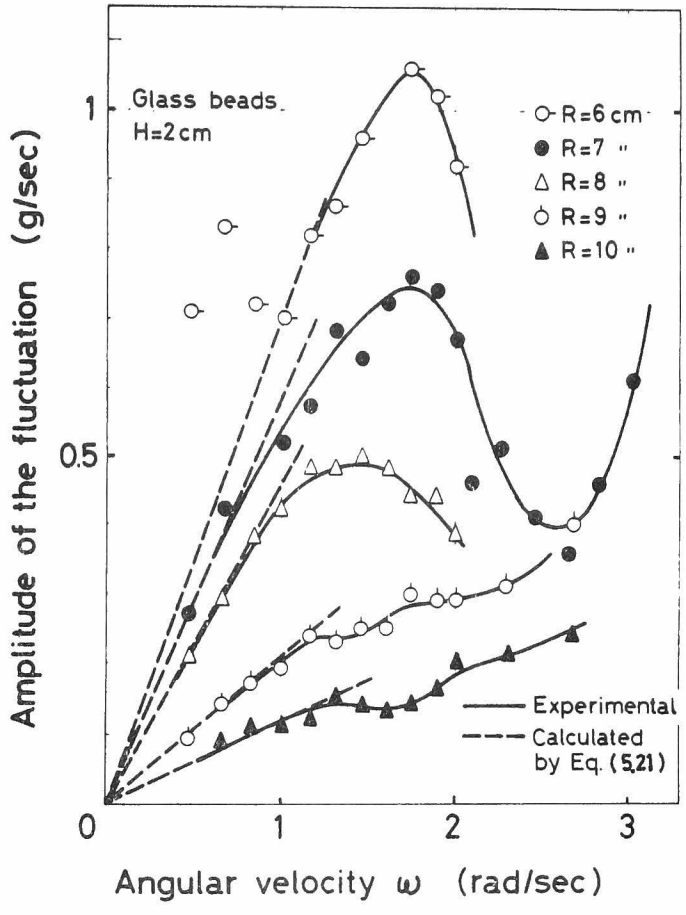

Fig.5.15 Amplitude of the fluctuation as a function of the angular velocity

Therefore, the relation between the measured amplitude A" and A is as follows:

$$A = \frac{1}{\sqrt{3}} A'' \quad \omega \tag{5.21}$$

Amplitudes A calculated by this equation are shown in Fig.5.15 with dotted lines. It is found that the calculated and experimental amplitudes are in good agreement up to 1 rad/sec.

The trend of the amplitude over the whole range may be explained as follows:
Let T_1 and T_2 denote the time constants of the measuring system and of another system respectively. Then the amplitude A in the low frequency range will be given by[5)]

$$A \simeq \frac{A' \quad \omega}{\sqrt{1 + (T_1\omega)^2} \quad \sqrt{1 + (T_2\omega)^2}} \tag{5.22}$$

where the time constant T_1 is about 0.4 second. It may be assumed that

$$T_1 \simeq T_2 \equiv T \tag{5.23}$$

From Eq.(5.22), it is found that the amplitude becomes a maximum at $\omega \simeq 1.8$ rad/sec. In a higher

frequency range than this, ($\omega T >> 1$), the following equation may be applicable

$$A \simeq \frac{Ke^{k\omega}}{(T\omega)^2} \qquad (5.24)$$

because the mass flow rate increases exponentially as shown in Fig.5.11. Eq.(5.24) can be rewritten as follows:

$$A \simeq K \{1 + k\omega + \frac{(k\omega)^2}{2!} + \frac{(k\omega)^3}{3!} + \ldots\ldots \}/(T\omega)^2$$

$$\simeq K\{\frac{1}{2!}(\frac{k}{T})^2 + \frac{1}{3!}\frac{k^3}{T^2}\omega + \ldots\ldots\} \qquad (5.25)$$

This equation means that the amplitude A increases monotonically with ω in the higher frequency range.

5.5 Intercepted Height of the Powder Bed as a Function of the Scraper Position : Y-curve

Some complementary explanations for the step responses of the discharge rate regulated by the scraper will be given in this section. As described in §5.2, there are two types of responses according to the kind of powder material and the operating conditions. It is shown that the factors affecting the responses are typified by the height of the bed

at the point of interception with the scraper in the steady state. The height as a function of the scraper position is herein called the Y-curve.

5.5-1 Measurements of Y-curve

The table feeder shown in Fig.5.9 was used in this study. The motor drive was taken off, and the table was turned slowly by manual operation. After turning the table for a while the steady state was attained, and the height Y was measured. The measurements were carried out varying the scraper position R and the skirt-clearance H. The powder materials used are listed in Table 5.2. Flowabilities of these powders increase in the order quartz sand No.8, quartz sand No.5 and glass beads.

Fig. 5.16 shows the Y-data for the quartz sand

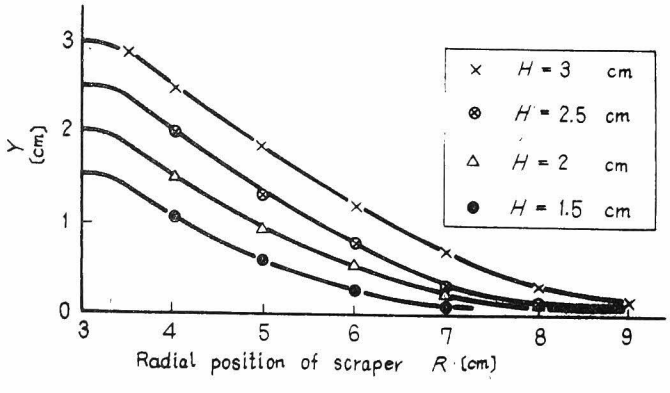

Fig.5.16 Y-data as a function of R
(quartz sand No.5)

No.5. In this figure, the Y-data is represented as a function of the scraper position R. Another representation of the Y-data is obtained, when a new variable X is introduced, defined by the following equation:

$$X = R - r_0 - \frac{H}{\tan \varphi_r} \qquad (5.26)$$

where X is the relative position of the scraper with respect to the intersecting point D as shown in Fig. 5.19-a. In this equation, r_0 denotes the inside radius of the hopper outlet pipe, and φ_r is the angle of repose of the powder. Fig.5.17-a shows the replotted data for the quartz sand No.5 using the relative scraper position X. The Y-data for the various skirt clearances H are almost fully represented by one curve. Fig.5.17-b and c show the Y-data for the quartz sand No.8 and glass beads, respectively.

5.5-2 Explanation of the step responses of the discharge rate regulated by the scraper

The slope of the Y-curve in the range of $X < 0$ *) is nearly equal to the angle of repose for the quartz

---

*) Strictly speaking, in the range $X < Xc$. Xc can be determined by Eq. (5.27).

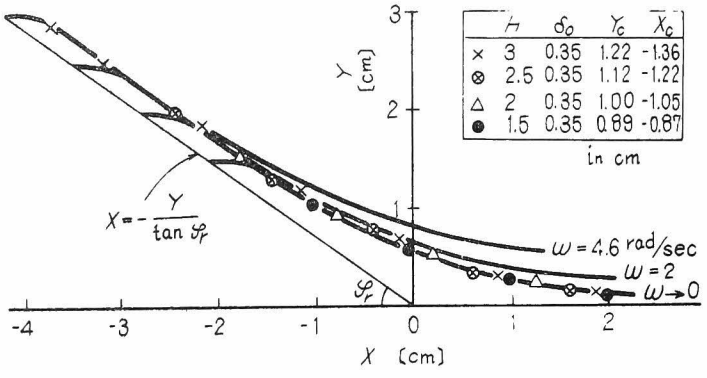

a) quartz sand No.5

$\varphi_r = 35.5°$

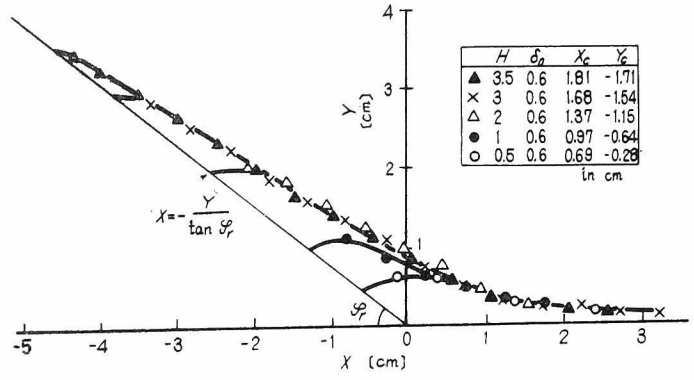

b) quartz sand No.8

$\varphi_r = 38°$

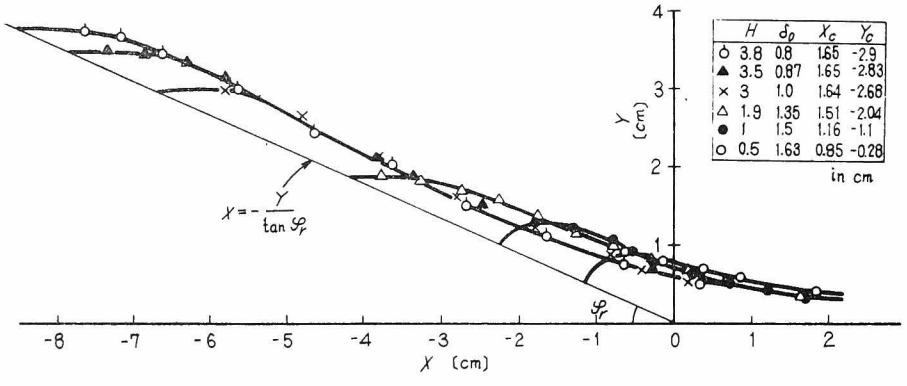

c) glass beads

$\varphi_r = 24°$

Fig.5.17 Y-data as a function of X

sand No.5, is smaller than the angle of repose for the quartz sand No.8, but larger than the angle of repose for the glass beads. It can be shown that the differences of the type of step response are attributable to these variations in the relation between the slope of the Y-curve and the angle of repose. Consider the case shown in Fig.5.18, where the slope is always smaller than the angle of repose, just as for quartz sand No.8. As the Y-curve represents the height of the powder bed relative to the scraper position in the steady state, it is independent of step change in the scraper position.

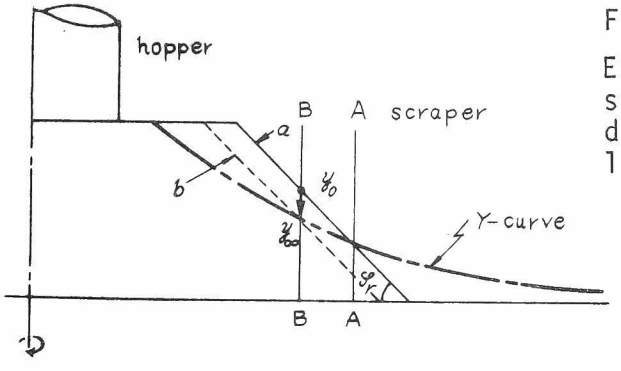

Fig.5.18
Explanation of the step responses of the discharge rate regulated by the scraper

On the other hand, the powder bed is affected by the step change. When the scraper position is A or B in Fig.5.18, the corresponding powder bed in the steady state is denoted by a or b. This is clear from the definition of the Y-curve. When the scraper is moved quickly from position A to B, the powder bed is not affected for the time of one revolution and is

also denoted by a. Therefore, the height of the powder bed at that time is indicated by y_0 on the line $\overline{BB}$. From this fact and the significance of the Y-curve, it is clear that the height of the powder bed y decreases from y_0 to y_∞ with the revolutions of the table. In this case, the step response is of the derivative type. In a similar way, the step response for the range where the slope of the Y-curve is larger than the angle of repose, can be shown to be of the time-delay-type. When the slope of the Y-curve is equal to the angle of repose the step response is of proportional type.

In this way, the differences between the type of the step responses become explicable. The responses following step decreases in the scraper position R can also be explained in a similar way.

5.5-3 Explanation of the effect of the powder properties on the Y-curve

The following discussion is concerned with the significance of the Y-curve. When the powder bed on the table reaches the scraper, part of the powder bed is separated and discharged and the remainder is rotated with the table again. The powder bed cut by the scraper crumbles. If the upper part of the crumbled powder bed is included inside the discharge pipe, powder stored in the hopper flows directly onto the table through the action of gravity. The

critical scraper position Xc may be assumed as X which satisfies the condition that the area of ΔCEF is equal to the area ABCD in Fig.5.19-a. Then, the following equation may be written.

$$Xc = \delta_0 - Yc / \tan \varphi r$$
$$Yc = \sqrt{2\ \delta_0\ H \tan \varphi r} \qquad (5.27)$$

where, δ_0 denotes the length $\overline{AB}$. Now the Y-curve can be divided into two parts by fixing the critical position Xc such that it satisfies the condition that the relative scraper position X is larger than the critical position Xc, or alternatively, that it satisfies the condition $X < Xc$.

(I) $X > Xc$ (cf. Fig.5.19-b)

In this case the length δ_1, Fig.5.19-b, is observed on the powder bed cut by the scraper. The powder bed spreads out further as the table continues to turn. The maximum spread-out length in one revolution of the table is denoted by δ_2. That is, during a single rotation the spread length varies progressively from δ_1 to δ_2. This means that the particles are receiving the energy required for the spreading motion from external sources. This work E will be a function of the position δ of a particle. Assume that the work E is represented by the following equation:

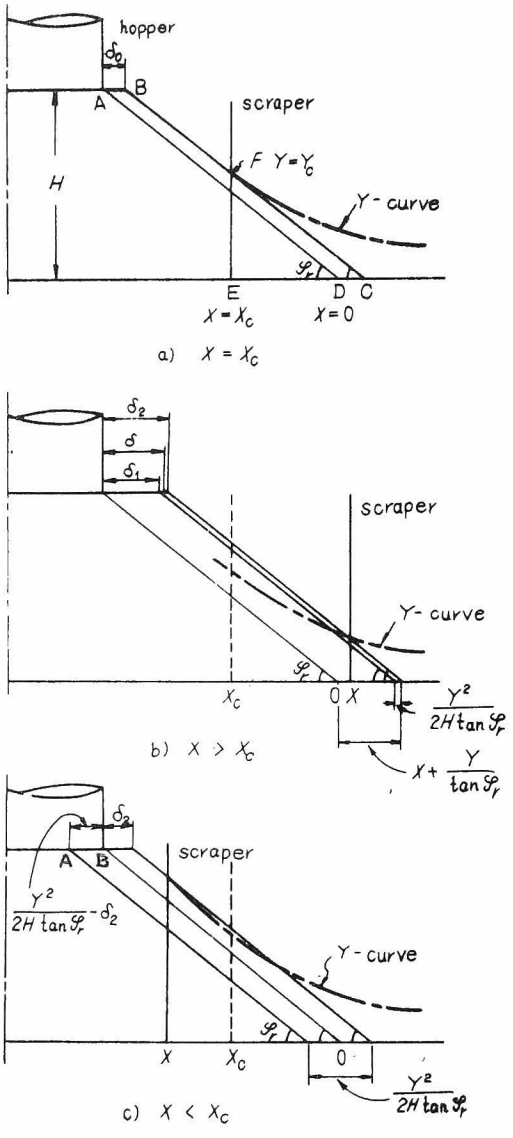

Fig.5.19 Relation between the Y-curve and the spread out length

$$dE / d\delta = k^{-1}\delta^{\alpha} \qquad (5.28)$$

Make the further assumption that the work E_1 received in one revolution of the table is constant. This is a fairly important assumption, but in view of the experimental results obtained, e.g. Fig.5.21, it seems reasonable. Then, if the scraper is not inserted, the total spread-out length δ after the N-th revolution will be given by

$$\int_0^{\delta} \delta^{\alpha}\, d\delta = kNE_1 \qquad (5.29)$$

Carrying out the integration of this equation, the following expression is obtained:

$$\ln\delta = \frac{1}{\alpha + 1} \ln N + \frac{1}{\alpha + 1} \ln \{kE_1(\alpha + 1)\} \qquad (5.30)$$

This equation means that the log.-log. plot of the total spread-out length δ vs. the cumulative number of revolutions N is a straight line, the slope of the line having the value $1/(\alpha + 1)$. Fig.5.20 shows the experimental results obtained. The data may be approximated by a straight line, and the slope of the line is about 1/4. Therefore, as far as these data are concerned, the assumptions made above are

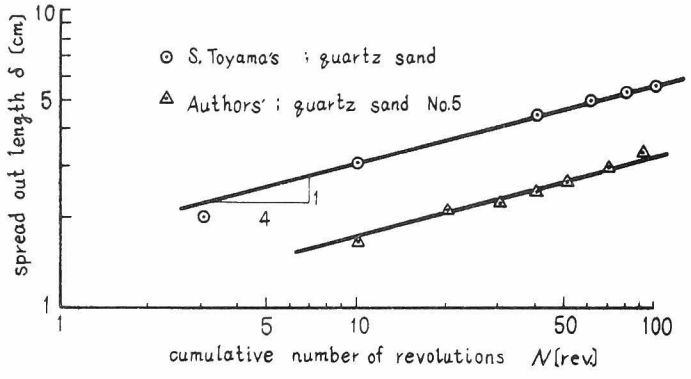

Fig.5.20 Spread out length in relation to the cumulative number of revolutions

admissible, and $\alpha \tilde{=} 3$. From Eq.(5.30), the constant kE_1 is obtained as follows.

$$kE_1 = \frac{1}{\alpha + 1} \delta_0^{\alpha+1} \tag{5.31}$$

The situation when the scraper is inserted as usual is dealt with similarly. In this case, $\alpha = 3$, $N = 1$, and the interval of the integration is $\delta_1 \sim \delta_2$. Therefore,

$$\int_{\delta_1}^{\delta_2} \delta^3 d\delta = kE_1 = \frac{1}{4} \delta_0^4 \tag{5.32}$$

The spread-out lengths δ_1 and δ_2 are represented by the following equations:

$$\delta_1 = X + \frac{Y}{\tan \varphi_r} - \frac{Y^2}{4H \tan \varphi_r} \quad ,$$

and $$\delta_2 = X + \frac{Y}{\tan \varphi_r} \quad .$$

The relation between X and Y can be obtained by carrying out the integration of Eq.(5.32) as follows:

$$X = \frac{Y}{\tan \varphi_r} + \frac{Y^2}{4H \tan \varphi_r} + \sqrt[3]{A} + \sqrt[3]{B}$$

where, (5.33)

$$\begin{pmatrix} A \\ B \end{pmatrix} = \left(\frac{H\delta_0{}^4 \tan^4 \varphi_r}{2Y^2} \pm \sqrt{\frac{H^2 \delta_0{}^8 \tan \varphi_r}{4Y^4} + \frac{Y^{12}}{3^3 \cdot 4^5 \cdot H^6}} \right)$$

A comparison between the calculated and experimental results for the quartz sand No.5 is shown in Fig.5.21. The value of δ_0 used in this calculation is 3.5 mm which can be obtained from Fig.5.17-a. The coincidence found between the calculated and the experimental results is satisfactory. As with the quartz sand No.8 and the glass beads, direct determi-

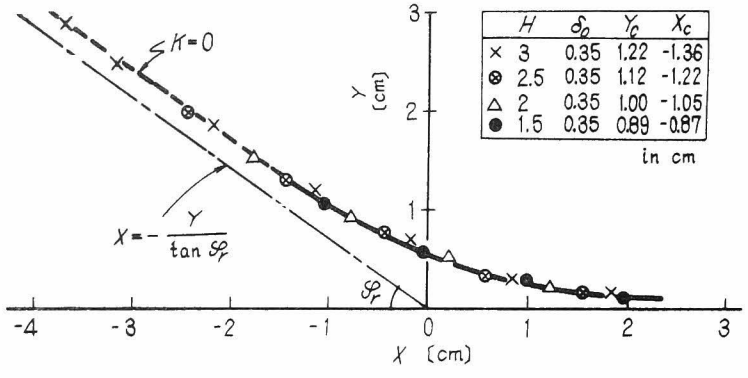

Fig.5.21 Comparison between the calculated Y-curve and experimental results (quartz sand No.5)

——— Eq.(5.33)

- - - - Eq.(5.37)

nation of the values of δ_0 cannot be carried out from Fig.5.17-b and c. However, assuming the trial value of δ_0, these Y-curves will also be represented by Eq.(5.33).

(II) $X \leq Xc$ (cf. Fig.5.19-c)

In this case powder stored in the hopper flows onto the table under the action of gravity. The rate at which the powder flows down may be affected by the length:

$$\frac{Y^2}{2H \tan \varphi_r} - \delta_2$$

which is contained in the discharge pipe and shown as $\overline{AB}$ in Fig.5.19-c. In the case of a powder of high flowability, the powder downflow-rate will increase with the length $(Y^2/2H \tan \varphi_r - \delta_2)$ because of the inertia of the particles. Therefore, the total spread-out length δ_2 will be approximated by the following equation:

$$\delta_2 = \delta_0 + \kappa\left\{\frac{Y^2}{2H \tan \varphi_r} - \delta_2\right\} \qquad (5.34)$$

where, κ is a positive number. This equation may be rewritten as

$$\delta_2 = \frac{\delta_0}{1 + \kappa} + \frac{\kappa}{1 + \kappa}\frac{Y^2}{2H \tan \varphi_r} \qquad (5.35)$$

In the case of a powder of low flowability, namely an adhesive powder, the powder flow-rate will decrease with the length $(Y^2/2H \tan \varphi_r - \delta_2)$ because of the adhesive force of the particles. In this case, the total spread-out length δ_2 will be approximated by Eq.(5.35) with "negative" κ. Differentiating Eq. (5.35) with respect to the parameter κ gives

$$\frac{\partial \delta_2}{\partial \kappa} = \left\{\frac{Y^2}{2H \tan \varphi_r} - \delta_0\right\}\frac{1}{(1 + \kappa)^2} \qquad (5.36)$$

From Eq.(5.27), the right hand side of this equation is positive for Y > Yc. Therefore, the total spread-out length δ_2 increases with the parameter κ. When $\delta_2 = \delta_0$, it can be seen from Eq.(5.35) that $\kappa = 0$. These results can be summarized as follows:

$$X = -\frac{Y}{\tan \varphi_r} + \frac{\delta_0}{1+\kappa} + \frac{\kappa}{1+\kappa} \cdot \frac{Y^2}{2H \tan \varphi_r} \quad , \qquad \text{for } X \leq Xc \tag{5.37}$$

where,

$$(-1 <)\ \kappa \begin{cases} > 0 : \text{for powder of high flowability such as glass beads} \\ = 0 : \text{for powder of moderate flowability such as quartz sand No.5} \\ < 0 : \text{for powder of low flowability such as quartz sand No.8} \end{cases} \tag{5.38}$$

For $\kappa = -1$, the corresponding real situation will be the failure of the discharge.

From Eq.(5.37), following equation is obtained:

$$\frac{d}{d\kappa} \left| \frac{dY}{dX} \right| = \tan \varphi_r \cdot \frac{Y}{H \{1 + \kappa(1 - \frac{Y}{H})\}^2} > 0 \tag{5.39}$$

Further, it is easily shown that:

$$\left|\frac{dY}{dX}\right| = \tan \varphi_r, \quad \text{for } \kappa = 0 \tag{5.40}$$

Therefore,

$$\left|\frac{dY}{dX}\right| > \tan \varphi_r, \quad \text{for } \kappa > 0 \tag{5.41}$$

and,

$$\left|\frac{dY}{dX}\right| < \tan \varphi_r, \quad \text{for } \kappa < 0 \tag{5.42}$$

From the above Eqs.(5.40 ~ 42), Eq.(5.38), and the discussion in §5.5-2, it can be said that:

(i) the step response for a powder of high flowability is of the time-delay type,

(ii) the step response for a powder of moderate flowability is of the proportional type,

(iii) the step response for a powder of low flowability is of the derivative type.

As described above, the step response of the discharge rate regulated by the scraper has been shown in relation to the properties of the powder

materials and the operating conditions. The following discussion is concerned with the mechanism of powder discharge. For this purpose, the following experiments are carried out.

The feeder is operated until a steady state of discharge is attained, colored particles are then added to the hopper. Steady state is attained again after sufficient revolutions. Then a dilute solution of Japanese isinglass is added slowly to the hopper. When the solution becomes hard the powder bed is cut. Fig. 5.22 shows one of the results obtained following the above procedure.

The white part in the figure is a dead zone. Particles move along the black part and are discharged. The border line between the dead zone and the moving zone is approximated by the slip line[6] calculated for the horizontal powder bed on which pressure is applied. The distribution pattern of the applied pressures is of isoscales triangle form, and the direction of the pressures is inclined downward. As the calculated slip line and the experimentally obtained border line are coincident, it seems that the powder bed of the table feeder receives a similar pressure. Then the particles at the shoulder part of the powder bed will be pushed up, and in the case of a large spread-out length, the particles will be piled up in this region. This phenomenon is observed for both the quartz sand No.8 and the glass beads when the skirt clearance H is small, as shown in Fig.5.17-b and c, where Y is higher than H.

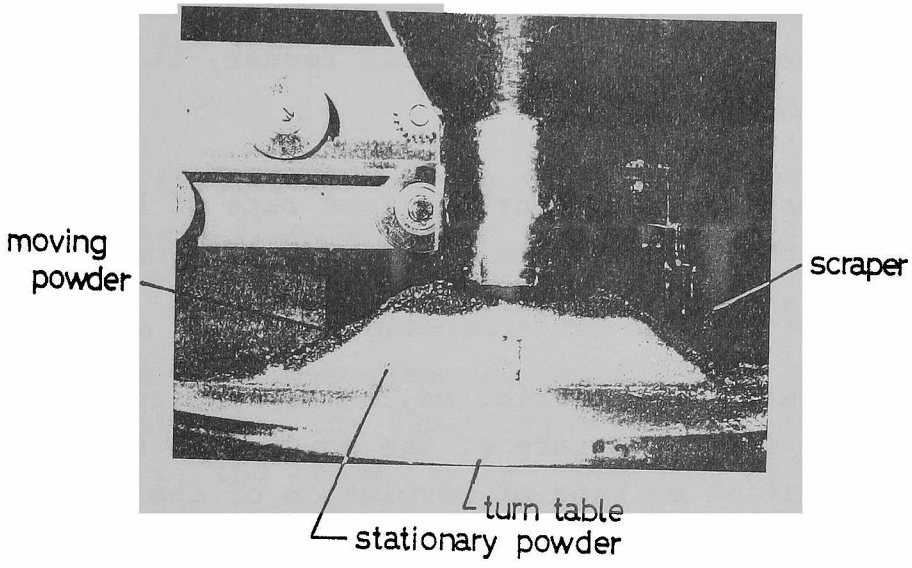

Fig.5.22 Discharge of powder from a hopper

5.6 Conclusion

From the above examination of the static and dynamic characteristics of a table feeder, it is concluded that:

1. In order to get a constant feed rate of high stability, the scraper should be inserted along the tangent of a concentric circle on the table.

2. The static characteristics, namely the relation between the discharge rate of the powder and the scraper position or rate of revolution of the table in steady state, can be estimated with fairly good accuracy if the shape of the powder bed is taken into consideration.

3. The shape of the powder bed can be estimated from a theoretical equation, Eq.(5.4).

4. The dynamic characteristic of the discharge rate when regulated by the scraper, may be derivative in nature, where the relative scraper position is large.

5. When the relative scraper position is small, the dynamic characteristic will be of time-delay, proportional, or derivative type for powders of high flowability, moderate flowability, or low flowability, respectively.

6. The dynamic characteristic of the discharge rate when regulated by changing the rotational speed of the table is of derivative nature, if the scraper position and the effect of the force $r|d\omega/dt|$ are large.

7. Any inclination in the installation of the table will cause a fluctuation in the mass flow rate. However, this fact suggests that the feeder may be used as a sine-wave generator for studies of powder flow rate. The experimental relationship between the amplitude of the fluctuation and the angular velocity of the table has been obtained and explained analytically.

8. The relation between the height at which the scraper cuts the powder bed and the relative scraper position is explained analytically.

9. The relationship, the Y-curve, depends on the powder properties. A parameter is introduced for taking the nature of the powder into consideration. The parameter is positive, zero, and negative for powders of high flowability, moderate flowability, and low flowability, respectively.

10. The internal part of the powder bed is stationary in the steady state. Particles move along the upper part of the powder bed and are discharged. The

border line between the dead zone and the moving zone is approximated by a specific slip line.

Nomenclature

A	amplitude of fluctuation of discharge rate, $A \equiv A'\omega$
A'	amplitude of fluctuation of discharge rate as a function of the angle of revolution
A''	amplitude measured following the procedure in §5.4-1, $A'' = \sqrt{3}A'$
E	energy required for spreading the powder bed
E_1	energy received in one revolution of the table
H	skirt clearance, cf. Fig.5.1 or 5.9
K	constant
k	constant

R	radial position of the scraper, cf. Fig. 5.1 or 5.9
R_m	$= r_m / R$
r	radial distance from the center of the table
r_m	maximum radius of the powder bed
T	time constant
W	discharge rate of particles in steady state
W_H	mass flow rate of particles from the hopper to the table
W_n	discharge rate of particles at n-th revolution
W_n^*	mass flow rate of particles through the cross section ABCO in Fig.5.7 at n-th revolution
X	relative scraper position represented by Eq.(5.26)
Xc	critical-relative scraper position given by Eq.(5.27)
Y	height at which the scraper cuts the powder bed in steady state

Y_c	Y for the case of X = Xc
y_n	height at which the scraper cuts the powder bed at n-th revolution
α, β, γ	angles in Fig.5.14
δ	spread-out length, cf. Fig.5.19
δ_0	spread-out length in the case X = Xc
δ_1	spread-out length as a lower limit of the integration of Eq.(5.32)
δ_2	spread-out length as a upper limit of the integration of Eq.(5.32)
θ (r, ω)	angle of the powder bed in Fig.5.3. θ(r, 0) represents the angle of repose
κ	parameter representing the properties of a powder
μ	tan φ_r
ρ_B	bulk density of particles
ϕ	angle of revolution of the table
φ_r	angle of repose
ω	angular velocity of the table

References

1) Kuwai, G., T. Ide, and G. Hōjo, "Feeding Mechanism and Characteristics of Table Feeder", Kagaku Kikai (Chem. Eng. Japan), 16, 313 (1952)

2) Toyama, S., "Studies on the Table Feeder - Its Application to the Discharge of a Moving Bed -", Kagaku Kōgaku, 30, 170 (1966)

3) Muchi, I., and K. Miwa, "Discharge Rate of Particles from Table Feeder", J. of Society of Materials Sci., Japan, 16, 370 (1967)

4) Synge, J. L., and A. Schild, "Tensor Calculus", p. 162, Toronto Univ. Press (1949)

5) Iinoya, K., and K. Hotta, "Process Seigyo no Kiso (Fundamentals of process control)", p. 63, Asakura Co., (Japan), (1967)

6) Соколовский, В.В., "СТАТИКА СЫПУЧЕЙ СРЕДЫ" (1960) translated into Japanese by K. Saitō et al. Ōhm Co., (1964)

CHAPTER 6

ROTARY FEEDER

6.1 Introduction

A rotary feeder is a simple powder feeder which is widely used as the final control device of a particulate process. However, comparatively little is known of its static and dynamic characteristics. The discharge mechanism of this feeder is such that the particles flow into the feed chambers of the rotor and are discharged through the exit pipe after a half revolution. In view of this mechanism, it seems that the discharged powder flow rate will increase with the rate of revolution of the rotor until the flow rate becomes equal to the discharge rate from the hopper without the rotary feeder, when the flow rate could be expected to remain constant. However in actual operation the flow rate gradually decreases with increasing speed of rotation before reaching the discharge rate of the powder from the hopper. This is attributable to the fact that the discharge of powder from the rotor is not perfect, part of the powder being raised again by the rotor blade. This fact will be confirmed by high-speed photography.

In this chapter the discharge mechanism is discussed and the experimental results examined. In addition the relationship between the discharged-mass flow rate and the rate of revolution of the rotor is studied with particular attention to the use of actual poly-disperse powders. Step responses of the discharge rate are also obtained.

6.2 Prediction of the Volumetric Efficiency

6.2-1 Theoretical study

The following discussion is based on the assumptions that:

(1) The rotor space is fully filled with the powder.

(2) No powder crumbling in a block occurs in the discharge process.

When the rotational speed of the rotor is very high, the impact force of the rotor blade will obstruct the inflow of particles. Then assumption (1) will not be applicable. However this problem is not dealt with in this study. On the other hand, assumption (2) is not admissible in low-speed rotation. However in this case the powder in the rotor space will be discharged fully and the analytical results will not be affected by failure of the assumption.

Consider the coordinates r and θ shown in Fig. 6.1, together with a third coordinate z, shown in Fig. 6.2. A particle is constrained by the surrounding particles, such that the motion of the particle is represented by the following equation:

$$\frac{d^2 r}{dt^2} = r\omega^2 + g\cos\theta - \left\{\frac{S}{m} - g\sin\theta\right\}\mu_p - \frac{3}{4} C_D \frac{\dot{r}}{D_p} \frac{\rho_a}{\rho_p} \qquad (6.1)$$

where, m denotes the mass of the particle, and μ_p the inter-particle friction factor. S represents the Coriolis' force and is given by

$$S = 2m\,\omega\,\dot{r} \qquad (6.2)$$

C_D denotes the drag-coefficient and is usually represented by a complicated function of the Reynolds' number. However in this case the drag-coefficient C_D is approximated by the Stokes' equation:

$$C_D = \frac{24}{Re} = \frac{24\ \mu_a}{D_p\ \rho_a\ \dot{r}} \qquad (6.3)$$

When the particle diameter D_p is large Eq.(6.3) is not applicable. However, under these circumstances

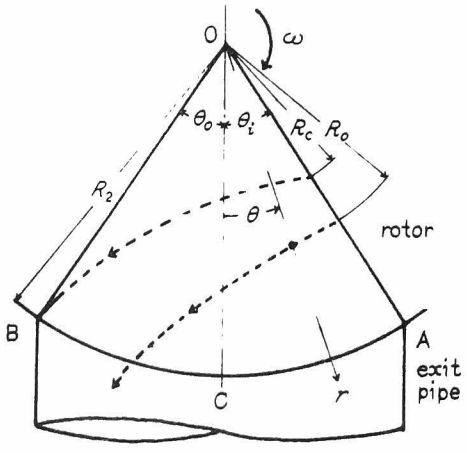

Fig.6.1 Trajectory of a particle in a rotary feeder

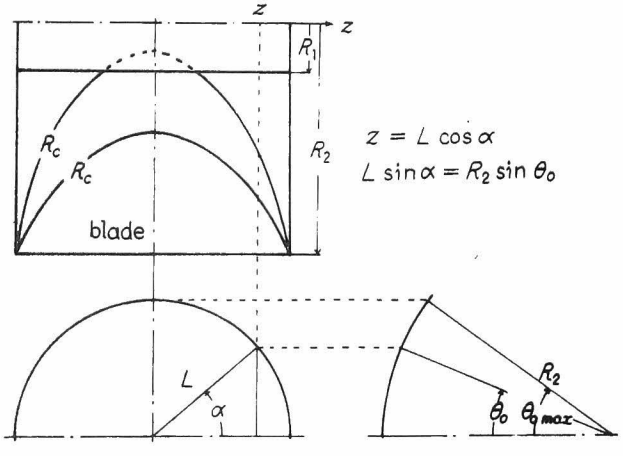

Fig.6.2 Relation between θ_0 and z

the fourth term of the right hand side of Eq.(6.1) is negligibly small, and Eq.(6.3) can be used[1].

When t = 0, the particle is on the line $\overline{OA}$ in Fig.6.1. The relation between the time t and the angle θ is represented by the following equation:

$$\theta = \theta i - \omega t \tag{6.4}$$

where θi is ∠AOC, which is constant. Substituting Eqs.(6.2 ~ 4) into Eq.(6.1), the following equation is obtained:

$$\ddot{r} + 2A\dot{r} - r\omega^2 = g\cos(\theta_i - \omega t) + \mu_p g \sin(\theta_i - \omega t) \tag{6.5}$$

where, $$A \equiv \mu_p \omega + 9\mu_a / D_p^{\,2} \rho_p \tag{6.6}$$

This differential equation is solved to yield

$$r(t) = C_1 e^{a_1 t} + C_2 e^{a_2 t} + C_3 \cos(\theta_i - \omega t) + C_4 \sin(\theta_i - \omega t) \tag{6.7}$$

where,

$$a_1 \equiv -A + \sqrt{A^2 + \omega^2}\ , \text{ and } a_2 = -A - \sqrt{A^2 + \omega^2} \tag{6.8}$$

By use of the initial condition: $r(0) = R_0$, $\dot{r}(0) = 0$, the integral constants $C_1 \sim C_4$ are determined, namely:

$$C_1 = \frac{1}{a_1 - a_2}\{-a_2 R_0 + (C_4\omega + a_2 C_3)\cos\theta_i - (C_3\omega - a_2 C_4)\sin\theta_i\} \tag{6.9}$$

$$C_2 = \frac{1}{a_1 - a_2}\{a_1 R_0 - (a_1 C_3 + C_4\omega)\cos\theta_i - (a_1 C_4 - C_3\omega)\sin\theta_i\} \tag{6.10}$$

$$C_3 = \frac{g(\mu_p A - \omega)}{2\omega(A^2 + \omega^2)} \tag{6.11}$$

$$C_4 = -\frac{g(\mu_p A - \omega)}{2\omega(A^2 + \omega^2)} \tag{6.12}$$

Now assuming that the trajectory of the particle is represented by Eq.(6.7), the volumetric efficiency of the rotary feeder may be obtained as follows.

At $\theta = -\theta_0$ ($\overline{OB}$ in Fig.6.1) or to put it in another way, at time t_0 given by

$$t_0 = (\theta_i + \theta_0)/\omega \qquad (6.13)$$

a certain particle will pass over the point B. The initial position R_c of this particle is given by

$$R_c = \frac{R_2 - C_5 e^{t_0 a_1} + C_6 e^{t_0 a_2} - C_3 \cos\theta_0 + C_4 \sin\theta_0}{(a_1 e^{t_0 a_2} - a_2 e^{t_0 a_1}) / (a_1 - a_2)} \qquad .....(6.14)$$

where,

$$C_5 \equiv \frac{1}{a_1 - a_2} \{(C_4\omega + a_2 C_3) \cos\theta_0 - (C_3\omega - a_2 C_4) \sin\theta_0\} \qquad (6.15)$$

$$C_6 \equiv \frac{1}{a_1 - a_2} \{(a_1 C_3 + C_4\omega) \cos\theta_0 - (a_1 C_4 - C_3\omega) \sin\theta_0\} \qquad (6.16)$$

Under some circumstances Eq.(6.14) may give values for R_c that are less than R_1, the inside radius of the rotor. However this is impossible physically, in which case R_c can be equated with R_1. Then the volumetric efficiency η of the rotary feeder is represented by the following equation:

$$\frac{\text{volume occupied by the discharged powder}}{\text{total effective volume of the rotor}}$$

$$= \frac{2\pi L(R_2^2 - R_c^2) - 2n\delta L(R_2 - R_c)}{2\pi L(R_2^2 - R_1^2) - 2n\delta L(R_2 - R_1)} \qquad (6.17)$$

where n is the number of the blades, δ is the thickness of the blade, and 2L is the width of the blade. When the exit hole is rectangular, Eq.(6.17) is applicable without modification. However, in the general case the exit hole is circular for convenient connection of a pipe. In this case, $\theta_0 (= \theta_i)$ is changed in the direction of z. Therefore, R_c and R_c^2 in Eq.(6.17) must be replaced respectively by the following expressions:

$$\overline{R_c} = \frac{1}{L}\int_0^L R_c dZ \quad , \text{ and } \quad \overline{R_c^2} = \frac{1}{L}\int_0^L R_c^2 \, dZ \qquad (6.18)$$

As shown in Fig.6.2, the relation between θ_0 and the coordinate z is represented by

$$\sin \theta_0 = \frac{L}{R_0}\sqrt{1 - (z/L)^2} \qquad (6.19)$$

$\overline{R_c}$ and $\overline{R_c^2}$ can be obtained by numerical integration of Eq.(6.18) using Eq.(6.19). Then the volumetric efficiency may be estimated by Eq.(6.17).

As far as the particle size is concerned in the discharge process, the size distribution must be taken into consideration. This is accomplished with Eq.(2.7), namely,

$$\overline{\eta} = \Sigma f(D_{pi})\ \eta(D_{pi}) \qquad (6.20)$$

6.2-2 Apparatus and experimental methods

The experimental set-up used for the measurement of the discharged mass flow rate from the rotary feeder is shown schematically in Fig. 6.3.

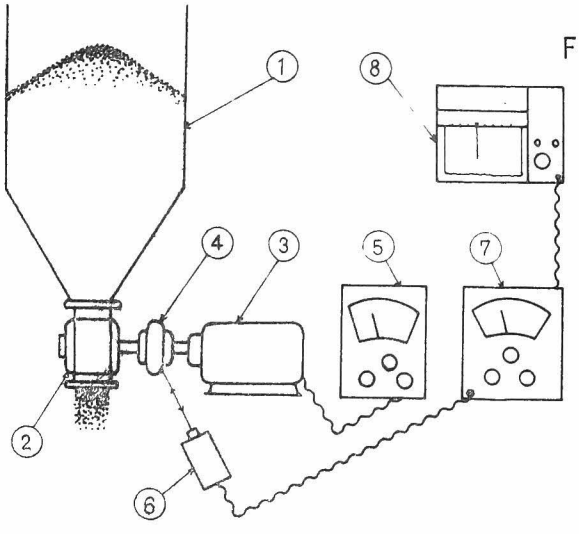

Fig.6.3 Schematic diagram of experimental arrangement

1. hopper
2. rotary feeder
3. VS-motor
4. coupling
5. controller
6. photo probe
7. amplifier
8. recorder

The pwoder flow rate is determined by sampling the powder for 20 ~ 60 seconds. The number of revolutions of the rotor during the test period is recorded through the photo-probe. When the rotational speed is very slow, the number of revolutions is determined by counting. The powder materials used are wheat, millet seeds, quartz sand No.8, quartz sand screened, and quartz sand-ultrafine. The properties of these powder materials are summarised in Table 6.1, where the inter-particle friction factor μ_p is calculated from the two-dimensional drain angle [2].

Table 6.1 Properties of the pwoder materials

material	density of particle ρ_p [g/cm^3]	bulk density ρ_B [g/cm^3]	drain angle (2-dimensional) [degree]	inter-particle friction factor $\mu_p = \tan\varphi$ [—]	angle of repose φ_r [degr]
Millet seed	1.31	0.789	41	0.87	33.0_4
Wheat	1.26	0.715	39	0.81	30.0
Quartz sand No. 8	2.64_5	1.234	74	3.50	38.3
Quartz sand screened	2.64_5	1.276	70.2	2.77	26.2_5
Quartz sand ultrafine	2.64_5	1.029	87~90	--	49.6

The size distributions of these powders are shown in Fig. 6.6. Two sets of rotary feeders, shown in Fig. 6.4, are examined in this study. When the quartz sand-ultrafine is used, a vibrator is installed at the hopper to prevent bridging of the powder.

Fig.6.5 shows the experimental installation for the measurement of particle trajectories. Transparent vinyl chloride boards were used in several parts to allow visual observation. Powder is poured into the feed space of the rotor, in such a way that a striped-pattern is made with vari-colored particles. The particle trajectories are recorded by a high-speed camera operating at 64 frames per second. The rate of revolution of the rotor becomes constant immediately after the feeder is started, the time lapse being determined by counting the number of frames.

6.2-3 Results and discussion

One of the results obtained by high-speed photography is shown in Fig.6.7. From such photographs the positions of the colored particles were measured and compared with the theoretical trajectories. The results are shown in Fig.6.8. The initial position R_0 required for the theoretical calculation was determined from the striped-pattern just before the exit. The coincidence between the theoretical and experimental trajectories for the case of the millet seeds is satisfactory. Differences between the theoretical and experimental trajectories

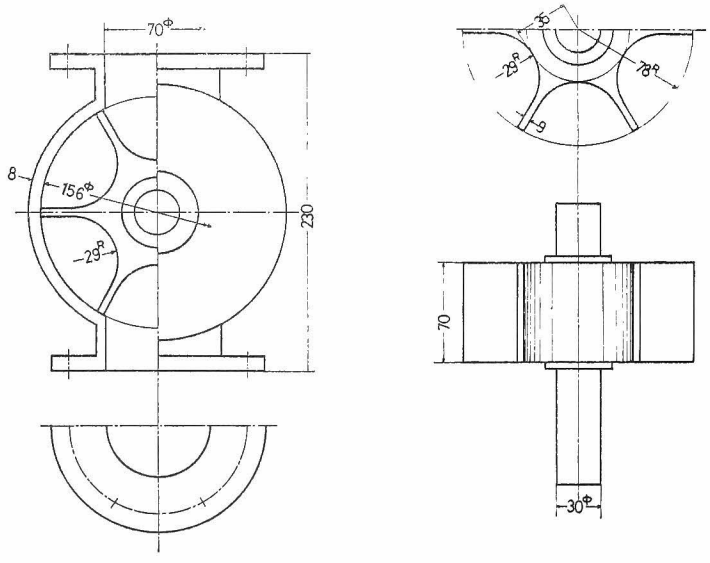

(a) 156φ rotary feeder

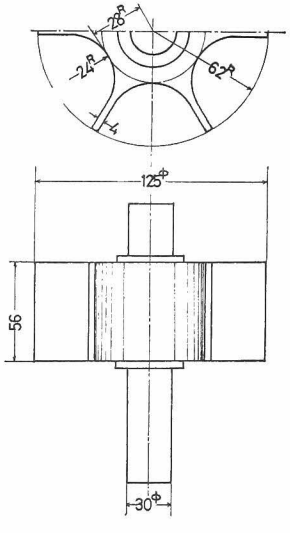

(b) 125φ rotary feeder (rotor)

Fig. 6.4 Rotary feeder

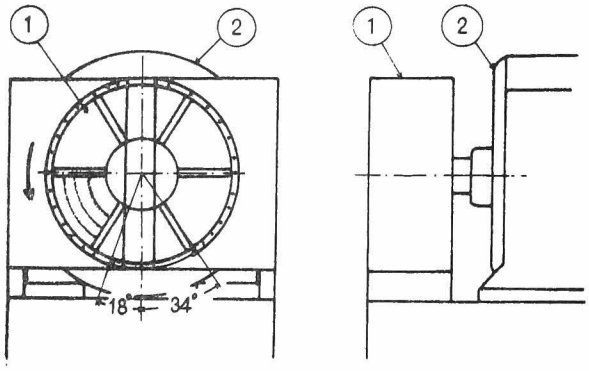

Fig.6.5 Schematic diagram of a rotary feeder for measurements of particle trajectories

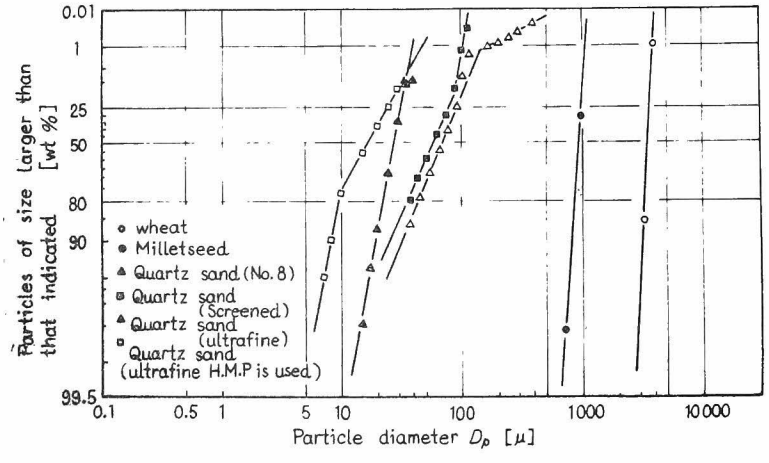

Fig.6.6 Size distribution of solid materials (RRS)

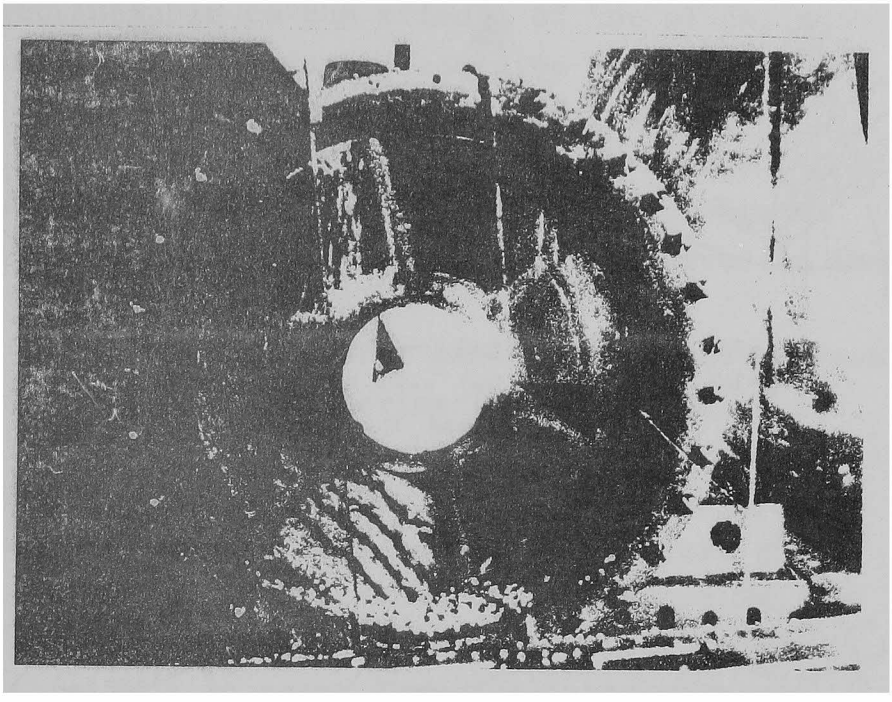

Fig.6.7 Particle trajectories

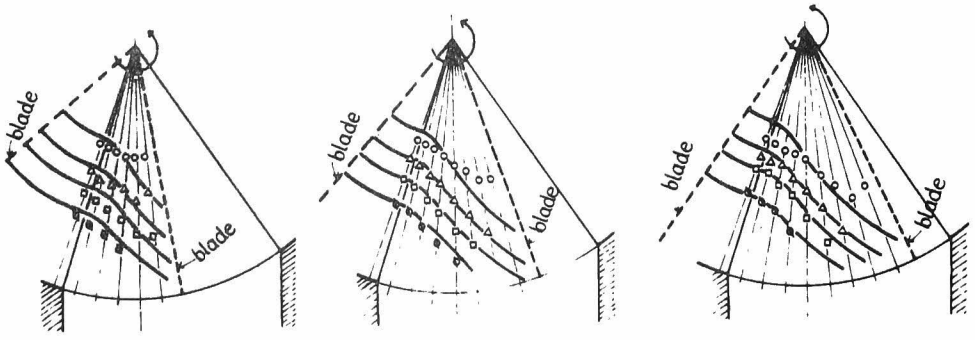

○ R_o = 2.60 [cm] □ R_o = 3.98 [cm] —— theoretical curve
△ R_o = 3.41 [cm] ▽ R_o = 4.71 [cm] - - - - Position of blade

(a) Millet seed, N = 72 rpm

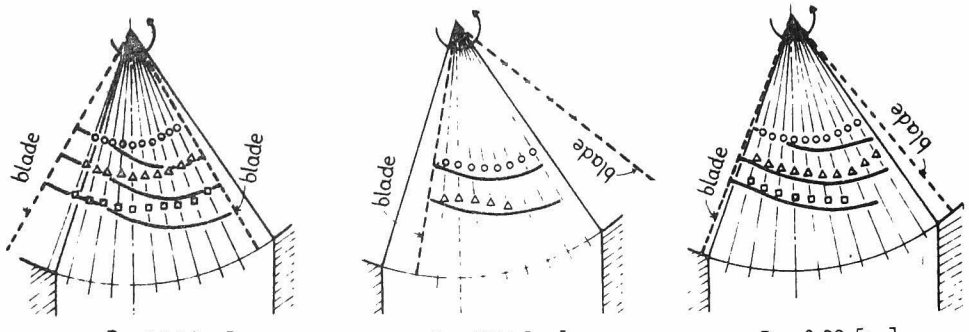

○ R_o = 3.06 [cm]
△ R_o = 3.85 [cm]
□ R_o = 4.71 [cm]
N = 83 [r.p.m]

○ R_o = 3.74 [cm]
△ R_o = 4.71 [cm]
N = 103.5 [r.p.m]

○ R_o = 3.22 [cm]
△ R_o = 4.13 [cm]
□ R_o = 4.79 [cm]
N = 103.5 [r.p.m]

—— theoretical curve - - - - position of blade

(b) Quartz sand

Fig.6.8 Particle trajectories

in the neighborhood of the center and of the blade are attributable to the effects of the blade, such as electrostatic force or adhesive force. However this effect decreases with the progress of the discharge process. Therefore the estimation of the volumetric efficiency will not be affected. Powder crumbling in a block was not observed in this case.

In the case of quartz sand, coincidence between the theoretical and experimental trajectories is good for high-speed revolution, but the agreement is not good for low-speed revolution. At low speeds the powder does not fall even if it is just above the exit hole. However once discharge begins, the whole of the powder is discharged instantaneously. From this fact it seems that the inter-particle friction factor μ_p varies with the progress of the discharge process. The adhesive force between the particles and the blade also affects the process.

These experiments on powder trajectories also confirm the hypothesis that part of the powder is raised up again by the blade at high-speed revolution.

Figs.6.9 and 6.10 show some of the results on the volumetric efficiency η, and $\omega\eta$, respectively. Coincidence between the theoretical and experimental results up to 100 rpm is satisfactory. However, at higher speeds of revolution, the experimental data are smaller than the theoretical values, and decrease with increasing speed of revolution. This can be attributed to:

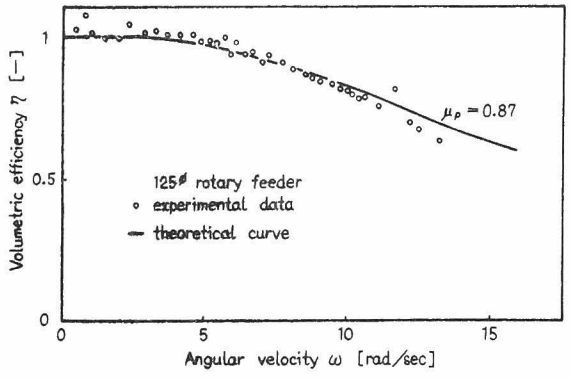

(a) Millet seed

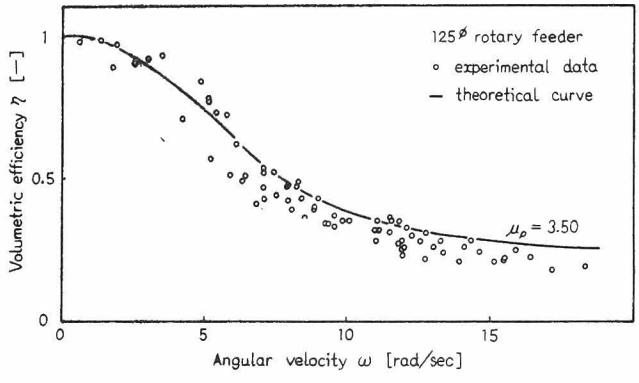

(b) Quartz sand (No.8)

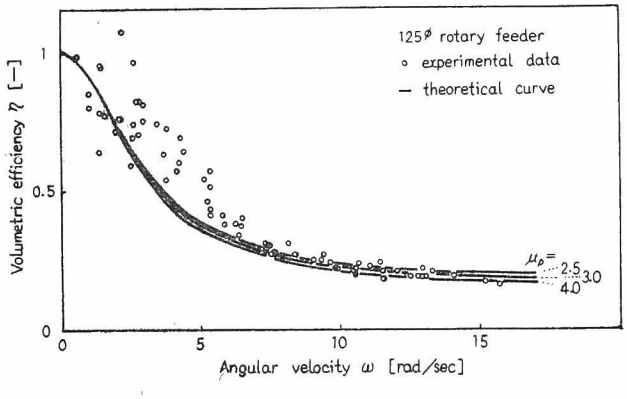

(c) Quartz sand (ultrafine)

Fig.6.9 Volumetric efficiency of rotary feeder vs. angular velocity

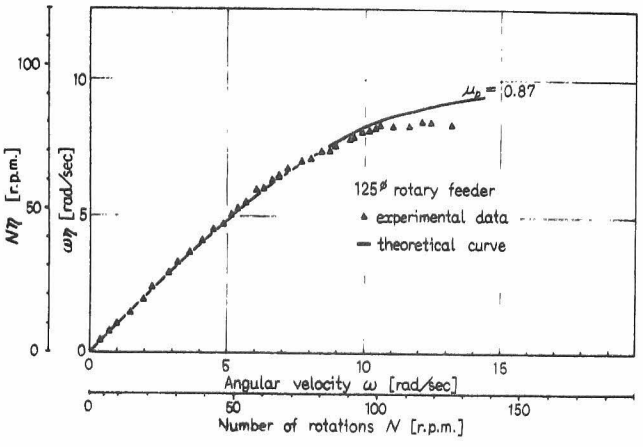

Fig.6.10
$\omega\eta$ vs. angular velocity

(a) Millet seed

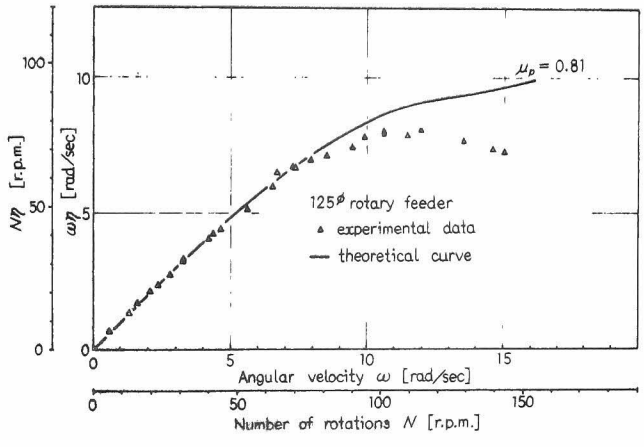

(b) Wheat

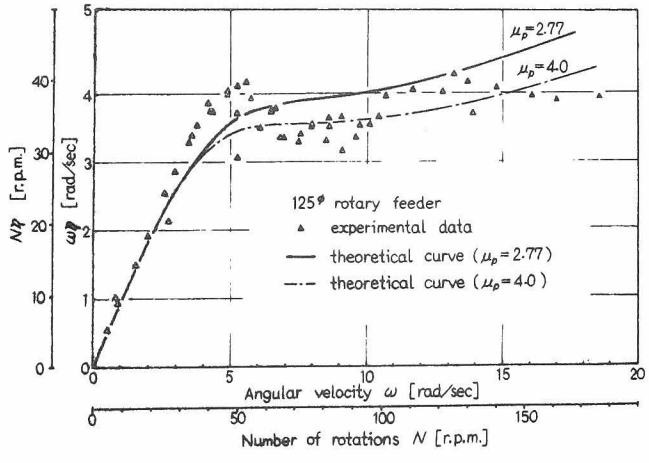

(c) Quartz sand (screened)

(1) blade action; the impact force of the blade obstructs the inflow of the powder. Under these circumstances assumption (1) fails.

(2) variation of the inter-particle friction factor; centrifugal force and Coriolis' force compress the powder, and the effective friction factor becomes large.

A theoretical curve calculated with large μ_p is shown for reference purposes in Figs. 6.9-c and 6.10-c.

The nature of the blade action is an interesting problem, but in practice the rotary feeder as the final control device should be used at low speeds of revolution in which case the effect of blade action is negligible. The maximum angular velocity ω will be approximated by $\sqrt{g/R_2}$.

The following discussion will be concerned with the effect of particle size on $\omega\eta$. Fig.6.11 shows the calculated results for the case $\mu_p = 3.5$. It is found that the effect is large when the particle size is small but that it becomes smaller as the particle size increases. This observation means that the drag force by air is smaller than any other force in this size range. Therefore, the effect of the particle size may offer no problem for systems using large particles. On the other hand, systems using small particles must be dealt with according to the method proposed in §2.2 or Eq.(6.20).

Fig.6.12 shows the calculated results concerning the effect of the dimension of the rotor on $\omega\eta$. From

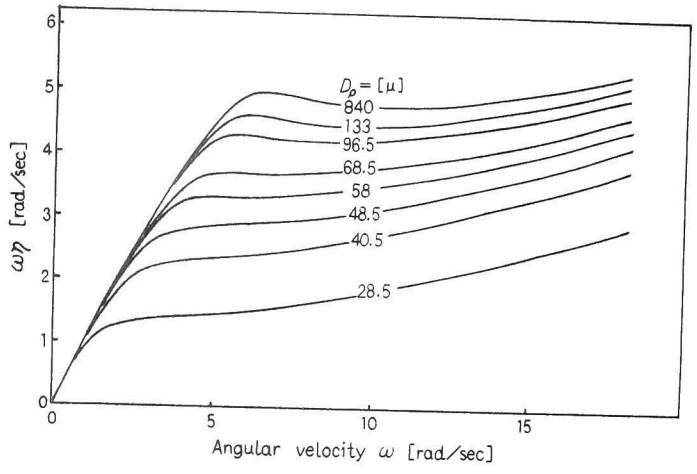

Fig.6.11 Effect of particle diameter on ωη

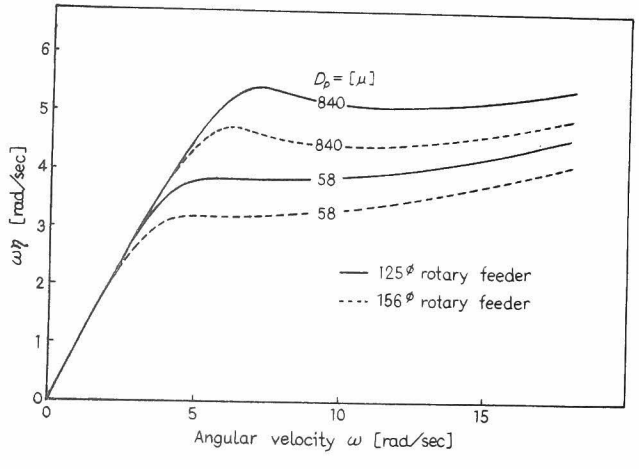

Fig.6.12 Effect of the dimension of rotor on ωη

the figure, it is seen that the volumetric efficiency decreases with increasing rotor diameter.

6.3 Step Response

Step responses of the discharged mass flow rate were studied by use of Impact-Line mass flow meter. Typical result is shown in Fig.6.13. Fluctuations in the instantaneous mass flow rate are fairly large. However, the variation of the mean of the mass flow rate is approximated by a first-order time delay. The time constant for the rotary feeder used here was found to be in the range of 4.5 ~ 5.5 sec.

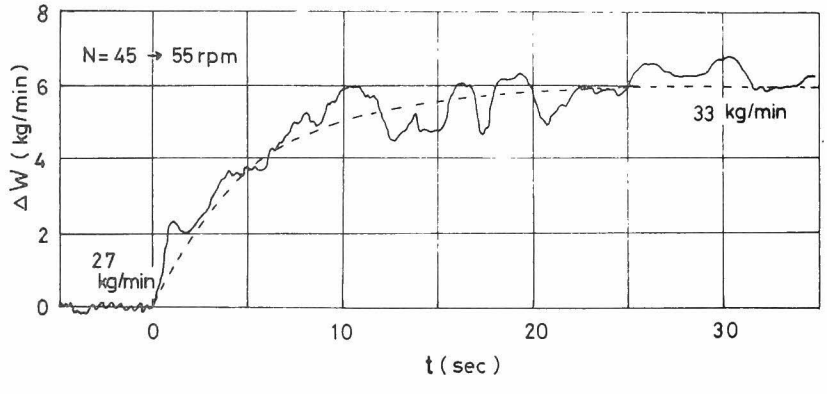

Fig.6.13 Step response of a rotary feeder

$$\Delta W = 6\{1 - \exp(-t/5.4)\}$$

6.4 Conclusion

In view of the study on the rotary feeder described above, it can be concluded that:

1. The discharge mechanism of this feeder can be represented by the use of particle mechanics, in which Coriolis' force and the frictional force between particles are taken into consideration.

2. The volumetric efficiency can be estimated by using the theoretical equation derived from an analysis of the discharge mechanism.

3. When systems involving fine particles are dealt with, the particle size distribution must be considered.

4. The inter-particle friction factor μ_p will vary with the progress of the discharge process. However, the whole discharge process observed during this study has been explained with a constant μ_p obtained by determination of the two-dimensional drain angle.

5. The volumetric efficiency decreases with increasing rotor diameter.

6. The dynamic characteristic of this feeder is that of a first-order time delay.

For practical application of this feeder as the final control means low speed operation is recommended because of the higher stability and the linear property of the static characteristics.

Nomenclature

C_1, C_2, C_3, C_4, C_5, C_6= constants

C_D drag coefficient

D_p particle diameter

$f(D_{pi})$ particle size distribution on the mass basis

L (width of blade)/2

m mass of a particle

n number of blades

N number of revolutions per unit time

R_0 initial position of a particle

R_1 inner radius of rotor

R_2 outer radius of rotor

R_c critical radius for a drained particle

S Coriolis' force

V total volume of a rotor section

r, θ, z coordinates

δ	thickness of a blade
η	efficiency of a rotary feeder
θ_i, θ_0	angles in Fig.6.1
μ_f	viscosity of air
μ_p	internal friction factor of particles
ρ_B	bulk density of particles
ρ_f	density of air
ρ_p	particle density
φ	two-dimensional drain angle
ω	angular velocity

References

1) Iinoya, k. and T. Yoneda: Res. Assoc. Powder Tech., Japan, 1, 48 (1964)

2) Isomura, I. and H. Igarashi, "On the Measurement of Angle of Repose", Res. Assoc. Powder Tech., Japan, 2, 329 (1965)

PART III

PRIMARY MEANS

MEASUREMENTS OF THE MASS FLOW RATES IN GAS-SOLIDS TWO-PHASE FLOW

CHAPTER 7

MEASUREMENT OF GAS FLOW RATE BY USE OF A HORIZONTAL DIFFUSER

7.1 Introduction

The measurement of the mass flow rate of solids, or of the flow rate ratio for solids to gas in a two-phase system is complicated by the fact that the measured value such as pressure drop along the pipeline is also a function of gas flow rate or velocity. Therefore the gas flow rate must be measured simultaneously by an independent method. A procedure is available for measuring the gas flow rate after separation of the solids from gas, but clearly it is desirable to make the measurement on the two-phase system with as little interference as possible to the flow pattern.

Farbar[1], Barth et al[2] Goto et al[3], and Sakata[4],

examined the possibility of using a diffuser to make such measurement on a two-phase system. They concluded that pressure-recovery in the diffuser decreased with increasing solids rate. However the manner in which the error varies with the distance along the diffuser has not yet been determined, as was mentioned by Sakata.

This chapter will examine the nature and extent of the error, and if it is the case that the error offers a problem, methods for estimating the error theoretically, and design methods for minimizing the error. In particular, it is shown that there is a design method for reducing the error to zero. Following the suggestion of Goto et al, the investigation is carried out for the horizontal part of a pneumatic conveyor.

7.2 Theoretical Approach

If it is assumed that the particles are uniformly suspended, and in rather low concentration, the wall-friction of particles may be regarded as negligible in a diffuser[2),3)]. Therefore, the following momentum balance equation is obtained.[5)]

$$- d P_m = \rho_a u du + m\rho_a u dv \qquad (7.1)$$

As far as Eq.(7.1) is concerned, the right hand side may have to be modified to account for the efficiency of conversion of momentum into pressure. This may

not be necessary, however, for dealing with the relative error, because the efficiencies for the first term and the second term may be nearly equal. The relative error is defined by the following equation:

$$E = m \frac{\int_{v_0}^{v} udv}{\int_{u_0}^{u} udu} = m \frac{\int_{0}^{x} uv'dx}{\int_{0}^{x} uu'dx} \qquad (7.2)$$

where, u_0 and v_0 denote the gas velocity and the particle velocity at the inlet of the diffuser, respectively. The prime represents the derivative with respect to the coordinate x. In this equation, the denominator shows the pressure recovery for gas flow alone, and the numerator shows the additional recovery by the solids momentum.

Assuming the incompressibility of gas flowing in the diffuser section, the velocity u can be expressed by the following equation;

$$u = \frac{u_0}{(1 + \alpha x)^2} \quad , \quad \alpha = \frac{\tan \theta}{r} \qquad (7.3)$$

where 2θ is the diverging angle of the diffuser, and r is the inside radius of the inlet tube.

On the assumption that the wall-friction of particles may be neglected in the diffuser, the

particle velocity v is given by the following equation of motion[5]:

$$v' = \frac{C_1(u - v) + C_2(u - v)^{5/3}}{v} \tag{7.4}$$

where, C_1 and C_2 are constants which are given by

$$C_1 \equiv 18 \frac{\mu_a}{D_p^2 \rho_p} \tag{7.5}$$

and,

$$C_2 \equiv 3 \frac{\mu_a}{D_p^2 \rho_p} \left\{ \frac{D_p \rho_a}{\mu_a} \right\}^{2/3} \tag{7.6}$$

In Eq.(7.4), the drag coefficient appeared in the study of Пашацкий et al[5] is used. However, the results obtained in this study are valid even in cases where other drag coefficients[6] are used. Fig.7.1 shows the velocities u, v and the trend of the relative error calculated by numerical integration using Schiller and Naumann's[7] drag coefficient. Particle velocity v_0 at the inlet is smaller than the corresponding gas velocity u_0, because the particles have been affected by wall friction in the straight pipe section just before the diffuser. On entering the diffuser, the particles are accelerated by the

gas, and the particle velocity v increases until it is equal to the gas velocity u. Then, the particles are decelerated by the

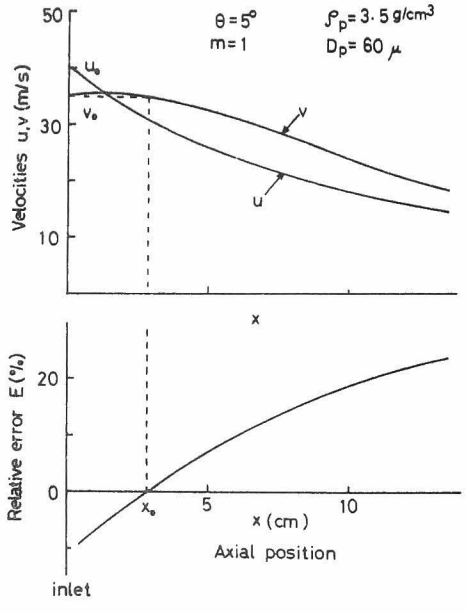

Fig.7.1 Velocities u, v and the trend of the relative error (numerical integration)

gas. After v is reduced to the initial velocity v_0, it approaches gradually to the gas velocity u. On the other hand, the relative error monotonously increases with the coordinate x. This trend of the error is analytically explained by Eqs.(7.2), (7.3) and (7.4).

From Eq.(7.2), it can be seen that the error is zero at $x = x_0$ or $v = v_0$;

$$Ex_0 = m \frac{\int_{v_0}^{v_0} udv}{\int_{u_0}^{u} udu} = 0 \qquad (7.7)$$

Applying L'Hospital's theoreom to Eq.(7.2), the limiting value of the error as $x \to \infty$ is given by the following equation;

$$\lim_{x\to\infty} E = m \lim_{x\to\infty} \frac{uv'}{uu'} = m \qquad (7.8)$$

These results can be summarized as follows: The relative error caused by the solids added to the gas flow is a monotone-increasing function of the coordinate x. The error is zero at x_0, negative for $x < x_0$, and positive for $x > x_0$. Further, it never exceeds the value of the mass flow ratio m.

Therefore, if the position x_0 can be estimated in some way, the gas flow rate in suspensions may be measured very accurately. Now, assuming that x_0 is determined, the residual error arising from the difference between the measuring point x and x_0, may be estimated from the gradient of the error curve at the position x_0. Taking the equation $E_{x_0} = 0$ into consideration, the following equation holds in the neighborhood of x_0;

$$E = m \frac{\int_0^x uv'dx}{\int_0^x uu'dx} \simeq 2m \frac{u_{x_0}}{u_0^2 - u_{x_0}^2} (v_0 - v) \quad (7.9)$$

If the relation; $v_0 - v \simeq |v'_{x_0}|(x - x_0)$ is substituted in the above equation, Eq.(7.9) reads;

$$E \simeq 2m \frac{u_{x_0}}{u_0^2 - u_{x_0}^2} |v'_{x_0}| (x - x_0) \quad (7.10)$$

Note that $E_{x_0} = 0$, and hence the differential form of this equation is

$$\frac{dE}{dx}\Big|_{x_0} \simeq 2m \frac{u_{x_0}}{u_0^2 - u_{x_0}^2} |v'_{x_0}| \quad (7.11)$$

Eliminating v'_{x_0} by use of the equation of motion (7.4), the more explicit form of Eq.(7.11) is obtained as;

$$\left.\frac{dE}{dx}\right|_{x_0} \simeq 36m \frac{\mu_a}{D_p^2 \rho_p} \left[1 + \frac{1}{6}\left\{\frac{D_p \rho_a}{\mu_a}(v_0 - u_{x_0})\right\}^{2/3}\right] \frac{u_{x_0}(v_0 - u_{x_0})}{v_0(u_0^2 - u_{x_0}^2)} \quad \cdots\cdots\cdots (7.12)$$

If the position x_0 is determined, u_{x_0} can be calculated from Eq.(7.3). Therefore, the gradient of the error is calculable with Eq.(7.12)

Now, the second term in the square brackets of the above equation is smaller than unity when $v_0 D_p < 3 \times 10^4$ [cm/sec. microns] in the case of pneumatic conveying. On the other hand, when $v_0 D_p > 3 \times 10^4$, the gradient of the error is fairly small. In practical applications, therefore, the second term in the brackets may be regarded as negligible. From this fact and the relation; $u_0 > v_0 > u_{x_0}$, Eq.(7.12) may be simplified as follows;

$$\left.\frac{dE}{dx}\right|_{x_0} \lesssim 18\, m \frac{\mu_a}{D_p^2 \rho_p v_0} \qquad (7.13)$$

This equation shows that the error presents a problem when the inertial force of a particle is smaller than the viscous-force of the fluid.

The next problem is to estimate the position at which the error vanishes. From the above results concerning the gradient of the error, the second term of Eq.(7.4) is seen to be negligible. Then Eq.(7.4) may be rewritten as

$$v' = C_1 \, (u/v - 1) \tag{7.14}$$

A first approximation by Picard's method[8] gives

$$v = v_0 + C_1 \left[\frac{1}{v_0} \left\{ \frac{u_0}{\alpha} - \frac{u_0}{\alpha(1 + x)} \right\} - x \right] \tag{7.15}$$

When the velocity v given by this equation is substituted into Eq.(7.14), an analytical solution with higher accuracy will be obtained. However, the result is very complicated, and proved to be useless in practice.

Now, the equation for x_0 is obtained from Eq.(7.15) where $v = v_0$:

$$\alpha x_0 = \frac{1 - \phi_0}{\phi_0} \quad , \text{ where, } \quad \phi_0 \equiv \frac{v_0}{u_0} \tag{7.16}$$

This equation shows that the first approximation of x_0 is determined by the dimensions of the diffuser and the velocity ratio ϕ_0. The characteristics of

the powder are not included explicitly in this equation.

7.3 Apparatus and Experimental Procedure

In this experiment, a pneumatic conveyor line operated under negative-pressure is used. The experimental set up is shown in Fig. 7.2. Two cyclones are installed for recovery of the solids. In the downstream side of this conveyor, there are installed a Western type Pitot tube, a flow-control valve, and a bag-filter. The diffusers used are shown in Fig. 7.3. Their diverging angles are 5°, 7°, 10° and 15°, respectively. The selected diffuser is placed in the horizontal section of the piping allowing the appropriate approach length. In order to charge the solid particles into the conveyor, a table feeder is used.

Table 7.1 Properties of the powder materials

materials	mass median dia. D_{p50} [microns]	mean particle dia. $\bar{D}_p$ [microns]	density of a particle ρ_p [g/cm^3]
Quartz sand No.8	51	45	2.65
Glass beads	55	52	2.42
Vinyl Chloride	115	108	1.41
Flour	57	28	1.44
Quartz sand No.5	380	295	2.65

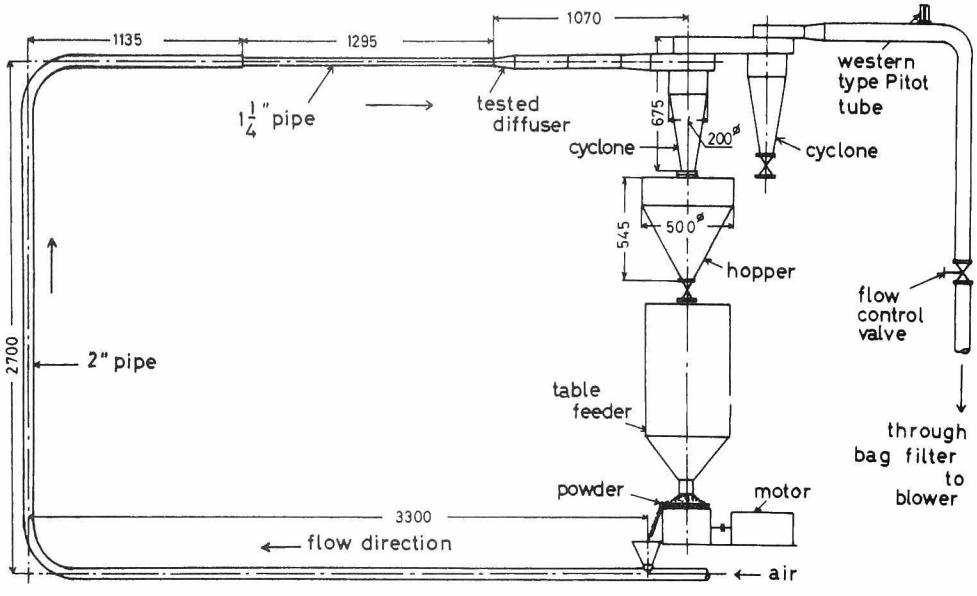

Fig.7.2 Schematic diagram of the experimental setup

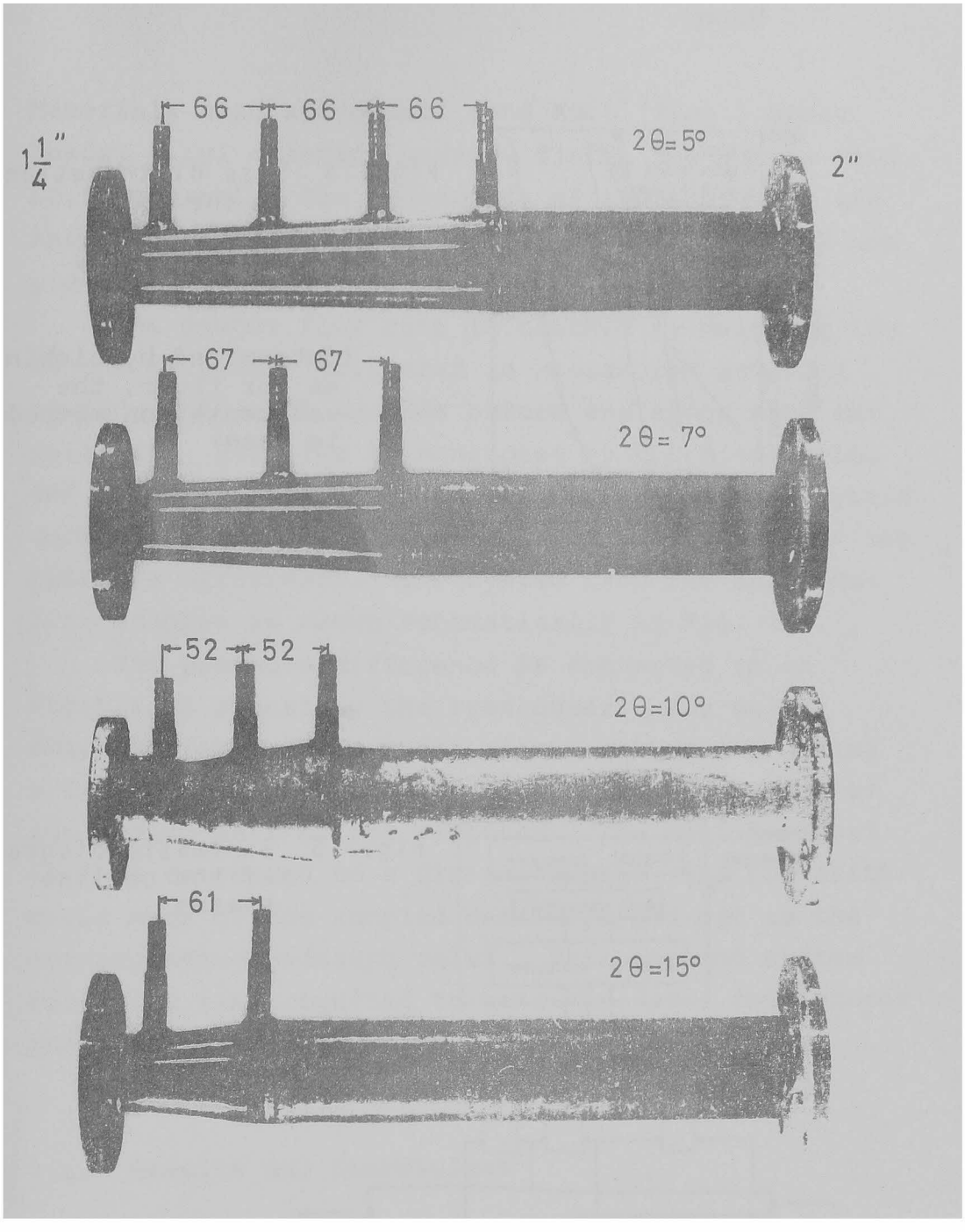

Fig.7.3 Diffusers used in the experiments

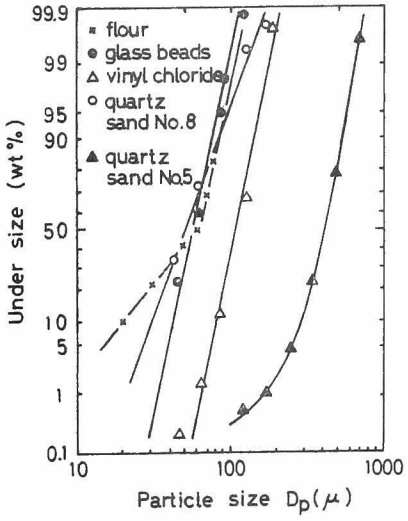

Fig.7.4 Size distribution of the solid materials (log-normal)

(determined by sieving; as for flour, the sedimentation method is used)

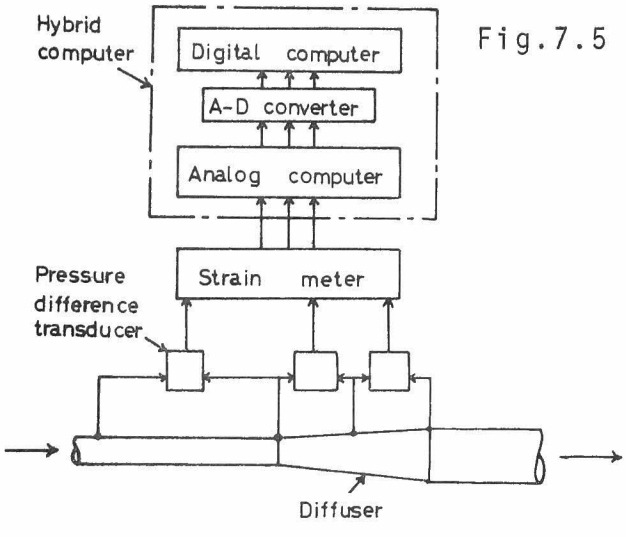

Fig.7.5 Schematic diagram of the on-line system

Materials used are quartz sand No.8 (fine), glass beads, vinyl chloride powder, flour, and quartz sand No.5 (coarse). The properties of these powders are shown in Table 7.1, and their size distributions are presented in Fig. 7.4.

The powder flow rate is checked by weighing the amount of powder collected in a measured sampling period of 15 ~ 200 seconds before and after each experiment. Air flow is monitored by the Pitot tube, and strain-gauges, transducers, and an on-line hybrid computer (CLAOP 2000) are used for measurement of the pressure difference. The system used for these on-line studies is shown schematically in Fig. 7.5.

The pressure difference is converted to an electrical signal by the transducer. Any noise, which is taken to be those signal components having a frequency higher than 10 H_z, is cut off by use of the analog part of the computer. The analog signal is then converted to a digital signal, and the arithmetic mean of the sampled data is typed out as the corresponding pressure value. This on-line system saves the time required to take the data, and reduces personal errors.

7.4. Results and Discussions

The analytical values calculated by Eq.(7.13) are compared with the results of the numerical integration obtained by the digital computer (FACOM 230-60). Fig.7.6 shows a set of the results on the gradi-

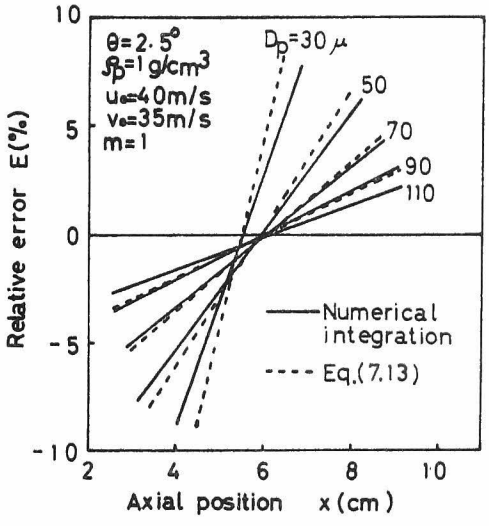

Fig.7.6

Comparison between the gradient of the error obtained by numerical integration and that calculated by Eq.(7.13)

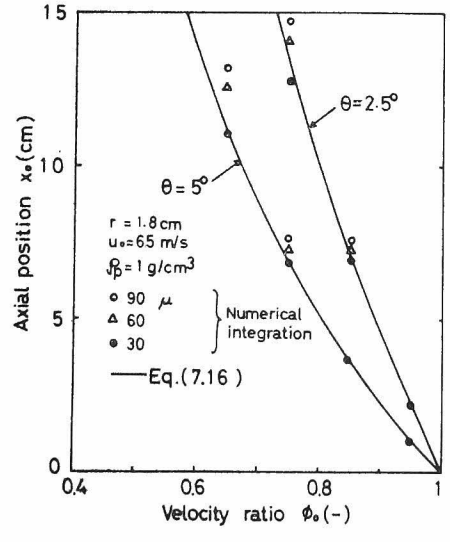

Fig.7.7

Comparison between x_0 calculated by Eq.(7.16) and that obtained by numerical integration

ent of the error. When particle size is small, the right hand side of Eq.(7.13) gives a little larger value than that calculated numerically. It is, however, sufficient as far as the estimation of the magnitude of the error is concerned. Fig.7.7 shows the comparison between x_0 calculated by Eq.(7.16) and x_0 obtained by numerical integration. When particle size is large, the coincidence of the analytical result and numerical one is not good. The disagreement is not serious, however, because the gradient of the error itself is very small in this case.

The relative error E has been defined in relation to the pressure difference measurements. Now, the corresponding relative error for measuring the gas flow rate is introduced as follows;

$$e \equiv \frac{Q_m - Q}{Q} \tag{7.17}$$

where, Q_m is the flow rate estimated by use of the pressure difference ΔP_m, and Q is the actual flow rate of the gas. As the pressure difference is in proportion to the square of the gas flow rate, Eq. (7.17) may be rewritten as:

$$e = \sqrt{\Delta P_m / \Delta p_a} - 1 \simeq \frac{1}{2}E \tag{7.18}$$

That is, the error e for measuring the gas flow rate is about the half the error E.

The results presented in Fig.7.8 indicate the magnitude of the error. Calculated values are shown by lines. The mean particle diameters defined by the following equation are used in the calculations.

$$\bar{D}_p = \sqrt{\frac{1}{\sum_i f_i / D_{pi}^2}} \qquad (7.19)$$

When the particle size distribution is log-normal, Eq.(7.19) is equivalent to

$$\bar{D}_p = \ln^{-1}\left(D_{p50} - \frac{\sigma^2}{2}\right) \qquad (7.20)$$

where, $\sigma = \ln D_{p84} - \ln D_{p50}$. The mean particle diameters of the quartz sand No.8, the glass beads, and the vinyl chloride powder are calculated using this equation. The particle velocity v_0 and the velocity-ratio ϕ_0 are calculated from the pressure difference measured at the straight pipe section just before the diffuser[9]. The variation of these values in the experiments made under constant dynamic pressure, is so small that the mean values are used.

The calculated values for the quartz sand No.8 and the flour are fairly large as shown in b) and c) of Fig.7.8. These differences between the experimen-

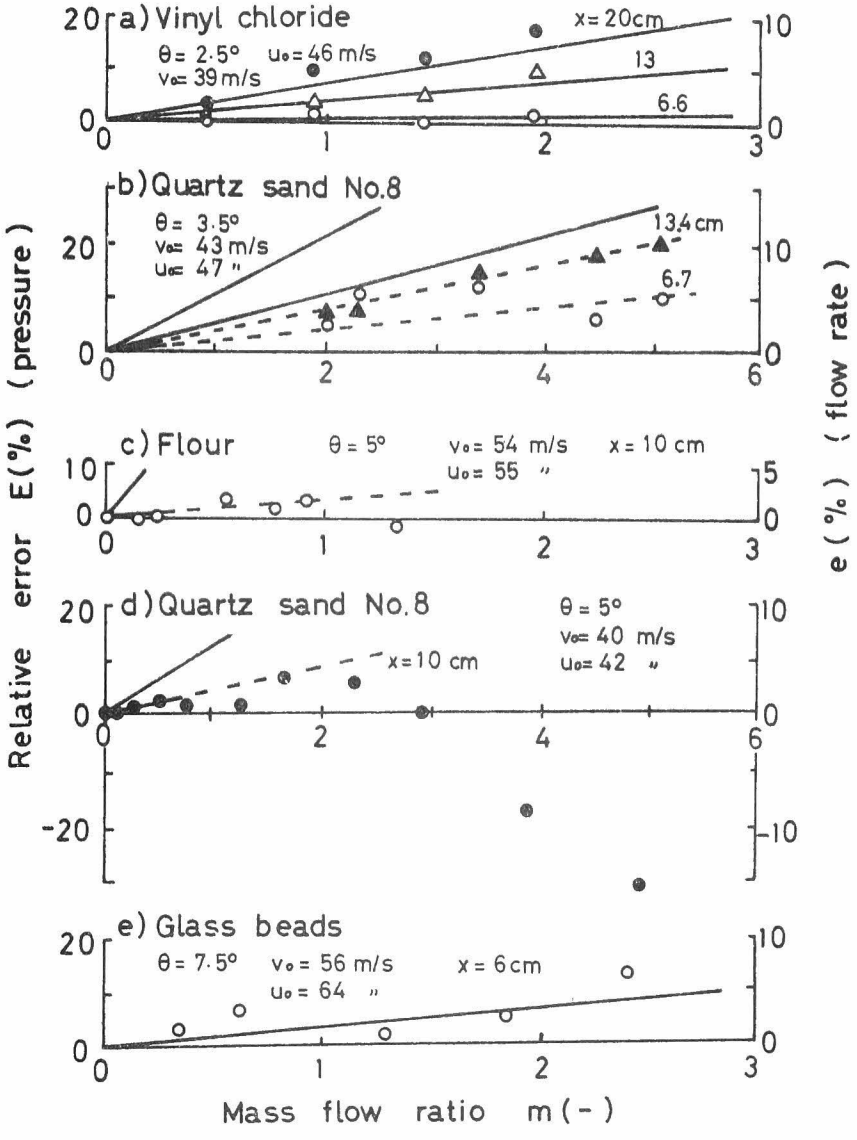

Fig.7.8 Relative error as a function of mass flow ratio

———— calculated by Eq.(7.13)
- - - - calculated as $\bar{D}_p$ = 70 μ for the quartz sand No.8, and $\bar{D}_p$ = 90 μ for the flour.

The symbols indicate experimental values.

tal and the theoretical results may be attributable to the agglomeration of the finer particles[10]. For reference, the mean particle diameter determined by the reverse calculation are, approximately, 70 and 90 microns for quartz sand No.8 and flour, respectively. In the case of the vinyl chloride powder and the glass beads, the calculated errors agree with the experimental data, as shown in a) and e) of Fig.7.8. In these cases, it is assumed that agglomeration has not occurred, because the vinyl chloride particles are fairly large on the one hand and the glass beads have good dispersibility on the other.

Fig.7.8-d) shows some of the results obtained using diffuser III ($\theta = 5°$). In this case, the error becomes negative with increasing particle velocity v_0 and mass flow ratio m. This phenomenon may arise from the separation of the fluid from the wall*). As the flow disturbance is aggravated by the particles, the separation occurs more readily. When the separation sets in, pressure recovery becomes smaller, even though the dynamic pressure is constant. When the diverging angle is fixed, this phenomenon occurs more easily at smaller mass flow ratios as the particle velocity becomes higher. As shown in Fig.7.8-e),

---

*) If we assume that this phenomenon arises from the failure of original assumption, that the wall-friction of the particles is negligible in the diffuser, we cannot explain the fact that the phenomenon is not observed when the diffuser with small diverging angle is used.

however, this phenomenon cannot be seen in the experiments with smaller mass flow ratio and lower particle velocity, even when $\theta = 7.5°$. Further, this phenomenon depends on the shape of the particle, and occurs more readily for quartz sand No.8 than for glass beads.

Fig.7.9 shows the experimental results proving the existence of a position x_0 at which the relative error is zero. Calculated values $x_{0,calc.}$ are also indicated in this figure. From these results, it is found that the coincidence between the experimental and the calculated x_0 is very satisfactory. Fig.7.9-c) shows the experimental results obtained when the measuring position x is shorter than the x_0 estimated by Eq.(7.16). In this case, the error is negative as estimated by the theory. These data are similar to that of Farbar, Barth et al, Goto et al and Sakata.

The following discussion is concerned with the effects of powder properties on the magnitude of the error. The difference in the magnitude of the error obtained by several authors using the coarse particles, may arise from differing values of $(x-x_0)$. That is, the error can be fairly large, even if the coarse particles are used. The equivalent difference $(x-x_0)$, which gives rise to an error of equal magnitude for the systems 1 and 2, is given by Eq.(7.21), which is developed from Eq.(7.13).

$$\frac{(x - x_0)_2}{(x - x_0)_1} = \left\{\frac{D_{p2}}{D_{p1}}\right\}^2 \cdot \left\{\frac{\rho_{p2}}{\rho_{p1}}\right\} \cdot \left\{\frac{v_{02}}{v_{01}}\right\} \qquad (7.21)$$

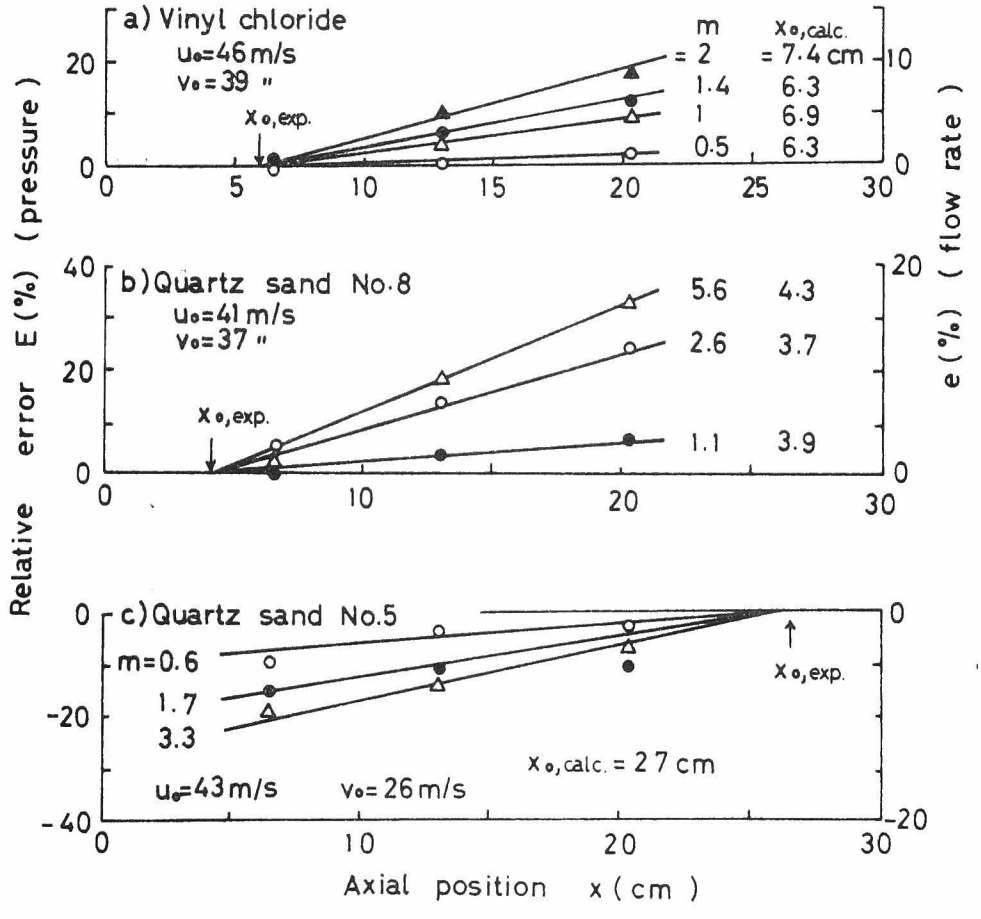

Fig. 7.9 Relative error as a function of axial position

Note: x_0 indicates the position at which the error vanishes. The values of $x_{0,\,calc.}$ are determined by use of Eq. (7.16).

In this equation, as the particle velocity v_0 is limited by the gas velocity, the effect of the powder properties on v_0 is small. However, the particle diameter D_p and the density ρ_p are independent of the flow conditions. The error involved in an experiment using coarse and heavy particles may, therefore, be smaller, when the difference of $(x-x_0)$ is kept the same, than in the case of fine, light particles. However, a large difference $(x-x_0)$ may cause a large error, even if heavy and coarse particles are investigated.

Summarizing the above discussion, the published data for large particles, and the results of this study for small particles, have been explained consistently taking into account the nature of the variation in the magnitude of the error and the fact that there is a position at which the error vanishes. Eq.(7.8), showing that the error does not exceed the mass flow ratio, will prove useful when a low mass flow ratio system as a dust collector is involved. The remark by Goto et al that the larger the diverging angle is, the smaller the error will be, may not be very important in the design of the diffuser. It may be more desirable to design the diverging angle less than 7°. In the system using large particles, the velocity ratio ϕ_0 is constant[11,12] without recourse to the mass flow ratio m and the gas velocity u. The position x_0 can, therefore, be estimated knowing the properties of the particles and the dimensions of the diffuser.

7.5 Conclusion

From the study in this chapter on the measurement of the gas flow rate in gas-solid suspensions by use of a diffuser, it is concluded that:

1. The relative error for the measurement is a monotone-increasing function of the measuring position, and the value of the error approaches that of the mass flow ratio.

2. There esists a position at which the error vanishes. This position, x_0, can be estimated by using Eq.(7.16).

3. The residual error, when the measuring position does not coincide with x_0, is estimable with Eq. (7.13).

In general, the error may be large in systems involving fine and light particles. In case of coarse and heavy particle systems the error may also be large, if the above remarks are not taken into consideration.

Nomenclature

C_1, C_2	constants, Eqs.(7.5) and (7.6)
D_p	particle diameter
$\bar{D}_p$	mean particle diameter, Eqs.(7.19) and (7.20)
E	relative error defined by Eq.(7.2)
e	relative error defined by Eq.(7.17)
f_i	particle size distribution
ΔP_m	pressure recovery of gas-solids suspensions flowing in the diffuser
Δp_a	pressure recovery of gas flow alone
Q_m	gas flow rate calculated by ΔP_m
Q	actual gas flow rate
r	inside radius of the diffuser inlet pipe
u	gas velocity
v	particle velocity
x	coordinate in axial direction
x_0	position at which the error E or e vanishes

Greek letters

α	constant determined with θ and r, defined by Eq.(7.3)
θ	half of the diverging angle of the diffuser
μ_a	viscosity of the gas
ρ_a	density of the gas
ρ_p	density of the particle
ϕ_0	velocity ratio defined by Eq.(7.16)

References

1) Farbar, L., "The Venturi as a Meter for Gas-Solids Mixtures", Trans. of the ASME, 75, 943 (1953)

2) Barth, W., R. Nagel, and K. van Waveren, "Neues Verfahren zur Bestimmung der augenblicklich geförderten Gutmengen im Luftstrom bei pneumatischer Förderung", Chemie-Ing.-Techn., 29, 599 (1957)

3) Iinoya, K. and K. Goto, "Solid-gas Two Phase Flowmeter", Kagaku Kōgaku, 27, 80 (1963)

4) Sakata, M., "Solid-Gas Two-Phase Flow in the Venturi Tube", Trans. of the Japan Soc. of Mech. Engrs., 37, 1560 (1971)

5) Пашацкий, Н. В. and Н.И. Сыромятников, "К РАСЧЕТУ ПЫЛЕРАСХОДОМЕРОВ", ИНЖЕНЕРНО-ФИЗИЧЕСКИЙ ЖУРНАЛ, 17, 26 (1969)

6) Tanaka, Z. and K. Iinoya, "New Approximate Equation of Drag Coefficient for Spherical Particles", J. Chem. Eng., Japan, 3, 261 (1970)

7) Schiller, L. and A. Naumann; Z.V.D.I., 22, 318 (1933)

8) Lapwood, E. R., "The International Encyclopedia of Physical Chemistry and Chemical Physics", Topic 1, Vol. 1, p. 179, Pergamon Press, London (1968)

9) Weidner, G., "Grundsätzliche Untersuchung über den pneumatischen Fördervorgang, imbesondere über die Vorhältnisse bei Beschleunigung und Umlenkung", Forschung, 21, 145 (1955)

10) Boothroyd, R. G., "Similarity in Gas-Borne Flowing Particulate Suspensions", Trans. of the ASME, ser. B, 91, 303 (1969)

11) Iinoya, K., T. Kamimura, and Y. Tsukada, "Some Studies on a Pneumatic Conveyor", Kagaku Kōgaku, 23, 400 (1959)

12) Barth, W., "Strömungsvorgänge beim Transport von Festteilchen und Flüssigkeitsteilchen in Gasen", Chemie-Ing.-Techn., 30, 171 (1958)

CHAPTER 8

CONCLUSION

The characteristics of powder feeders and of the methods for measuring the gas flow rate in gas-solids two-phase flow are studied. The basic problems peculiar to particulate processes are also discussed. The significance of the mean particle diameter in relation to the analysis of particulate processes and the scatter of the experimental data attributable to the particle size distribution are discussed in Part I. The static and dynamic characteristics of a screw feeder, Vibra screw feeder, Flo-tron, belt feeder, table feeder and a rotary feeder are studied in Part II. The venturi-type Gas-flow meter used generally for measuring gas flow rate in gas-solids two-phase flow is examined in Part III. As a result of this study it is recommended that it be used as a basic device for measuring the powder flow rate in the two-phase flow.

The main results obtained in Part I are that the mean particle diameter is one of the most important factors in the analysis of the data obtained using poly-disperse powder, and that the particle size distribution can cause appreciable scatter of the experimental data. The mean particle diameter

is defined most exactly by

$$\bar{D}_p = y^{-1}(\bar{y}) \tag{2.8}$$

where y^{-1} is an inverse function of the mono-disperse particle process variable and $\bar{y}$ a linear estimate of the poly-disperse particulate process variable. If the experimental data are studied using this mean particle diameter, the scattering arising from the ambiguous use of the mean particle diameter is eliminated. On the other hand, the scatter of data caused by the size distribution may increase with the standard deviation and other factors. When the size distribution is log-normal and the process is represented by

$$y = K D_p^{\alpha}$$

the distribution of $\ln \bar{D}_p / \bar{D}_p^{\cdot}$ is given by

$$f(\ln \bar{D}_p/\bar{D}_p^{\cdot}) = \frac{\sqrt{n}}{\sigma\sqrt{2\pi}\ \sqrt{2c^2\sigma^2 + 1}}\ e^{-\frac{\varphi^2}{2}}\ \Phi\ (z) \tag{3.16}$$

where

$$\varphi \equiv \frac{\sqrt{n}(\ln \bar{D}_p / \bar{D}_p^{\cdot} + c\sigma^2/n)}{\sigma\sqrt{2c^2\sigma^2 + 1}}$$

$$z \equiv \sqrt{\frac{n}{2(2c^2\sigma^2 + 1)}} \left(2c \ln \frac{\bar{D}_p}{\bar{D}_p^{\cdot}} + 2c^2\sigma^2 + 1\right)$$

and $$\Phi(z) = \frac{1}{\sqrt{2\pi}} \int_{-\infty}^{z} e^{-\frac{z^2}{2}} dz$$

This sampling distribution shows a bias, $\bar{D}_p^{\cdot}\{\exp(-c\sigma^2/n) - 1\}$. Fortunately, this bias becomes rapidly smaller with increasing number of particles n. The number of particles required to ensure that a desired percentage of the data is within a designated range of error is given by

$$\log n_* = -2 \log \delta + \log \omega \qquad (3.27)$$

where,

$$\omega \equiv u^2\alpha^2\sigma^2(2c^2\sigma^2 + 1)$$

$$\Phi(-|u|) = \frac{1 - P(|e| \leq \delta)}{2}$$

and $P(|e| \leq \delta)$ is a probability that the experimental data may be within the range of relative error $-\delta$ to $+\delta$. It is possible to use this equation in calculating the number of particles required in an experiment, and also in estimating the error when the number of particles is given.

Part II gives the results on the characteristics of several kinds of feeder. It is found that almost all of these feeders have delay-times. In addition, the table feeder shows a derivative response in a particular operating range. Because of this, a table feeder is well suited for use as a final control means.

It is found that the shape of the powder bed on the table can be represented by the following equation:

$$y = Y - \frac{g}{\omega^2}\left(1 + \frac{1}{\mu^2}\right)\ln\frac{g + \mu r\omega^2}{g + \mu R\omega^2} + \frac{1}{\mu}(r - R) \qquad (5.4)$$

The relationship between the discharge rate of the particles and both the scraper position and rotational speed of the table in the steady state, can be estimated with fairly good accuracy provided the shape of the powder bed is taken into consideration. The dynamic characteristic of the discharge rate regulated by the scraper is of derivative nature

when the relative scraper position is larger than X_c determined by

$$X_c = \delta_0 - Y_c/\tan \varphi_r \qquad (5.27)$$

This characteristic is attributable to the fact that the slope of the Y-curve is larger than the angle of repose in the above case. The different type of step response under various operating conditions can be explained on the basis of the relation between the slope of the Y-curve and the angle of repose. The response can be approximated by the following equation:

$$W_n = \frac{\rho_B \omega}{2} \frac{y_n^2}{\tan \theta} \left(\frac{1}{3} \frac{y_n}{\tan \theta} + R \right) \qquad (5.16)$$

where

$$y_n = R\left\{ \sqrt[3]{1 + \frac{3y_{n-1}}{R \tan \theta} + \frac{6W_H}{R^3 \rho_B \omega \tan\theta}} - 1 \right\} \tan \theta$$

..... (5.15)

It is also found that the Y-curve depends on the properties of the powder. This fact is represented by a parameter κ;

$$\kappa \text{ is } \begin{cases} \text{positive, for powders of high flowability} \\ \text{zero , for powders of moderate flowability} \\ \text{negative, for powders of low flowability} \end{cases} \tag{5.38}$$

The dynamic characteristic of the discharge rate regulated by changing the rotational speed of the table is also derivative in nature, when the scraper position and the effect of the force $r|d\omega/dt|$ are large.

An inclination in the installation of the table causes a periodic fluctuation in the discharge rate of the particles. This fact suggests that the table feeder may be used as a sine-wave generator for studies in the dynamic characteristics of a particulate process.

The discharge rate of particles from a rotary feeder inherently fluctuates. However the mean discharge rate can be estimated as shown earlier. The motion of a particle in the rotary feeder can be approximated by the following equation:

$$\frac{d^2r}{dt^2} = r\omega^2 + g\cos\theta - \left(\frac{S}{m} - g\sin\theta\right)\mu_p - \frac{3}{4}C_D\frac{\dot{r}}{D_p}\frac{\rho_a}{\rho_p} \tag{6.1}$$

where, μ_p denotes the inter-particle friction factor, S denotes the Coriolis' force and C_D denotes the drag-coefficient. The volumetric efficiency can be estimated up to 100 rpm. The effect of the particle size distribution on an estimation can be represented by

$$\bar{\eta} = \Sigma f(D_{pi})\eta(D_{pi}) \qquad (6.20)$$

It is also found that the dynamic characteristic of the rotary feeder is approximated by a first-order time delay.

The main results obtained in Part III are that the relative error for the measurement of the gas flow rate in gas-solids two-phase flow is a monotone-increasing function of the measuring position, that the value of the error approaches that of the mass flow ratio, and that there exists a position where the error vanishes. This position can be estimated by

$$\alpha x_0 = \frac{1 - \phi_0}{\phi_0} \quad , \quad \text{where} \quad \phi_0 = \frac{v_0}{u_0} \qquad (7.16)$$

The residual error, when the measuring position does not coincide with x_0, is estimable with the following equation:

$$\left.\frac{dE}{dx}\right|_{x_0} \lesssim 18\, m\, \frac{\mu_a}{D_p^{\,2} \rho_p v_0} \qquad (7.13)$$

The physical significance of the mean particle diameter and the scatter of data due to the particle-size-distribution have been clarified. The relation between the properties of the powders and the characteristics of the powder feeders, and the important factors in the measurement of air flow rates in gas-solids two-phase flow have also been obtained.

The results reported in this dissertation are of interest in many ways and it is believed that they will be useful to engineers who seek information about the physical phenomena involved, as a basis to their design of a control system for a particulate process. Further studies into the measurement of powder flow rate in gas-solids two-phase flow are needed to attain more satisfactory control of particulate processes.